UNCLASSIFIED

AD 277 750

Reproduced
by the

ARMED SERVICES TECHNICAL INFORMATION AGENCY
ARLINGTON HALL STATION
ARLINGTON 12, VIRGINIA



UNCLASSIFIED

NOTICE: When government or other drawings, specifications or other data are used for any purpose other than in connection with a definitely related government procurement operation, the U. S. Government thereby incurs no responsibility, nor any obligation whatsoever; and the fact that the Government may have formulated, furnished, or in any way supplied the said drawings, specifications, or other data is not to be regarded by implication or otherwise as in any manner licensing the holder or any other person or corporation, or conveying any rights or permission to manufacture, use or sell any patented invention that may in any way be related thereto.

DASA-1272

277750

Final Report

GEOPHYSICAL EXPERIMENTS PERTINENT TO NUCLEAR BLACKOUT STUDIES

Prepared for:

HEADQUARTERS
DEFENSE ATOMIC SUPPORT AGENCY
WASHINGTON 25, D.C.

ATTENTION: MAJOR BILLY M. McCORMAC
RADIATION DIVISION

CATALOGED BY ASTIA AS AD No.

STANFORD RESEARCH INSTITUTE

MENLO PARK, CALIFORNIA



277 750

ASTIA
RECEIVED
JUL 16 1962
TISIA B

STANFORD RESEARCH INSTITUTE
MENLO PARK, CALIFORNIA

December 31, 1961

Final Report

GEOPHYSICAL EXPERIMENTS PERTINENT TO NUCLEAR BLACKOUT STUDIES

Prepared for:

HEADQUARTERS
DEFENSE ATOMIC SUPPORT AGENCY
WASHINGTON 25, D.C.

ATTENTION: MAJOR BILLY M. McCORMAC
RADIATION DIVISION

By: *I. G. Poppoff* *R. C. Whitten* *S. D. Softky* *A. H. Samuel*
T. O. Passell *E. T. Pierce* *R. B. Dyce* *C. J. Cook* *D. C. Lorents*
R. A. Young *J. B. Chown* *J. E. Nanevicz* *E. F. Vance*

SRI Project No. PAU 3709

Approved:

Clinton M. Kelley

CLINTON M. KELLEY, DIRECTOR
CHEMICAL PHYSICS DIVISION

Copy No. 159

LETTER OF PROMULGATION

This report was prepared for the Defense Atomic Support Agency as an aid in planning research programs for the investigation of atmospheric processes involved in the production of nuclear blackout. The specific objective of this study was to consider geophysical experiments involving naturally occurring ionizing events. In order to make the necessary reference material easily accessible, pertinent aspects of both natural and nuclear weapon radiations are presented. The interaction of these radiations with the upper atmosphere to produce various ionospheric phenomena is then considered and the relevant features of ionization events caused by both nuclear weapon tests and solar-terrestrial phenomena are summarized.

Potentially rewarding areas of geophysical research are described. Feasible geophysical experiments are suggested and analyzed with respect to the kinds, numbers, and accuracies of measurements that should and could be made as well as the amount of information that could be derived either under ideal circumstances or in the event of partial malfunction of equipment. Although it is evident that geophysical experiments could provide data that would be very useful in the absence of actual nuclear weapons tests, it is noted that these data would also be very useful in understanding the results of investigations conducted during weapons tests.

This report is published for the information and guidance of all concerned.

Robert H. Booth

ROBERT H. BOOTH
Major General, USA
Chief, DASA

FOREWORD

Interest in D-region* ionization and recombination processes was considerably enhanced by observations of radio propagation anomalies caused by the detonation of nuclear weapons at high altitudes. Although theory substantiates the general interpretation that the anomalies were caused by excess ionization of the D-region--which was sufficient to cause serious absorption of HF radio signals over very large areas--insufficient specific data are available to allow confident predictions of the extent and duration of the absorption effects.

Similar effects have been observed as the result of either solar-flare or auroral activity. Thus, an obvious correlation would seem to exist between the ionospheric effects caused by nuclear weapon detonations and those caused by naturally occurring geophysical phenomena. It would also seem obvious that knowledge derived from studies of natural geophysical phenomena could, therefore, be applied to military problems concerned with the effects of high altitude nuclear weapon detonation.

Unfortunately, the state-of-knowledge of D-region perturbation and relaxation processes is not sufficient at present to provide the required basic data. Hence, it has been suggested that pertinent geophysical events be studied in order to make the data available.

In exploring the similarities between nuclear weapon and geophysical events, several important questions, such as the following, arise.

1. How similar are these events?
2. Which natural events are most amenable to study?
3. What geophysical experiments can be conducted?
4. What measurements should be made and with what precision should they be made?

---

*Used in this report to designate any ionized region below the E-region.

5. How much information pertinent to nuclear weapon effects can be obtained from such experiments?

The purpose of this report is to provide the information necessary to answer these questions.

We have attempted to provide enough background material and references to be useful in evaluating most geophysical experiments proposed as well as to substantiate the value of the specific experiments suggested in this report.

Specifically, the characteristics of ionizing radiation emitted by nuclear weapons and by the sun are reviewed and summarized (Chapters I and II). The effects of these radiations on the atmosphere are discussed and similarities between nuclear weapons effects and solar-terrestrial relationships are discussed and summarized (Chapters II, III, and IV).

Promising areas of geophysical research and a general schedule for the progress of such research through the 1963-67 period is suggested (Chapter VI). Finally, specific rocket probe experiments utilizing geophysical events are suggested and analyzed (Chapter VI). These experiments are considered from the viewpoint of obtaining sufficient information regarding atmospheric relaxation parameters to allow predictions of nuclear weapons effects or confirmations of theoretical models of weapons effects.

CONTENTS

FOREWORD iii

LIST OF FIGURES xi

LIST OF TABLES xiii

I ORIGIN AND CHARACTERISTICS OF IONIZING RADIATION 1

A. Ionizing Radiation Expected from Bomb Detonation 1

1. Electromagnetic Radiation 1

a. Prompt X- and γ-Radiation 1
b. Fission Products 1
c. Bremsstrahlung 3

2. Particles 5

a. Prompt Electrons 6
b. Fission Product Electrons 6
c. Neutron Decay Electrons and Protons 8
d. Prompt Protons and Heavier Particles 9
e. Neutrons 10

B. Ionizing Radiation Expected from Solar Activity 11

1. Electromagnetic Radiation 11

a. Continuously Emitted X-ray 11
b. Flare X-ray and γ ray 14
c. Bremsstrahlung X-ray 15
d. Proton-γ Reactions 23

2. Particles 23

a. Electrons from Solar Activity 23
b. Flare Ejected Protons 24
c. Solar Wind Protons 26
d. Neutrons and Heavy Ions in Solar Radiation . . . 27

C. The Van Allen Radiation Belts 27

REFERENCES 33

CONTENTS (Continued)

II GEOPHYSICAL PHENOMENA CAUSED BY IONIZING RADIATIONS. 37

A. Aurora. 37

1. Optical. 37
2. Radio Reflection and Transmission. 38

a. Introduction. 38
b. Reflection. 39
c. Transmission. 41
d. Conclusions 42

B. Auroral Zone and Polar Cap Absorption 43

C. Sudden Ionospheric Disturbances 47

D. Normal D-Region 49

E. Geophysical Effects of the Solar Wind 49

REFERENCES. 51

III ATMOSPHERIC IONIZATION AND RELAXATION PROCESSES. 55

A. Ionization Processes. 55

B. Relaxation Processes. 62

1. Chemical Reactions 63
2. Ion-Atom Interchange 64
3. Electron Attachment. 66
4. Electron Detachment. 67
5. Dissociative Recombination 68
6. Ion-Ion Recombination. 69
7. Radiative Recombination. 69
8. Temperature Effects. 70

REFERENCES. 71

CONTENTS (Continued)

IV PERTINENCE TO NUCLEAR DETONATION EVENTS 75

A. Auroral and Bomb Events 75

1. Ionization 75
2. Radio Effects 76

a. Prompt X-ray, γ-ray, and Neutron Radiation . . . 76
b. Prompt Charged-particle Radiation 77
c. Delayed X-ray and γ-ray Radiation 77
d. Delayed Charged-particle Radiation 78

B. Sudden Ionospheric Disturbances (SID) and Bomb Events . . 80

1. Ionization 80
2. Radio Effects 81

a. Natural Origin 81
b. Absorption Effects 82
c. Effects at VLF 85
d. Radio Effects Not Due to D-Region Ionization . . 87
e. Nuclear Origin 87

C. "Quiescent" Conditions and Bomb Events 89

1. Ionization 89
2. Radio Effects 89

REFERENCES 93

V SOLAR ACTIVITY EXPECTED DURING THE 1963-67 PERIOD 95

REFERENCES 99

VI PERTINENT GEOPHYSICAL EXPERIMENTS 101

A. General 101

1. Value and Limitations 101
2. Pertinent Areas of Research 102

a. Aurora 102
b. Polar Cap Events 102
c. Sudden Ionospheric Disturbances 103
d. "Quiescent" Solar Conditions 103

3. Research Phases. 103
4. Recent and Current Geophysical Investigations. . . 104

a. Satellite Observations of Solar X-rays. . . . 104
b. Rocket Observations of Solar X-rays 105
c. Injun Satellite 105
d. Lockheed Satellite Experiments. 106
e. Balloon Observations of Auroras 106
f. Solar Proton Experiments. 106
g. Quiescent D-region Experiments. 107

B. Specific Experiments. 107

1. Design Philosophy. 107

a. Polar Cap Absorption (PCA). 108
b. Sudden Ionospheric Disturbances (SID) 110
c. Quiescent D-region. 110
d. Auroral Bremsstrahlung. 111

2. Measurement of Ionizing Radiation. 111

a. Particle Fluxes 111
b. X-rays in the 2-8A Wavelength Range 119
c. Auroral Brehmsstrahlung 122

3. Measurements of Electron and Ion Concentrations, Electron Temperature, and Collision Frequency. . . 124

a. General 124
b. Propagation Experiments 125
c. Impedance Probes. 129
d. Conductivity Measurements 132
e. Langmuir Probes 133
f. Ion Traps 135
g. Recommended Measurement Techniques. 135
h. Conclusions 146

4. Measurement of Density 147

CONTENTS (Concluded)

5. Ancillary Measurements and Observations 147

a. Riometers 147
b. Solar Patrol 148
c. Auroral Features 148

6. Solar Aspect Measurements 148
7. Data Reduction 149

a. Ionizing Flux: Protons 149
b. Ionizing Flux: X-rays 150
c. Measured Electron Concentration and Time Rate of Change of Electron Concentration . . . 153
d. Measured Negative Ion-Electron Concentration Ratio and Its Time Rate of Change 154

8. Interpretation 154

a. Relaxation Parameters 154
b. Electron Collision Frequencies 163

9. Information Obtainable if Errors are Large or Part of the Equipment Malfunctions 169

C. Summary 170

REFERENCES 175

FIGURES

Fig. I-1	Typical Distribution of Energies for β-emission from a Mixture of Artificial Radioactive Isotopes . .	4
Fig. I-2	Typical Distribution of Energies for γ-emission from a Mixture of Artificial Radioactive Isotopes . .	4
Fig. I-3	Range in Atmosphere of 2 mev β and 1.5 mev γ Radiation	5
Fig. I-4	Typical Shapes of Neutron Decay Beta Spectra	9
Fig. I-5	Estimated Spectrum of Quiescent Solar X-Radiation During Sunspot Maximum	13
Fig. I-6	Estimated Shape of a Solar Flare X-ray Pulse	17
Fig. I-7	Estimated Spectrum of X-Radiation from a Solar Flare	18
Fig. I-8	Shape of 2-8 A X-ray Pulse for Two Flares Observed by Solar Satellite eta II	19
Fig. I-9	An Example of Auroral Bremsstrahlung Observations . .	22
Fig. I-10	Energy Distribution of Protons from a Solar Flare . .	25
Fig. I-11	The Van Allen Bands in Meridian Section	28
Fig. I-12	Spectrum of Protons in Inner Belt	29
Fig. I-13	Changes in Outer Van Allen Band During a Solar Storm	31
Fig. II-1	Integral Spectrum of Interplanetary Particles	46
Fig. III-1	Interactions of Electrons with Air, N_2, and O_2 . . .	56
Fig. III-2	Interactions of Protons with Air, N_2, and O_2	57
Fig. III-3	Interactions of Alpha Particles with Air, O_2, and N_2.	58
Fig. III-4	Absorption cross section for X-rays in Air as a Function of Wavelengths	60
Fig. III-5	Mass Attenuation Coefficients for Photons in Air . .	61

FIGURES (Concluded)

Fig. IV-1 Electron Density Profiles for SID and Normal Conditions 83

Fig. IV-2 Absorption Coefficients for SID and Normal Conditions 84

Fig. IV-3 Attenuation Coefficients for SID and Normal Conditions 86

Fig. V-1 Predicted and Observed Sunspot Numbers 97

Fig. VI-1 Time Sequence of Most of the Important Chromospheric Flare Effects Observable at the Earth. 109

Fig. VI-2 Range-Energy Curves for Protons in Air (A) and Aluminum (B) 113

Fig. VI-3 Block Diagrams of the Circuit for use with the Semi-conductor Particle Detector 117

Fig. VI-4 Modified Langmuir Probe. 138

Fig. VI-5 Variations of Sheath Structure about Plane Probe in Rocket Skin. 140

Fig. VI-6 Possible Refinements of Plane Probe. 141

Fig. VI-7 Cylindrical and Spherical Langmuir Probes. 143

Fig. VI-8 Observed X-ray Spectrum. The Blocks Represent the Mean Spectral Radiance in the Appropriate Wavelength Interval. The Broken Line Represents the Estimated X-ray Spectrum 152

Fig. VI-9 Total and Momentum Cross Sections of Electrons (Q and Q_d, respectively) in N_2 as a Function of Energy 163

Fig. VI-10 Total and Momentum Transfer Cross Sections (Q and Q_d respectively) for Electrons in O_2 as a Function of Energy. 164

Fig. VI-11 Typical Electron Concentration Profiles Occurring during SID's[58] and PCA Events;[59] Electron Collision Frequencies According to Phelps and Pack 167

Fig. VI-12 HF Absorption Coefficients Based on the Data Presented in Figure V-11. The Signal Frequencies are 10 mc (SID) and 20 mc (PCA). 168

TABLES

Table I-1	Radioactivity Associated with a 20-KT Fission Bomb	2
Table I-2	Continuous Solar Radiation in the 2-8 A Spectral Region	14
Table I-3	Summary of Rocket Observations of X-Ray Flares	16
Table I-4	Balloon Observations	16
Table I-5	Observed Auroral and Subauroral X-Radiation	21
Table IV-1	Pertinent Ionizing Events	90
Table VI-1	Atmospheric Layer Equivalent in Proton Stopping Power of a 20μ Silicon Detector	112
Table VI-2	Energy Loss in Sensitive Layer	116
Table VI-3	X-Ray Detector Transmission Windows	120
Table VI-4	Spectral Response of G-M Counters	121
Table VI-5	Examples of Transmission Windows for Absorbers Transmitting 25% Radiation at K-Edge	123
Table VI-6	Differential Absorption of HF Signals	169
Table VI-7	Information Obtainable if Errors are Large or Part of the Equipment Malfunctions	170
Table VI-8	Summary of Data That can be Derived from Geophysical Experiments	172
Table VI-9	Summary of Instrumentation Requirements	174

I ORIGIN AND CHARACTERISTICS OF IONIZING RADIATION

In evaluating the pertinence of studies of geophysical phenomena to phenomena produced by nuclear weapon detonations, it is important to consider the available information regarding the ionizing radiations responsible for both kinds of phenomena. In this chapter the characteristics of these ionizing radiations are discussed; in Chapter IV, pertinent characteristics are compared.

Although only unclassified (and, therefore, incomplete) weapon data are used, this constraint does not significantly affect the conclusions.

A. Ionizing Radiation Expected from Bomb Detonation

1. Electromagnetic Radiation

a. Prompt X- and γ-Radiation

Unclassified sources* report that ... "the case temperature of the weapon is so high that the thermal radiation will be released as X-rays. ... These X-rays will have between one and five kev of energy and, because of the extreme temperature of the bomb case (on the order of 15×10^6 degrees K), will be radiated in less than 10^{-6} sec." It is also noted that ... "a one megaton weapon detonated 3×10^8 km" ... (in space) ... "will deposit 1.5 Mev of X-ray energy per square centimeter" ... at the earth.

The same source states that---"Only about one percent of the total energy of a detonation will be carried away by gamma rays and neutrons."

b. Fission Products

An explosion based on a fission reaction is quoted[1] as producing 3×10^8 curies of radioactive debris per kt one hour after the explosion. Further unclassified information[2] given in Table I-1 agrees with the above figure.

* Missiles and Rockets, October 23, 1961 issue, pp 12-13, 49.

Table I-1

RADIOACTIVITY ASSOCIATED WITH A 20-KT FISSION BOMB
(Low Altitude Burst)

Time After Explosion	Total Radioactivity (curies)	Radius of Cloud Occupied by Debris (km)
One minute	10^{12}	0.6
One hour	6×10^{9}	4
One day	10^{8}	35
One week	10^{7}	90

The decay of the radioactivity is reasonably well represented by the simple relation $Q = Q_o T^{-1.2}$ where Q is the total amount of radioactivity, T is the time in hours, and Q_o is the activity one hour after the explosion ($\approx 3 \times 10^{8}$ curies per kt). The figures given in Table I-1 for the radii of the cloud refer to dissemination in the troposphere. They are hardly applicable to megaton weapons for which it is known[3] that the fireballs, even for ground detonation, extend upwards well into the stratosphere.

Most radioactive substances decay by an emission involving β particles or γ radiation; often both are emitted during a radioactive change. Thus it is a reasonable assumption to regard the radioactive debris resulting from a fission explosion as being primarily a source of energetic electrons and of γ radiation.

The energy distribution of the β and γ emission will of course be dependent upon the particular isotopes involved; these, in turn, will be functions of the bomb characteristics, the place of detonation, and the time after the explosion. However, since the radioactive debris will contain many varieties of radioactive isotopes, it is probably not unreasonable to take the energy distribution as corresponding to that of the general family of radioactive isotopes. Energy distributions have been plotted in Figs. I-1 and I-2 using the data quoted for the artificial radioactive isotopes listed in the Smithsonian Physical Tables.[4] It can be seen that the median energy is about 2 Mev for the β particles

and somewhat less for the γ emission. If some allowance is made for the fact that Figs. I-1 and I-2 are based on data tending to give the peak energy associated with a decay transition, a simple approximate approach would be to take monochromaticity with each disintegration as being responsible for a 1-Mev electron and a 1-Mev γ ray, the number of disintegrations per second being 3.7×10^{10} Q.

The absorption of the emissions in the atmosphere is critical in determining where most ionization is generated. This absorption is a sensitive function of the height of origin for the emissions. γ rays are absorbed according to the law

$$I = I_o \, e^{-\rho \mu_m x}$$

where

ρ is the air density

μ_m the mass absorption coefficient, and

x is the absorption path length.

An effective range, within which most of the ionization is deposited, may be defined by $\rho \mu_m x = 1$. This range is plotted in Fig. 1-3 for 1.5-Mev ($\mu_m \approx 0.05$ cm^2/gm) γ rays traveling vertically up or down from given heights in the atmosphere. An effective range may also be defined somewhat similarly for the β emissions; this is also plotted in Fig. 1-3 for 2-Mev electrons, any effects due to the earth's magnetic field being neglected. The range of the β particles relative to that of the γ rays depends upon the height of origin of the emission, but is usually about an order of magnitude less.

c. Bremsstrahlung

Neutron decay electrons trapped by magnetic field lines, and radioisotope decay electrons are potential sources of bremsstrahlung. Although only a few percent of the total energy loss of the electrons would be represented by bremsstrahlung, the increased range of the bremsstrahlung photons may make this process important. For example, a 1-Mev electron has a range of only 0.5 g/cm^2, whereas the mean path

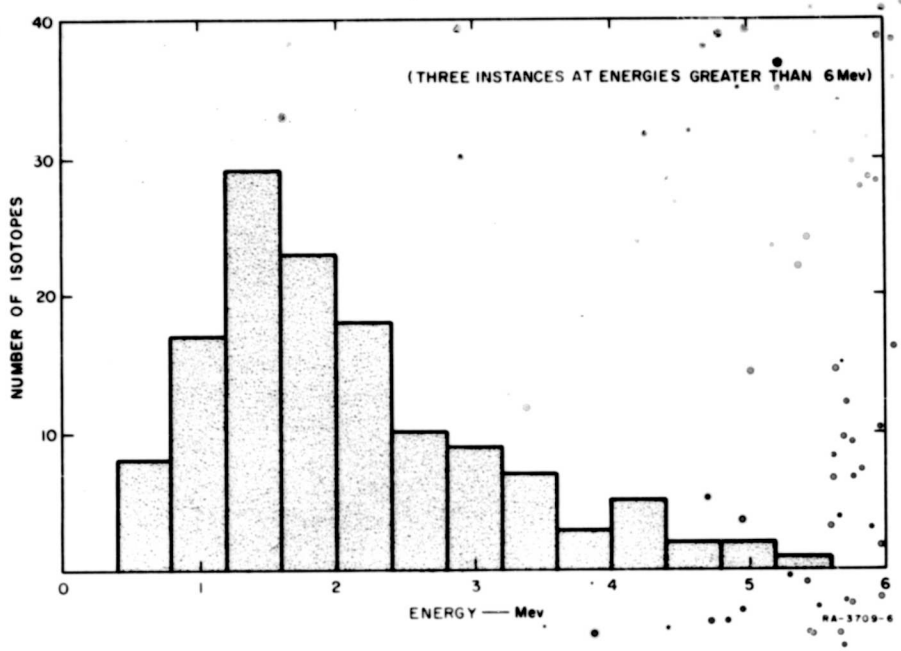


FIG. I-1 TYPICAL DISTRIBUTION OF ENERGIES FOR β_- EMISSION FROM A MIXTURE OF ARTIFICIAL RADIOACTIVE ISOTOPES

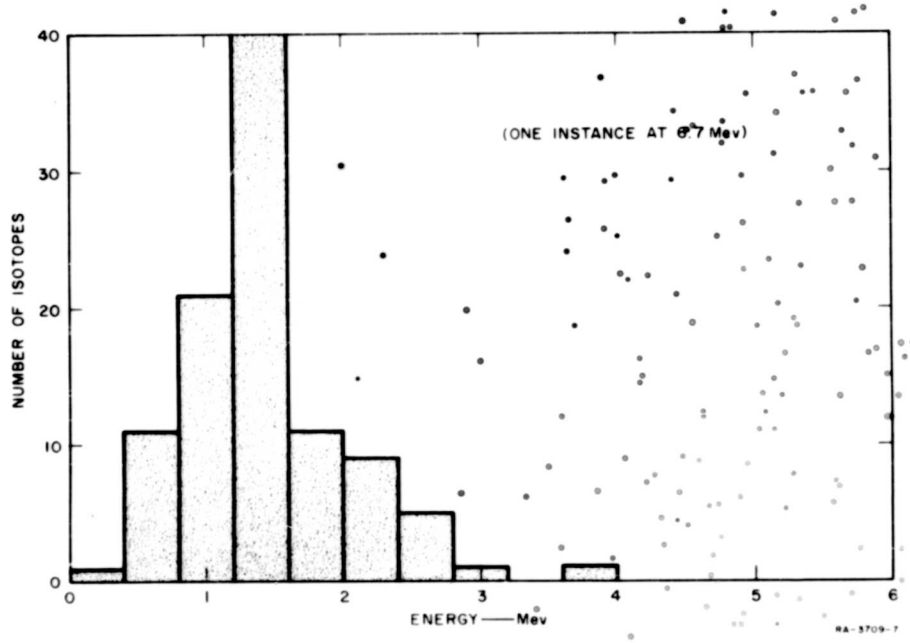


FIG. I-2 TYPICAL DISTRIBUTION OF ENERGIES FOR γ EMISSION FROM A MIXTURE OF ARTIFICIAL RADIOACTIVE ISOTOPES

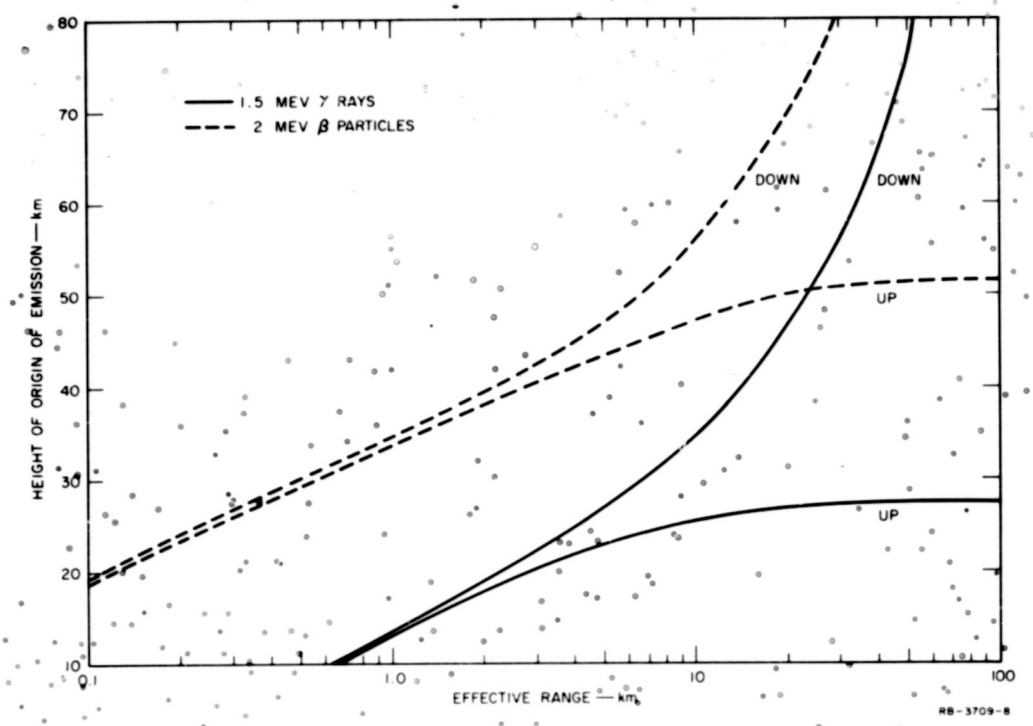


FIG. I-3 RANGE IN ATMOSPHERE OF 2 mev β AND 1.5 mev γ RADIATION

length for a 1-Mev photon is > 14 g/cm^2. This means that 1-Mev electrons impinging on the atmosphere would be absorbed above 55 km whereas 1-Mev photons would be absorbed in the vicinity of 30 km. For calculations of ionization produced by mixed fission products, bremsstrahlung would not be important except as a small correction to the γ ray ionization. On the other hand, for consideration of the possible longer range effects of neutron decay, bremsstrahlung should be considered.

2. Particles

There are two sources of energy which are used in nuclear devices, fusion (a thermonuclear reaction), and fission (of some heavy element). Presently used fusion devices require the release of a substantial amount of fission energy in order to trigger the fusion reactions. As a consequence, the products of fission are all found to a greater or

lesser degree as the result of a nuclear explosion. A nuclear explosion in vacuo, which will be discussed here, involves no interaction of the nuclear reaction products with air, and so the particles which could conceivably be important products of the explosion are:

1. Promptly emitted electrons
2. Electrons from decay of fission products
3. Electrons from decay of neutrons emitted
4. Protons or other heavy charged particles due to nuclear reactions or neutron decay
5. Neutrons
6. Positions from pair production by γ-rays interacting with atoms in the device.

a. Prompt Electrons

No electrons can escape the plasma formed by a nuclear explosion in vacuo. This is guaranteed by the electrostatic force which would exist according to Coulomb's Law if any substantial charge separation took place. If one coulomb of electrons separated radially one meter from the explosion, the radial voltage difference would be $1/4\ \pi k_o$ or about 10^{10} volts. Consequently the prompt electron emission is limited to a very small fraction of a coulomb, consistent with energies certainly no more than a few Mev for electrons.

b. Fission Product Electrons

One fission event contributes about 180 Mev or 2.9×10^{-4} erg to the energy of a nuclear detonation. One kiloton is equivalent to 4.18×10^{19} erg and it therefore follows that the number of fission products (two per event) is 2.9×10^{23} per kiloton-TNT-equivalent of fission. Fission product nuclei are produced as multiple-charged positive ions because of the high temperature in the explosion, and the positive charge is increased by a series of beta decays. As there are about 8 beta decays per fission, the total number of electrons from fission product decay is about 1.2×10^{24} per (fission) kiloton.

Since the range of fission products is only a few (3.0 in air) milligrams per square centimeter, they will in general be thermalized in the bomb and expand with the fireball. Although the fireball is dense enough to be considered as a fluid, hydrodynamic cooling will take place and may result in partial neutralization of the charge. However, complete neutralization is considered unlikely. The half-time for the first radioactive decay is of the order of 1 second for most primary fission products, and it is anticipated that, when they have moved far enough from the site of the detonation so that the mean free path is that characteristic of the altitude, they will exist as singly or multiply charged ions. After the first ten seconds, an empirical rule gives their radioactivity as proportional to $t^{-1.2}$, where t is the time after detonation.

It follows that at suitable altitudes the fission products, as well as the electrons they emit, may be geomagnetically trapped. They would then constitute a trapped source of electrons. The electrons would be emitted at energies of up to 6 Mev and their velocities would be almost completely unaffected by the energy of the parent. In addition, geomagnetically trapped fission products would produce gamma rays which would be absorbed in part at lower levels of the atmosphere, perhaps of the order of 10 g/cm^2, and would produce ionization there. This would be somewhat below the D-layer and should be detectable.

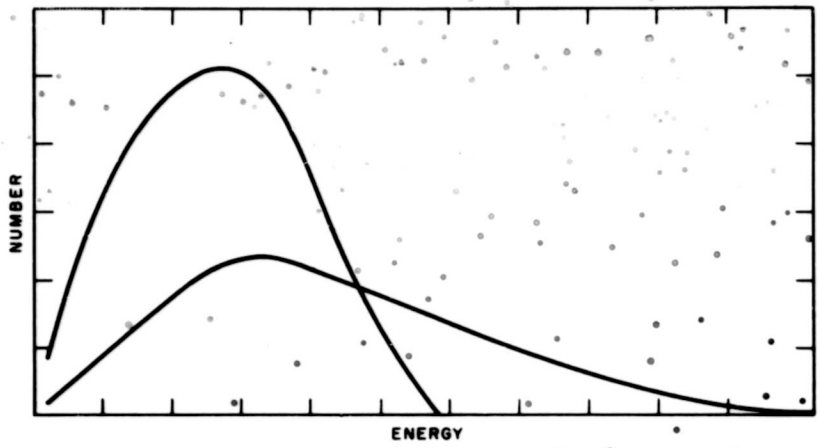
In the Argus experiments, as interpreted by Welch and Whitaker,[5] only the electrons produced by fission product decay in the first few seconds after detonation are assumed to be geomagnetically trapped. The decay of trapped electrons is observed to follow roughly a t^{-1} law, consistent with the theory of their gradual loss by multiple-small-angle Coulomb scattering on atmospheric constitutents near the mirror points.[5] It appears to have been overlooked that the observed t^{-1} decay is very nearly identical with the decay law of gross fission products ($t^{-1.2}$). Furthermore, whereas scattering theory predicts a hardening of the spectrum of trapped electrons with increasing time, a softening is observed.[6] A softening is expected if fission fragments are the geomagnetically trapped particles, since electrons emitted from long-lived nuclei are of lower energy than those emitted from short-lived nuclei. (See note on p. 35.)

A detailed description of the decay rates of fission products has been given by Hunter and Ballou.[7] Their curves can be combined with the formula which has been given for fission product decay and with the known characteristics of the individual beta rays for a computer calculation of fission product electron yields. A rough formula for the electron spectrum from fission products used by Welch and Whitaker[5] is $P(E) = P_0 \exp(-E/1.3)$ for $0.5 \text{ Mev} < E < 6 \text{ Mev}$.

c. Neutron Decay Electrons and Protons

Both fusion and fission reactions cause the release of large numbers of neutrons in the Mev range of energy. Approximately one neutron per fission escapes a fission device;[8] these neutrons have the well-known spectrum associated with fast fission. This corresponds to about 10^{23} neutrons per kiloton of fission yield. The chief reaction leading to neutrons in a thermonuclear device is the burning of H^3 by H^2, yielding one 14-Mev neutron per reaction within the device. However, there is no way of knowing what fraction of these neutrons escapes the device without knowing the function and design of the device in detail.[8] It is true that most fusion devices absorb a large fraction of these neutrons with a consequent great reduction in the external yield of 14-Mev neutrons.

Both fission and fusion neutrons will decay (with a half-life of about twelve minutes) into proton-electron pairs. The neutrons, having energies in the Mev range, will have velocities of the order of one tenth that of light. The neutron decay electrons will have velocities relative to their parent very close to that of light ($\beta \sim 0.8$). Consequently, the neutron decay beta spectrum will have an upper energy limit of 782 kev and a shape similar to the spectra shown in Fig. 1-4. In other words, the energy spectrum will not be changed much by the additional velocity of the decaying neutron and as a result, one should expect to find some electrons in the energy range below 800 kev magnetically trapped in the earth's field after a detonation above the atmosphere. Since the parent neutrons will diffuse with a velocity up to 3×10^4 km/sec, the parent neutrons will constitute a diffuse source



SOURCE: Friedlander and Kennedy, Introduction to Radiochemistry 1st ed. p. 132.

RA-3709-9

FIG. I-4 TYPICAL SHAPES OF NEUTRON DECAY BETA SPECTRA

of electrons relative to an earth radius of 6000 km. Indeed, attempts to explain the inner Van Allen belt as fed by a cosmic ray neutron source have been made.[9]

The energetic protons from neutron decay are the only protons to be expected in the particle yield directly from a nuclear explosion. Since the proton and neutron masses are almost equal and neutrons would not be moderated in vacuo, the energy spectrum of neutron decay protons should be the same as the fission or fusion spectrum of neutrons. Such protons could be expected to be diffusely spread throughout the geomagnetic field, trapped wherever the source neutrons happened to decay.

d. Prompt Protons and Heavier Particles

The reason no prompt protons or other charged particles escape a nuclear explosion in vacuo is esentially twofold; (1) the previously mentioned charge separation voltage would forbid large yields of charged particles in any case, and (2) in a thermonuclear device none of the fast charged particles from fusion reactions could penetrate the mass represented by the vaporized outer part of the device. Relatively small yields of protons may be expected due to secondary reactions of neutrons with the matter of the outer part of the device, but as a source of ionizing particles this would be negligible relative to the major products.

A microsecond or so after the explosion, the hot plasma of the device will have radiated most of the energy as black-body radiation (X-rays) and the plasma will expand rapidly. These plasma ions must all have energies well below 1 kev and so are not important as sources of penetrating ionization, although they will become magnetically trapped, and the fission products will provide decay radiations as mentioned.

e. Neutrons

The subject of neutrons from fission and fusion devices has been treated extensively under (c) above. The number of excess neutrons from a fission device (those not consumed in initiating other fissions) is about 1.5×10^{23} per kiloton. Their initial energy spectrum is given by

$$N(E) = (2/\pi e)^{1/2} \, e^{-E} \sinh(2E)^{1/2}$$

where $N(E)\,dE$ is the fraction of neutrons emitted in the energy range between E and E + dE and E is in Mev. The average neutron energy is ~ 1.6 Mev. Neutrons from fusion are mostly produced at 14 Mev, and the number per kiloton is appreciably less. In actual devices, the neutrons will undergo some moderation before leaving the device. Nevertheless their velocities should be great enough for all neutrons except those decaying in the first fraction of a second (less than 0.1%) to escape from the vicinity of the earth if their paths do not intersect the earth or the atmosphere. Crain and Tamarkin[10] have calculated that for a megaton explosion the small fraction of decaying neutrons would suffice to give observable effects.

The effect of neutrons decaying in flight as postulated by Crain and Tamarkin is to produce geomagnetically trapped electrons which will move along spiral paths and hit the atmosphere at large distances from the explosion. The effects near the explosion will be several orders of magnitude greater since nearly all neutrons hitting the atmosphere will be moderated and decay or undergo nuclear reaction rather than escape. During moderation, the neutrons may undergo the reaction $N^{14}(n,p)C^{14}$; in this case the emitted proton will produce ionization in the air.

If the neutron is successfully thermalized, the most probable reaction is $N^{14}(n,\gamma)N^{15}$, though other reactions with A^{40} and H^1 have probabilities only an order of magnitude less. (The probability of reaction with H depends on the water vapor content.) If thermalization occurs below 70 km altitude, as is most likely, capture of neutrons will predominate over decay, and at the most probable altitude for thermalization, capture will be the fate of the overwhelming majority of neutrons. The $N^{14}(n,\gamma)N^{15}$ reaction is exoergic by 10.8 Mev and this energy will be deposited in the atmosphere and eventually cause ionization (approximately 1 ion-pair/34 ev).

B. Ionizing Radiation Expected from Solar Activity

1. Electromagnetic Radiation

a. Continuously Emitted X-ray

The continuous X-radiation from the sun is produced in the hot solar corona. An excellent review of the present state of knowledge regarding X-ray emission by the quiescent sun was published recently by Elwert.[11] A similar study, but not as comprehensive or recent, was made by Kazachevskaya and Ivanov-Kholodnyi.[12]

Briefly, the theoretical approach is to determine the temperature, electron density and energy distribution, atomic particle density and energy state, and then calculate the energy distribution and flux of photon emission resulting from free-free and free-bound transitions, recombinations, and line emissions. Three solar regions or conditions are considered: the innermost corona (estimated temperatures of 1-2 x 10^6 ^oK and electron densities of 5 x 10^8 cm^{-3}); chromosphere-corona transition region (estimated temperatures 4 x 10^4 ^oK and particle densities of 10^{12} cm^{-3}); and short-lived hot coronal condensations (estimated temperatures of 3-6 x 10^6 ^oK and electron densities of 10^{10} cm^{-3}).

Results of these two studies[11,12] indicate that normal solar conditions do not provide a basis for postulating a flux in the $< 10A$ (> 1200 ev) region of the X-ray spectrum sufficient to ionize the D-region to any significant extent. These results are substantiated by citing

results of the earlier Naval Research Laboratory rocket observations[13,14,15] made during periods of sunspot minimum (May 1952 to October 1955). For this period of low solar activity, theoretical estimates are somewhat lower than the measured values for the spectral region below 8 A, even though the measured values above 8 A are within the limits of the theoretical estimate. During periods of increased solar activity (1959), measured values were found to be higher than theoretical values by factors of one or two orders of magnitude.[16] These latter measurements indicated that, at least during periods of high solar activity, the "quiescent" solar X-ray flux may be sufficient to account for the normal D-region ionization.[17]

A spectrum of "quiescent" solar X-radiation in Fig. I-5 during sunspot maximum was estimated by Whitten and Poppoff[17] using rocket data supplied by Kreplin.[16] The results of observations by the 1960 eta II* solar radiation satellite show that insofar as X-radiation is concerned, it is rather difficult to define a "quiescent" condition. X-ray fluxes in the spectral region 2-8 A on the order of 10^{-3} ergs/cm^2 sec were observed frequently for hours at a time, but without any clear correlation with visible or r.f. solar activity.

Thus, one of the important unresolved problems in solar physics (insofar as the D-region ionization processes are concerned) is to provide adequate information, both theoretical and observational, regarding the short wavelength X-radiation from the quiescent sun. Only two possibilities exist at present to explain the discrepancies between theory and observation and neither seems to be considered very tenable. These are that the coronal temperatures are actually greater than 2×10^6 ^{o}K, or that coronal hot condensations occur quite frequently or for long periods. Apparently neither of these suppositions is consistent with solar observations.

The situation at present is summarized in Table I-2.

---

*Private communication. R. W. Kreplin. U.S. Naval Research Laboratory.

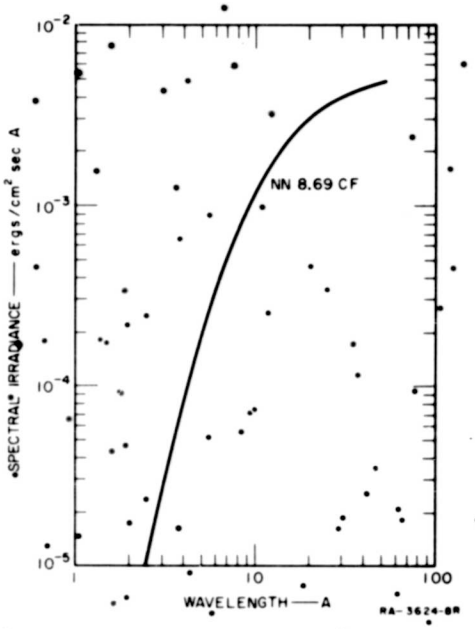


FIG. I-5 BACKGROUND SOLAR X-RAY SPECTRUM CONSTRUCTED FROM DATA OBTAINED BY SUNFLARE II PROBE NN 8.69 CF AT 15:59 UT ON 8/14/59

Table I-2

CONTINUOUS SOLAR RADIATION IN THE 2-8 A SPECTRAL REGION

Calculated (for the following coronal temp)	Flux (erg/cm² sec)	
	Elwert, 1961	Kazachevskaya and Ivanov-Kholodnyi, 1960
1×10^6 1.5×10^6 2×10^6	$\approx 9 \times 10^{-8}$ $\approx 4 \times 10^{-6}$	1×10^{-8} 2.5×10^{-6} 3×10^{-5}
Observed (Naval Research Laboratory Programs)*		
5/1/52 5/5/52 11/15/53 11/25/53	2×10^{-5} 0.6×10^{-5} 0.2×10^{-5} 1.5×10^{-5}	Low sunspot number
8/7/59 8/14/59	0.1×10^{-2} 0.1×10^{-2}	High sunspot number

*Chubb, et al:[14] and Kreplin[16]

b. Flare X-ray and γ ray

Rocket and balloon observations over the past several years have resulted in the accumulation of a limited but convincing body of data regarding the enhancement and hardening of the solar X-ray emissions during solar flares. It seems clear at this point, that the various manifestations of increased ionization in the D-region during flare activity can be attributed to X-radiation.

Peterson and Winckler[18] suggested that the hard γ-rays they observed at balloon altitudes during a solar flare were bremsstrahlung produced by the deceleration of fast electron jets emitted by a source in the corona or chromosphere and directed toward the photosphere. This suggestion has recently been investigated theoretically by de Jager[19] and extended to include all enhanced X- and γ-radiation emitted during

flares. He finds that thermal mechanisms cannot account for the observed emissions since this would require temperatures in excess of 10^7 ^oK and such temperatures have never been observed on the sun. Instead, de Jager postulates the acceleration of electrons near shock fronts in the collapsing field of two bi-polar sunspot groups. He calculates possible energies of the order of Mev, and even Bev on rare occasions.

Rocket and balloon measurements are summarized in Tables I-3 and I-4, and Figs. I-6 and I-7. The limited satellite data currently available are presented in Fig. I-8.

Most lacking at this point are observational data regarding the spectral distribution of solar flare X-rays and the time dependence of both the spectra and flux. A pulse shape for a flare of importance 2* (see Fig. 1-6) has been estimated by Poppoff and Whitten.[20] An estimated spectrum of solar flare X-radiation[20] based on U.S. Naval Research Laboratory results is presented in Fig. I-7. Fig. I-8 shows the shape of the 2-8 A X-ray pulse for two flares as observed by the solar satellite eta II.

c. Bremsstrahlung X-ray

Several observers have reported measurements of X-ray fluxes during auroras at balloon altitudes in the auroral and subauroral zones.[21-25] The radiation has not been observed in the magnetic polar regions, even during highly disturbed geomagnetic field conditions; however, it has been observed even during lightly disturbed conditions in the auroral and subauroral regions.

It seems to be universally agreed that this radiation is bremsstrahlung produced by soft electrons impinging on the top of the atmosphere. The source of the electrons and their precise energy ranges and fluxes are not definitely established. Some estimates, however, have been made of the electron energies and these along with the observed X-ray

* Flare importance is defined in terms of area (as estimated by the observer). Importance is designed in intervals from 1- to 3+, the latter designating the largest flares observed.

Table I-3

SUMMARY OF ROCKET OBSERVATIONS OF X-RAY FLARES*

Date	Observation Time (UT)	Flare Importance	Wavelength Range of Sensor (A)	Observed Flux (erg/cm^2 sec)	Remarks
7/20/56	1217	1	3-8	5×10^{-3}	Late in flare
8/20/57	0949	1+	2.5 - ?	$> 3 \times 10^{-3}$	
8/29/57	1412	2	3-8	$> 2 \times 10^{-2}$	
9/18/57	1054	3	1.5 - ?	$10\text{-}50 \times 10^{-2}$	
8/24/59	2246	2+	2-8	2.6×10^{-2}	Optical max 2239
			8-20	16×10^{-2}	
			44-60	< 0.41	
8/31/59	2252	2+	0.3-0.9	2.5×10^{-5}	Xtal spectrometer
			2-8	$> 22 \times 10^{-2}$	Optical max 2252
			8-20	$> 45 \times 10^{-2}$	
			44-60	< 1.8	
9/1/59	1659	2+	2-8	$> 8.8 \times 10^{-2}$	Optical max 1702.
			8-20	$> 90 \times 10^{-2}$	

*Byram, et al.;[13] Chubb, et al.;[14] Kreplin;[16] Friedman.[15]

Table I-4

BALLOON OBSERVATIONS*

Date	Observation Time (UT)	Flare Importance	Energy (kev)	Flux ($ergs/cm^2$ sec)	Remarks
3/20/58	1304-5	2	200-500	2×10^{-5}	Simultaneous with observed flash and cm radio burst. Coincident with observed optical max.
8/11/60	1926	2+	30	3×10^{-5}	Optical max 1930. Simultaneous with observed flash. Correlated with type III radio bursts which began at 1925.8 UT.

*Peterson and Winckler;[18] Winckler, et al.[21]

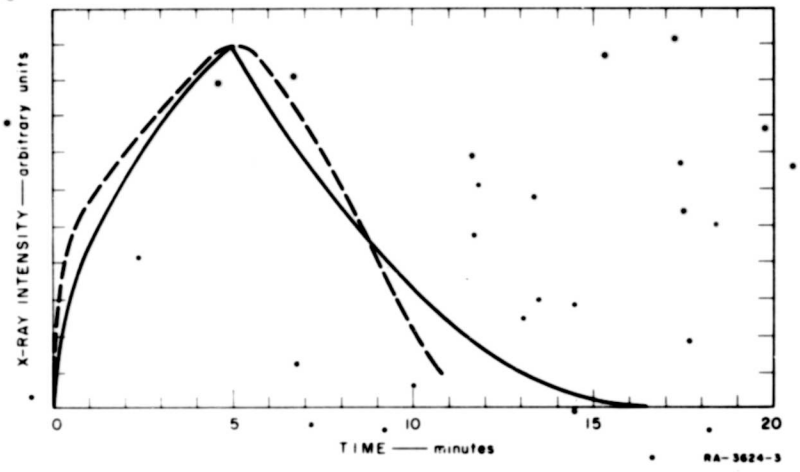


FIG. I-6 MODEL OF SOLAR RADIATION INTENSITY (λ = 2 to 8A) AS A FUNCTION OF TIME FOR THE FLARE OCCURRING ON 31 AUGUST 1959. THE SOLID LINE REPRESENTS THE FUNCTION $a\, t^{1/2}$, $0 \leq t \leq 5$ MIN. AND $a'\,(11.7 - t)^2$, $t > 5$ MIN. THE BROKEN LINE REPRESENTS THE ESTIMATED X-RAY INTENSITY

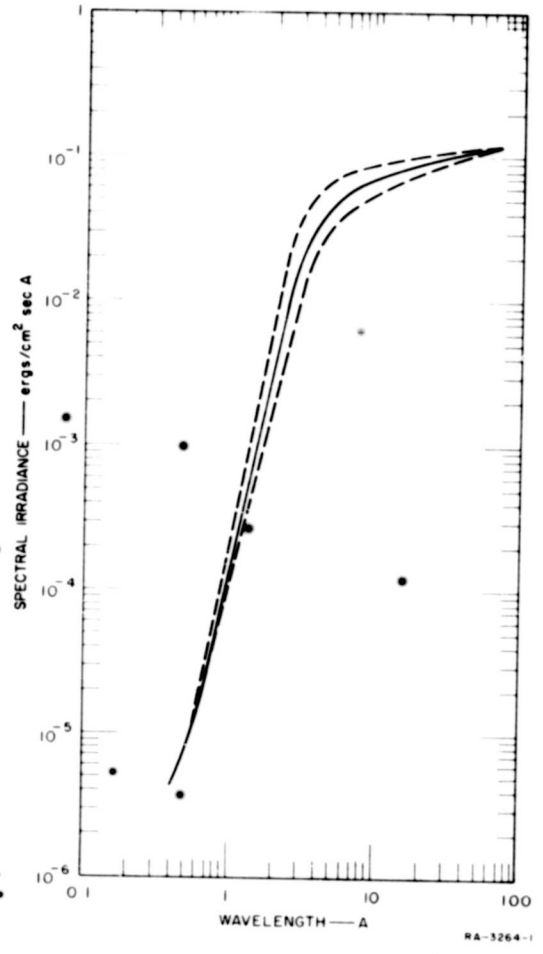


FIG. I-7 X-RAY SPECTRUM OF THE FLARE OBSERVED AT 22:50 UT ON 31 AUGUST 1959. THE SOLID CURVE REPRESENTS THE MOST PROBABLE SPECTRUM BASED ON EXTRAPOLATED DATA. THE BROKEN LINES REPRESENT THE ESTIMATED UPPER AND LOWER LIMITS OF INTENSITY.

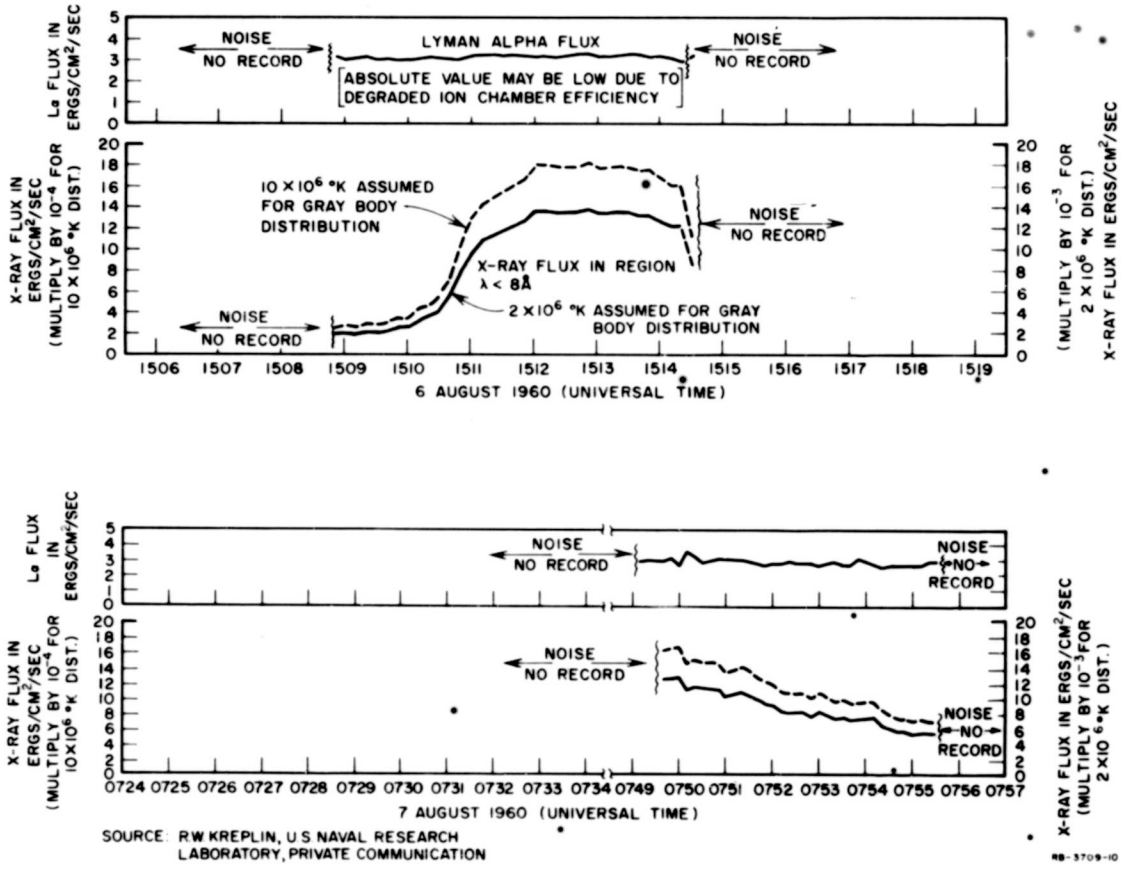


FIG. I-8 SHAPE OF 2-8 A X-RAY PULSE FOR TWO FLARES OBSERVED BY SOLAR SATELLITE ETA

fluxes and energies are presented in Table I-5. Calculations based on the assumption that the radiation is bremsstrahlung indicate that the source electrons have an energy distribution described by $N_e(E) = KE^{-\gamma}$ where gamma is usually 5 for long time-averages. A gamma of 7 was found to be a good fit for the auroral peak measurement denoted by A in the table. Actually the observed X-ray spectra cannot be described by assuming a simple exponential distribution of source electrons. However, more accurate calculations apparently have not been made.

There seem to be some differences between the observations made in the auroral and subauroral zones: (1) a harder component in the subauroral measurements; and (2) little or no background X-radiation in the subauroral region, whereas a sporadic flux has been observed for long periods in the auroral zone.

The X-ray pulse durations seem to vary considerably in both zones, from tenths of seconds (with rise times of ~ 0.01 sec) to hours. Correlations of bursts with geophysical events indicate that they usually accompany geomagnetic disturbances, visible auroral emissions, and radio absorption. However, the correlations are loose*--this may well be due to limitations in observational programs. For example, the bremsstrahlung sources seem to be typically of small areal extent; and whereas the flux measurements are made from balloons, the other measurements are typically made from fixed ground stations some distance away from the balloons. If the events are localized (as they seem to be), measurements of other parameters, particularly of radio absorption, must be made near the same point that the X-ray measurements are made.

An example of records obtained from these balloon observations is presented in Fig. I-9.

---

*Rather tight for subauroral zone auroras but loose for auroral zone auroras.

Table I-5

OBSERVED AURORAL AND SUBAURORAL X-RADIATION

A. From Bhavsar (1961)[24]

Photon Energy (kev)	> 22	> 35	>55	> 265	
Photons/cm^2 sec	539	48	19	6	(0835 UT, peak of aurora)
	72	25	13	1	(Avg 0805 to 0925, duration of aurora)

Notes:

Meas. at depth of 10 g/cm^2 near Minneapolis on 5/17/59.
Estimated electron flux (>22 kev) to produce the observed bremsstrahlung is $\sim 10^9/cm^2$ sec at peak and $\sim 10^{12}/cm^2$ for total period.

B. From Anderson and Enemark (1960)[23]

1. Photon Energy (kev) 25-40 40-90 100-300
   Photon Intensity cm^{-2} sec^{-1} 974 260 2

Notes:

Meas. on Aug. 16, 1959 at Fort Churchill.
Corrected to zero atmospheric depth.
Estimated peak electron flux (>50 kev) 4 x 10^6 to 6 x $10^7/cm^2$ sec (Brown 1961) daily avg flux 6 x $10^{10}/cm^2$.

2.

Photon energy (kev)	> 45	> 85	>170	> 380	
Counts per sec	220	85	5	bckgnd	1930 UT
	80	35	bckgnd	bckgnd	0300 UT

Notes:

Meas. at Fairbanks 15-16 April 1959.
Data are for peaks of two prominent bursts.
Observational data, uncorrected.

3.

Photon energy (kev)	> 34	>60	> 150	> 300	
Counts per sec	32	12	bckgnd	bckgnd	1630 UT
	36	12	bckgnd	bckgnd	2015 UT

Notes:

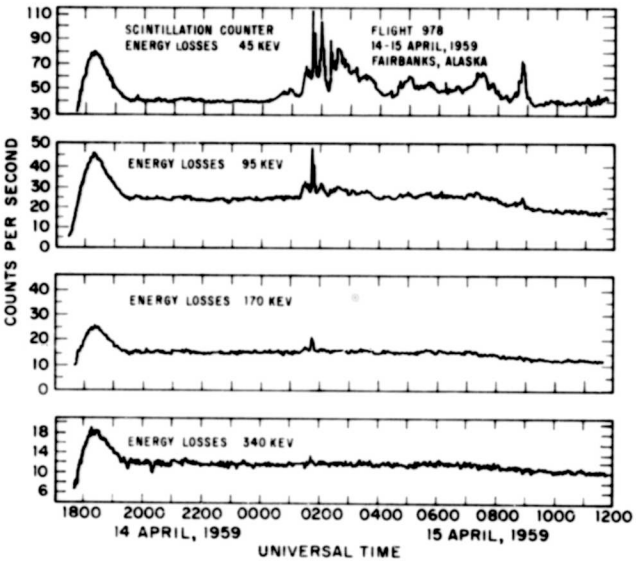
Meas. made at Fort Churchill Aug. 8, 1959.
Data are for peaks of two prominent bursts.
Observational data, uncorrected.

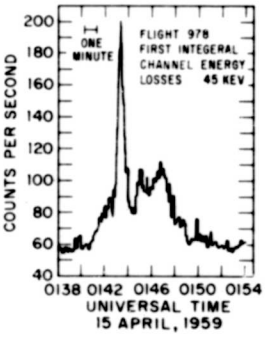
4.

Photon energy (kev)	> 25	> 40	> 100	> 300	
Counts per sec	180	120	10	bckgnd	1310 UT
	50	20	bckgnd	bckgnd	1410 UT
	240	170	6	bckgnd	1730 UT

Notes:

Meas. at Fort Churchill Aug. 16, 1959.
Data are for peaks of three prominent bursts.
Observational data, uncorrected.





SOURCE ANDERSON, K.A., J. GEOPHYS. RES. 65, 554 (1960)

FIG. I-9 AN EXAMPLE OF AURORAL BREMSSTRAHLUNG OBSERVATIONS

d. Proton-γ Reactions

The presence of photons resulting from p, γ reactions between solar protons and atmospheric nuclei has been observed by Bhavsar.[24] The following data from Bhavsar compares fluxes and energies of this gamma radiation with bremsstrahlung.

	Photon Energy (kev)	>22	>35	>55	>263
Peak of aurora	γ-ray photons (cm^{-2} sec^{-1})	54	47	24	11
	Bremsstrahlung photons	539	48	19	6
1 hr 20 min average	γ-ray	43	37	19	9
	Bremsstrahlung	72	25	13	1

2. Particles

a. Electrons from Solar Activity

The flux of particles from the sun is apparently divided into two parts. One is the normal flux or solar wind, whereas the other is the flux associated with solar surface events and especially flares.

The solar wind is a plasma which is the outer extension of the corona. Its motion is essentially diffusional. The proton component is believed to have a density of about $10^3/cm^3$ (or less) near the earth's orbit and the proton velocity is believed to be of the order of 10^8 cm/sec. Since to maintain electrical neutrality, both the concentration and the flux of electrons must be similar to the proton values, the electrons must have similar velocities. This means that the electrons are in the energy range 1 to 10 ev and carry less than 0.1% of the energy. This in turn means that no great charge separation can occur as the retarding potentials would quickly reach 1 to 10 volts. Effects due to solar wind electrons are therefore probably negligible. However, the plasma must necessarily cause losses in deep space radio communications.

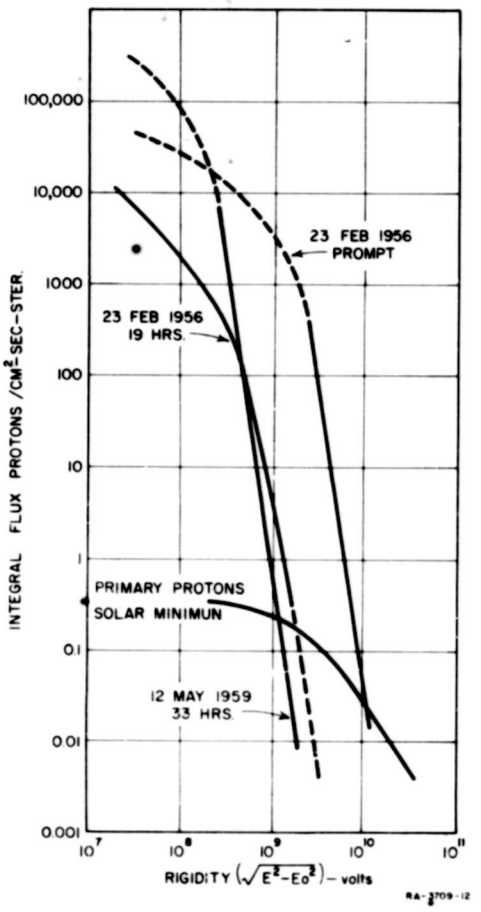
The particle fluxes from solar flares are so large that it appears impossible for charge separation to be extensive. However, no effects of energetic electrons have been detected. It appears likely in this case also that electrons carry only a minor fraction of the energy. It seems possible that electrons have energies up to about 1 Mev, in which case their range would be less than 1 g/cm^2 and most of the ionization caused by them would be in the D-layer or higher, if they reach the atmosphere. However, solar electrons would be geomagnetically trapped if they impinged on the Van Allen belt regions at suitable angles. Subsequent leakage into the auroral zones was thought to be an important aurora-producing process. Recent observations, however, show that insufficient energy is available in the radiation belts to account for auroras.

b. Flare Ejected Protons

The small fraction of solar flares that are accompanied by polar proton events occur with a frequency of the order of one per month during the more active portions of the sunspot cycle. Most of them cause no direct ionization at sea level. Exceptional events, perhaps one every five years, produce sea level ionization. Protons are the main detectable particle constituent of flares.

Flares are large eruptions of plasma from the surface of the sun. It is now believed that the plasma carries magnetic lines of force with it into interplanetary space and these extend back to the sun. It is believed that these lines cause geomagnetic storms about one day after the flare is seen.

A good summary of data on solar flare protons is given by Winckler.[26] Figure I-10 shows the energy distribution of protons from a normal flare (12 May 1959) and an exceptional flare (23 February 1956). It is noted that the exceptional flare has many more protons at high energies. (Note that the abscissa is the "rigidity" which is related to the energy as shown in the caption. The ordinate shows integral flux, i.e., particles of that energy or more.) The decay of the exceptional flare is also shown.



SOURCE: WINCKLER, J.R., RADIATION RESEARCH 14, 521 (1961) FIG 3

FIG. I-10 ENERGY DISTRIBUTION OF PROTONS FROM A SOLAR FLARE

Protons from exceptional flares are detected simultaneously with visual observation of the flare; protons from ordinary flares are detected about one hour after the flare is seen, and arrive nearly isotropically. In both cases, the proton intensity drops as the square of the time after the first hour of observation. Thus most of the ionization caused by flares comes in the first hour.

Winkler estimates that the total energy deposition from ordinary flares is of the order of 10 to 40 rads and from exceptional flares as much as 1000 rads. One rad corresponds to 1.9×10^{12} ionizations per gram. This will represent the total number of ion pairs formed in the outermost atmosphere. At lower depths it is necessary to consider: (1) the reduction in the number of protons due to the stopping of the less energetic ones, and (2) the recombination of ions which takes place during deposition. The calculation is fairly complicated but it can be performed by computers as adequate data are available. For all except the most energetic protons this ionization is stongest near the magnetic poles.

c. Solar Wind Protons

It was first suggested by L. Biermann[27] that there exists a steady radial stream of protons from the sun. The evidence[27] for this was the "blowing aside" of comet tails in the solar system with forces greater than those due to radiation pressure alone. The calculations indicated that the proton stream must consist of at least 200 protons/cm^3 with energies of about one or two kev at one A.U. from the sun. Later theoretical calculations on solar dynamics,[28,29] based upon different models, also predict the existence of such a "solar wind" of protons. These protons must actually be in a neutral plasma in order to conserve charge neutrality, and this plasma probably has magnetic fields "frozen" into it which originated at the sun.[29] A further observation which supports this order of magnitude estimate of the solar wind is the diurnal variation of the latitude of aurorae.[30] This variation is shown to agree well in magnitude and phase with what would be expected from the day-side compression of the geomagnetic field by the pressure of the solar wind; and satellite measurements of the shape of the Van Allen bands support this hypothesis. It has been suggested[31] that the aurora is actually caused by solar wind protons which find their way into the geomagnetic field at the neutral point where the geomagnetic field meets the interplanetary magnetic field. Other theories have generally hypothesized some kind of turbulence as allowing the entrance of the solar plasma with consequent Fermi acceleration in the geomagnetic field.

Measurements[32] of the intensity of the Lyman lines from interplanetary hydrogen have led to an estimate of the interplanetary electron density as under 45 e/cm^3, and this is difficult to reconcile with the electron density which is associated with the plasma of the solar wind. Measurements of the polarization of the zodiacal light[33] will only fit an interplanetary electron density of about 20/cm^3. These contradictory data concerning the quiescent electron density of space pose a serious question about the magnitude of the solar wind which has not yet been answered.

d. Neutrons and Heavy Ions in Solar Radiation

There is little evidence regarding the presence of neutrons and heavy ions in radiation of solar origin. Freden[34] has reported that the neutron flux as measured by BF_3 counters on Atlas missiles is enhanced at the time of a large solar storm (but this may be due to p,n reactions in the atmosphere). No ionization effects due to these components of the solar radiation have been reported. He, C, N, O, and F nuclei from flares have been measured by several balloon and rocket experiments (July 1959 and November 1960).

C. The Van Allen Radiation Belts

There exists a region of radiation intensity orders of magnitude greater than that of cosmic rays in the altitude range from 4000 km to 90,000 km. This radiation is now known to consist of protons and electrons which are magnetically constrained to the region by the geomagnetic field. The discoverer of the bands of radiation is J. A. Van Allen, who first reported them in May 1958 as a result of measurements taken aboard the U.S. Satellites 1958 alpha and gamma.[35] Figure I-11 shows these radiation regions in meridian section, the particle fluxes being 1.9 times the counting rates on the contours. (Fluxes are in (cm^2 sec 4π sr)$^{-1}$.)

In the last three years extensive measurements of these trapped particle fluxes have been made by many investigators using different types of radiation detectors. These experiments have shown that there are actually two* distinct zones of trapped particles which appear to meet at about 18,000 km from the center of the earth. The inner zone consists of protons with energies from 5 Mev to 700 Mev and electrons

* Very recent explorations have changed this concept to one of several bands or one large band with considerable structure.

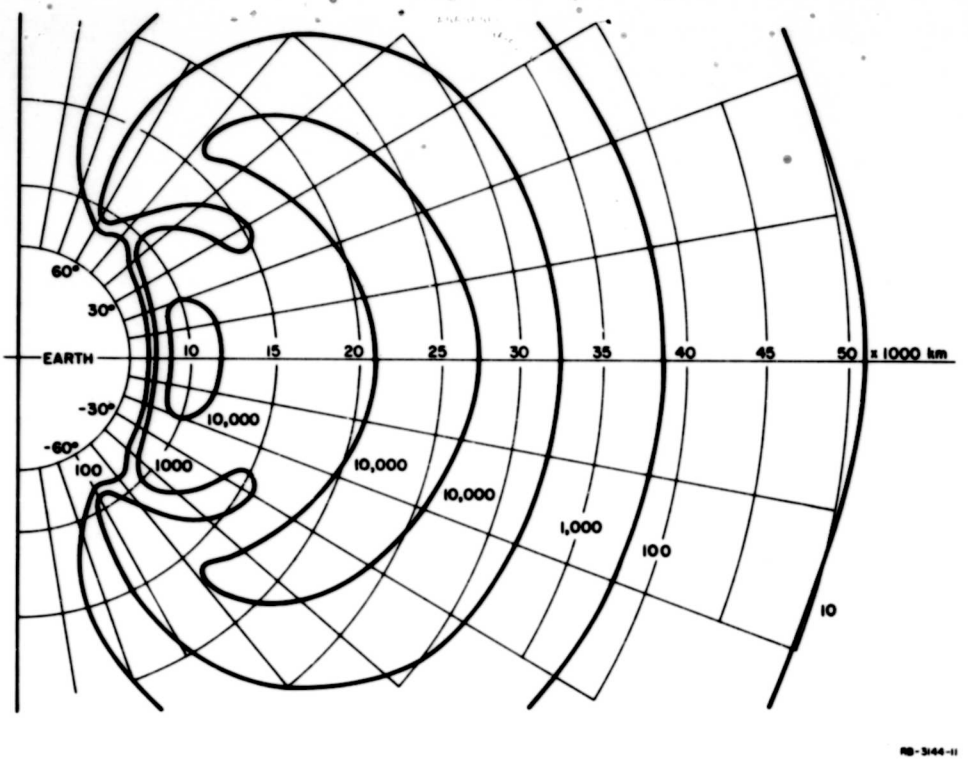


FIG. I-11 THE VAN ALLEN BANDS
IN MERIDIAN SECTION

with energies from below 20 kev to an upper limit of 800 kev. The outer zone appears to consist mainly of electrons of about the same energy as the inner zone electrons. The spectrum of inner zone protons as measured by nuclear emulsions flown on Atlas rockets is shown for high energies[36] in Fig. I-12 where the ordinate is in omnidirection proton flux (Mev cm^2 sec)$^{-1}$.

Although the spectra of both the belt protons and electrons are reasonably well known, and the intensity of the protons is agreed upon, there appears to be a certain margin for disagreement upon the absolute intensity of the electrons in both inner and outer bands. A comparison of the results of several experiments[37] leads to an estimate of about 10^{12} electrons/m^2 sec 4π sr above 30 kev in the outer band. A reasonable estimate[38] of the electron flux above 180 kev in the inner band is 10^{11} electrons/m^2 sec 4π sr.

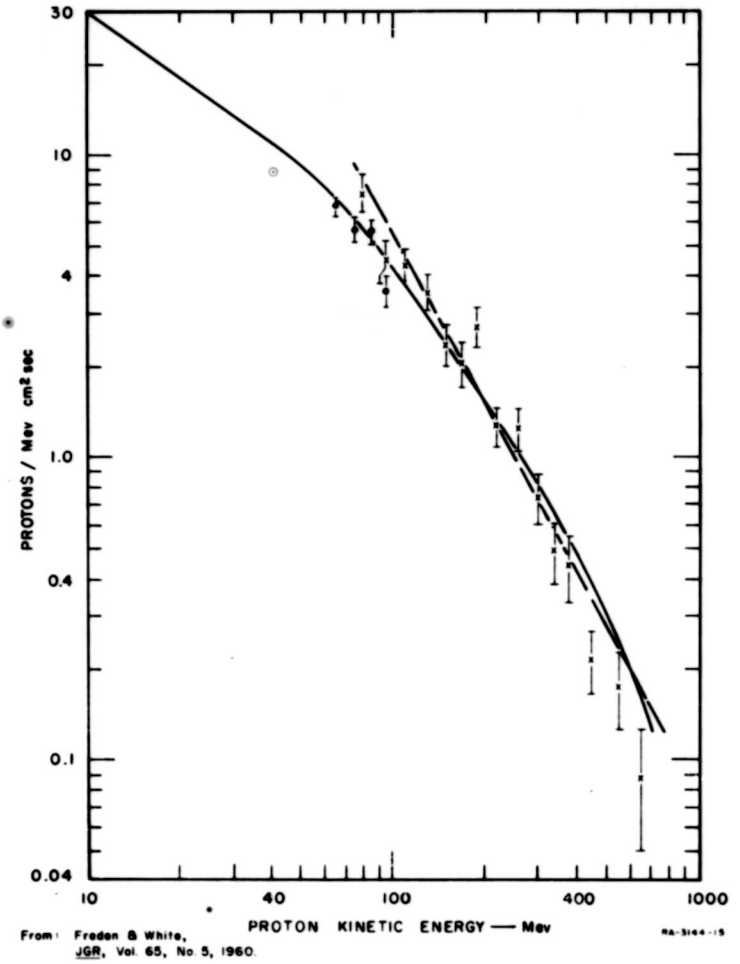


FIG. I-12 SPECTRUM OF PROTONS IN INNER BELT

Most of these estimates of intensities are only approximate because the shape and intensities of the trapped particle zones have been observed to change with solar activity. This is particularly noticeable for the outer zone which can change by orders of magnitude during a solar storm.[39]

Figure I-13 shows three passes of Explorer VI through the outer Van Allen bands, respectively at the beginning of a storm, 24 hours later, and 48 hours later.

The interaction of the Van Allen radiation and solar activity is currently among the most interesting problems of space physics. It seems almost certain at this time that some of the electrons, at least, find their way into the Van Allen bands from solar plasma streams. The problem is rendered complex by the interaction of the geomagnetic field with solar plasma clouds and the solar wind. When the geomagnetic "bubble" (of magnetic field) is either compressed or expanded, it is possible that this changes the energy spectra of the Van Allen particles. Such a change would appear to simple counters as an increase or decrease of particle density, due to the steep dependence on energy of most of these spectra. However, as mentioned in the discussion on the solar wind, it has been shown possible for particles either to leak into the geomagnetic field at its neutral points where it meets the interplanetary magnetic field, or to leak in at the region of disordered fields next to the interface with the solar wind. This problem is also closely related to the origin of the protons and electrons which cause aurora, since the particular changes observed in Fig. I-13 were observed to correlate in time with the appearance of a large low latitude aurora.[39] Unfortunately, all aurora cannot be so correlated; many investigators believe the auroral particles were never geomagnetically bound.

Only the origin of most of the protons in the inner band seems to be fairly well explained.[38] These protons apparently come from the decay of neutrons which are produced in the atmosphere by cosmic rays. Calculated spectra agree well with experiments, but even this explanation for the protons fails to show conclusively that the electrons from these beta-decaying neutrons constitute the major part of the electron content of the Van Allen bands.[40] The solution to the problem of the origin of the Van Allen electrons must still await more complete information on the relation of the band to solar phenomena.

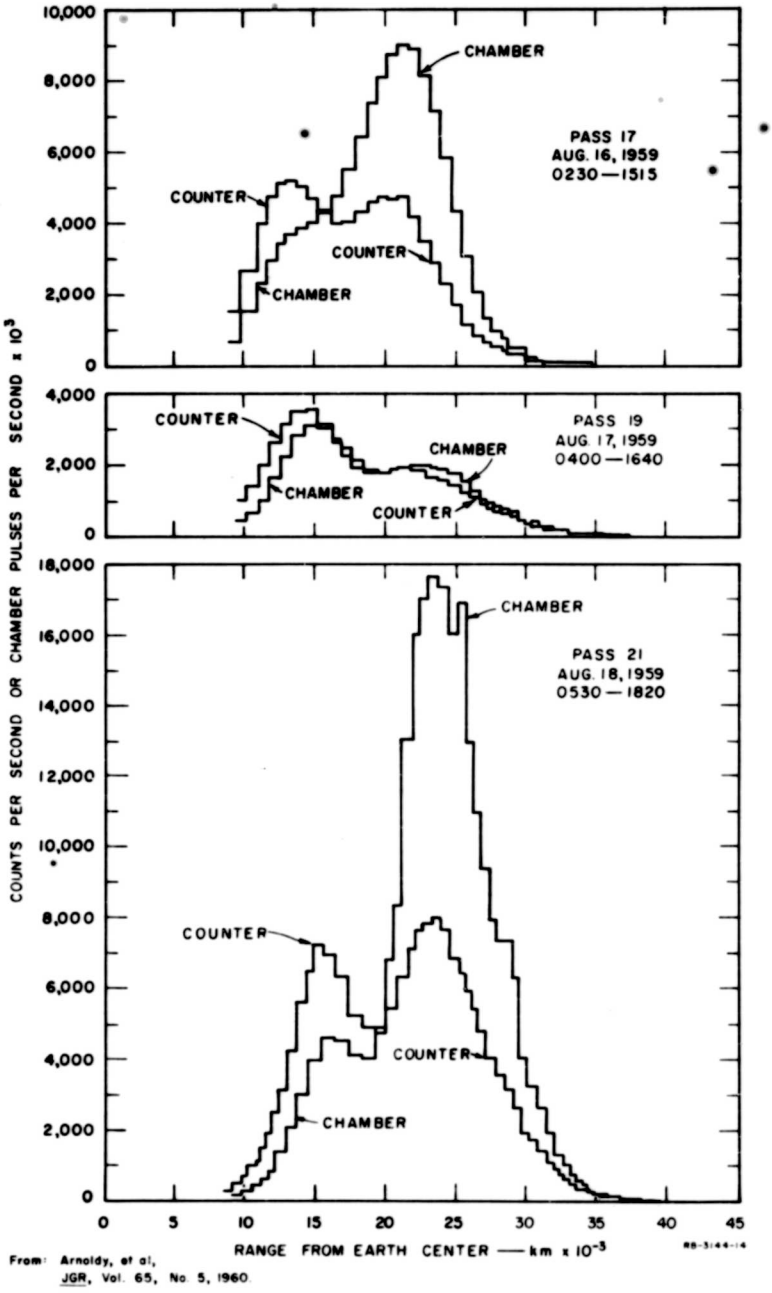


FIG. I-13 CHANGES IN OUTER VAN ALLEN BAND DURING A SOLAR STORM

REFERENCES

1. Report of the Conference of Experts to Study the Possibility of Detecting Violations of a Possible Agreement on the Suspension of Nuclear Tests. United Nations General Assembly Document A13897 (28 August 1958)

2. Effects of Atomic Explosions on Weather. Atomic Energy, Vol. 2, No. 2, Science Publication Association, Peking, China (April 1957). Translation from Chinese available as Air Intelligence Information Report 1162011

3. Martell, E. A. Atmospheric Aspects of Sr-90 Fallout. Science 129, 1197-1205 (1959)

4. Smithsonian Physical Tables (Smithsonian Institution, Washington, D.C., ninth revised edition, 1954)

5. Welch, J. A. Jr., and W. A. Whitaker. Theory of Geomagnetically Trapped Electrons from an Artificial Source. J. Geophys. Res. 64, 909 (1959)

6. Allen, L., Jr., J. L. Beavers II, W. A. Whitaker, J. A. Welch, and R. B. Walton. Ibid, p. 893

7. Hunter, H. F. and N. E. Ballou. Fission-Product Decay Rates. Nucleonics 9, No. 5 C-2 (1951)

8. McMaster, W. Lawrence Radiation Laboratory, Livermore. Private communication.

9. Hess, W. N. The Radiation Belt Produced by Neutrons Leaking Out of the Atmosphere of the Earth. J. Geophys. Res. 65, 3107 (1960)

10. Crain, C. M. and P. Tamarkin. A Note on the Cause of Sudden Ionization Anomalies in Regions Remote from High-Altitude Nuclear Bursts. J. Geophys. Res. 66, 35 (1961)

11. Elwert, G. Theory of X-ray Emission of the Sun. J. Geophys. Res. 66, 391 (1961)

12. Kazachevskaya, T. V. and G. S. Ivanov-Kholodnyi. Continuous Solar Emission in the X-ray Region. Soviet Astronomy 3, 937 (1960)

13. Byram, E. T., T. A. Chubb, and H. Friedman. The Solar X-ray Spectrum and Density of the Upper Atmosphere. J. Geophys. Res. 61, 251 (1956)

14. Chubb, T. A., H. Friedman, and R. W. Kreplin. X-ray Emission Accompanying Solar Flares and Non-flare Sunspot Maximum Conditions. Space Research, ed. by H. Kallmann, North-Holland Publishing Co., Amsterdam (1960)

15. Friedman, H., T. A. Chubb, J. E. Kupperian, Jr., and J. C. Lindsay. X-ray and Ultraviolet Emission of Solar Flares. IGY Rocket Report Series, No. 1 (30 July 1958)

16. Kreplin, R. W. Solar X-rays. Annales de Geophysique, Tome 17, No. 2, p 151 (1961)

17. Whitten, R. C. and I. G. Poppoff. The Possible Role of Solar X-rays in the Formation of the Normal D-region. To be published.

18. Peterson, L. E. and J. R. Winckler. Gamma-Ray Burst from a Solar Flare. J. Geophys. Res. 64, 697 (1959)

19. de Jager, C. The X-radiation of the Sun. Space Research, Proc. of the First International Space Science Symposium, Nice, 1960 (North-Holland Publishing Co., Amsterdam, 1960)

20. Poppoff, I. G. and R. C. Whitten. The Shape of a Solar Flare X-ray Pulse. Unpublished work.

21. Winckler, J. R., T. C. May and A. J. Mosley. Observation of a Solar Bremsstrahlung Burst at 1926 UT, August 11, 1960. J. Geophys. Res. 66, 316 (1961)

22. Anderson, K. A. Balloon Observations in the Auroral Zone I. J. Geophys. Res. 65, 551 (1960)

23. Anderson, K. A. and D. C. Enemark. Balloon Observations of X-rays in the Auroral Zone II. J. Geophys. Res. 65, 3521 (1960)

24. Bhavsar, P. D. Scintillation-Counter Observations of Auroral X-rays During the Geomagnetic Storm of May 12, 1959. J. Geophys. Res. 66, 679 (1961)

25. Brown, R. R. Balloon Observations of Auroral-Zone X-rays. J. Geophys. Res. 66, 1379 (1961)

26. Winckler, J. R. Primary Cosmic Rays. Radiation Res. 14, 521 (1961)

27. Biermann, L. The Tail of Halley's Comet in 1910. Z. Naturforsch. 7a, 127 (1952)

28. Parker, E. N. Suprathermal Particle Generation in the Solar Corona. Astrophys. J. 128, 677 (1958)

29. Chamberlain, J. W. Properties of the Interplanetary Gas. J. Geophys. Res. 65, 2481 (1960)

30. Liemohn, H. The Outer Radiation Belt and Aurorae. Nature 188, 394 (1960)

31. Dungey, J. W. Interplanetary Magnetic Field and the Auroral Zones. Phys. Rev. Lett. 6, 47 (1961)

32. Friedman, H. Rocket Observations of the Ionosphere. Proc. IRE 47, 272 (1959)

33. Blackwell, D. W. Interplanetary Electron Densities. Paper presented at 41st Annual Mtg. Amer. Geophys. Union, Washington, D.C. April 27-30, 1960

34. Freden, S. C. Space Research at the Lawrence Radiation Laboratory. J. Geophys. Res. 66, 1554 (1961)

35. Van Allen, J. A., G. H. Ludwig, E. C. Ray, and C. E. McIlwain. Observation of High Intensity Radiation by Satellites 1958 Alpha and Gamma. Jet Propulsion 28, 588 (1958)

36. Freden, S. C. and R. S. White. Particle Fluxes in the Inner Radiation Belt. J. Geophys. Res. 65, 1377 (1960)

37. Dessler, A. J. Discussion of paper by R. L. Arnoldy, R. A. Hoffman, and J. R. Winckler. Observations of the Van Allen Radiation Regions During August and September 1959, Part 1. J. Geophys. Res. 65, 3487 (1960)

38. Hess, W. N. The Radiation Belt Produced by Neutrons Leaking out of the Atmosphere of the Earth. J. Geophys. Res. 65, 3107 (1960)

39. Arnoldy, R. L., R. A. Hoffman, and J. R. Winkler. Observations of the Van Allen Radiation Regions During August and September 1959, Part 1. J. Geophys. Res. 65, 1361 (1960)

40. Walt, M. and W. M. MacDonald. Energy Spectrum of Electrons Trapped in the Geomagnetic Field. J. Geophys. Res. 66, 2047 (1961)

Note (to Section A 2b).

A more complete analysis and interpretation of the Jason rocket data was recently published by Cladis and Walt (Final Report, Analysis of Jason Data. SWC TR 61-82, Lockheed Missiles and Space Division, Contract No. AF 29(601) 2862, October 1961.) The hypothesis of trapped fission fragments is supported to some degree by the new evidence. Walt (private communication), however, feels that it is unlikely that fission fragments are themselves trapped, even though he believes the decay of Argus electrons is controlled by decay of fission fragments and not by scattering losses of trapped electrons. The experimental evidence seems insufficient to support or contradict a trapped fission fragment hypothesis.

II GEOPHYSICAL PHENOMENA CAUSED BY IONIZING RADIATIONS

A. Aurora

1. Optical

Auroras are extremely complicated. As they are natural phenomena we have scant control of the variables that govern their character. This necessitates either a "case history" discussion of a specific aurora or a statistical description of a general group of auroras. This description should include their morphology, their development in time, an enumeration of the specific radiating systems, and their associated ionization. As complete a description as is presently possible and a thorough discussion of auroral phenomena may be found in recent reviews by Bates,[1,2] and by Chamberlain and Meinel[3].

There are two parts to an understanding of visual auroral phenomena: the characteristics of the incident charged flux, and the characteristics of its interaction with the upper atmosphere.

Auroras are produced by the interaction of energetically charged particles with the upper atmosphere, predominantly in the 100-200 km region. The impinging charged particles often are confined to sharp beams which excite well-defined regions of the atmosphere and produce distinct auroral features. A very bright aurora (with an international brightness coefficient* of IV) of 5,000 kilorayleighs (5×10^{12} photons/cm^2 sec) is equal to the illumination of the full moon. The character of the radiation depends upon the composition of both the upper atmosphere and the exciting particle flux. It is not surprising that the predominant radiation consists mostly of molecular nitrogen and oxygen bands with conspicuous, sharp features due to atomic oxygen and nitrogen since this reflects the composition of the auroral region of the atmosphere. Because the mean density at auroral heights is low (less than 10^{-3}mm Hg), deactivating collisions are rare and much forbidden radiation is observed. Atomic hydrogen lines appear which are broadened and shifted by the Doppler effect indicating that protons are part of the exciting flux striking the upper atmosphere. To penetrate to the 100-km level these protons must have approximately 100 kev of energy and in dissipating this energy they will

* International brightness coefficient (IBC) is defined in terms of the green (5577 A) oxygen line. IBC: I = 1 kilorayleigh (kR), II = 10 kR, III = 100 kR, and IV = 1000 kR.

produce many secondary electrons and ions. These, along with those originally in the incident particle stream, will produce further excitation of atmospheric constituents. However, it is now believed that only rather rare auroras are primarily excited by protons; the majority are caused by the energetic (≈ 4-10 kev) electron component of the incident flux.

The detailed processes by which the observed radiation is excited are not well known: (1) because of the limited measurements of excitation functions of atmospheric gases by protons and electrons over a wide range of energy; (2) because of the unknown composition and energy distribution of the incident beam; and (3) because of the unknown changes in the composition and energy distribution of the flux as it penetrates the earth's atmosphere. Work is in progress to measure the necessary excitation functions and, with new techniques, should be successful. Satellite experiments are planned to measure directly the nature of the incident beam at the top of the atmosphere. Computer programs are being written to calculate the changes in the exciting particle flux as it penetrates the atmosphere although more inelastic scattering data are necessary. Hopefully, altitude luminosity curves for defined auroral features will also be obtained either to supplement or to check the calculation program and the experimental parameters fed into it.

The morphology and time variation of the aurora are determined by the distribution and time variation of the incident particles penetrating the atmosphere. Certainly the earth's magnetic field influences the spatial extent of the exciting flux (auroral arcs lie along circles of magnetic latitude, etc.) and probably its energy distribution. The time variation of the source of the exciting particles is reflected by auroras. However, since these particles may have been stored in current belts about the earth, auroral phenomena may be related to the characteristics of these belts, such as their stability and density, which in turn are dependent upon other factors (such as sun spot activity, etc.).

2. Radio Reflection and Transmission

a. Introduction

In addition to its visible emissions, the aurora has the ability

to reflect or scatter radio waves and to influence the propagation of radio waves between, for example, the earth and the moon. Attention is directed here to the reflection and transmission of radio waves at frequencies of about 100 to 1000 Mc.

b. Reflection

For more than a decade, it has been known that the aurora is capable of reflecting or scattering a radio wave back to the earth at frequencies above 30 Mc, where direct reflection back from the ionosphere is not normally expected.[4]

The echoes fluctuate randomly at a rapid rate of the order of a few hundred cycles per second at 100 Mc, at least an order of magnitude faster than any other ionospheric echo. The echoes occur coincidently with geomagnetic disturbances, and statistics of auroral echoes agree with statistics of the visible aurora. An individual auroral echo is not necessarily accompanied by visible light, although at least some auroral light is usually observed.

Early in these studies, it was found that the earth's magnetic field plays an important role in the reflection process.[5,6] Echoes are possible at 30 Mc only when the exploring radio ray is directed no more than 20 degrees from the normal to the earth's magnetic field lines; this angle is even smaller at higher frequencies. Thus, at Arctic latitudes, echoes are not obtainable from aurorae appearing in the zenith, but are most readily observed about 700 km magnetically north of the station at large zenith angles. This suggests that an auroral region consists of bundles of rod-shaped scatterers, each one aligned parallel to the earth's field lines and scattering most effectively at right angles to its long axis. Echoes from aurorae have been studied by Stanford Research Institute using 60- and 142-foot diameter parabolic antennas and high-power transmitters in a radar (single-station) configuration capable of measuring range, azimuth, elevation, and Doppler shift.

With this equipment, two types of echoes called "discrete" and "diffuse" are observed, having the following characteristics:

(1) Discrete:

(a) Nighttime occurrence--associated with visible aurorae.

(b) Position along a line parallel to a line of latitude (range a function of azimuth).

(c) Narrow elevation angle; by measuring simultaneously the slant range and elevation angle, the heights are found to be about 110 $\pm$ 30 km.

(d) Observed frequently by our Alaskan station but rarely by our Scotland station.

(2) Diffuse:

(a) Occurrence when the ionosphere is sunlit at times of disturbed magnetic conditions (aurorae might be present but not visible because of sunlight).

(b) Coverage of an extended area of the sky, about 1000 km in north-south and east-west extent.

(c) Occurrence in a narrow height stratum located at about 100 km height. If the elevation angle is changed, a corresponding change of range is noted.

If one assumes that simple reflection is taking place (i.e., the plasma frequency is equal to or greater than the radar operating frequency), an electron density of about 10^{15} per cubic centimeter is required, far exceeding the values calculated by considering ionizing reactions indicated by the optical emission. A more satisfactory theory is that in which Booker, Gartlein, and Nichols postulate a mildly scattering medium having irregularities ideally of the order of a wavelength, without the necessity of an enhanced mean electron density over that already present in the ionosphere.[5] Unfortunately, there are many parameters in this calculation, combinations of which can be varied without changing the resultant echo strength.

Based on observed echo strengths, a calculation of the "reflection coefficient" of a typical aurora reveals that less than one part in a

million of the energy striking the aurora is scattered backward in the direction of the receiver. Thus, the aurora, although capable of giving strong echoes on a sensitive radar, is quite transmissive to radio waves above about 100 Mc.

Doppler shift studies at 400 Mc have shown that the reflected energy can appear several kc away from the transmitted frequency. An east-to-west motion is observed before magnetic midnight and a west-to-east motion after midnight. The direction is related to the direction of the magnetic disturbance vector.

c. Transmission

A radio wave capable of penetrating the ionosphere (above 30 Mc, for example) is subject to several perturbing effects that occur normally, not requiring the presence of visible auroras.[7] Amplitude and angular "scintillation" effects are noted, similar to twinkling and poor seeing conditions at optical frequencies. Polarization twist is also experienced, due to the Faraday effect of free electrons in the presence of the earth's magnetic field, an effect not present in optical astronomy. When radio waves pass through the aurora, the scintillation effects increase by about one order of magnitude. Most of these experiments have involved the observation of extra-galactic point sources of radio noise by receivers located on the earth's surface.

A cooperative experiment between the Stanford Research Institute at College, Alaska, the Defence Research Telecommunications Establishment at Ottawa, and the M.I.T. Lincoln Laboratory at Boston was performed by transmitting a radio wave through the aurora and using the moon as a passive reflector to return the wave to the earth. The experiment was carried out during the winter of 1958-59. A continuous 440-Mc wave was transmitted from College, Alaska, using the 60-foot antenna beamed toward the moon. By comparing the signals received at Ottawa and Boston with observations of visible auroras in Alaska, several conclusions were reached:

1. The echo coming back from the moon fluctuates irregularly because the lunar surface is rough, and is changing its aspect

with respect to an observer on the earth. This "libration fading" normally occurs[2] at a rate of about one cycle per second at 400 Mc and is calculable. Occasionally the signal received showed fluctuation rates of twice this amount, which could be correlated with the presence of an aurora between the transmitter and the moon.

2. By integrating the signal for about one minute, one can make the system sensitive to changes of over-all system loss with an accuracy of about ± 25 percent. No aurorally associated loss of signal occurred equal to or greater than this value.[8] This observation is in agreement with the fact that even during intense overhead auroras the ionospheric absorption only rarely exceeds 10 db at 30 Mc (using the cosmic noise monitoring technique of Little and Leinbach[9]).

3. When a 10- to 1000-Mc radio wave travels through the ionosphere, the simultaneous presence of ionization and the geomagnetic field causes a linearly polarized wave to be twisted (clockwise looking toward the zenith in the Northern Hemisphere whether energy is being transmitted or received). Since the magnetic field of the earth can be considered known, this "Faraday rotation" can be used to study the ionization content of the ionosphere. The 440-Mc experiment showed increases in electron column density during auroras of the order of 10^{17} electrons per square meter. This represents an approximate doubling of the normal column density of the ionosphere above College, Alaska, and is equivalent to an electron density of 10^{6} per cubic centimeter in a layer 100 kilometers thick.

d. Conclusions

These observations show that in the 100- to 1000-Mc region the aurora appears as a region of weak scatterers, capable of reflecting a radio wave if correctly oriented but not extracting appreciable energy from the forward direction. Because of the large volumes present, strong echoes are nevertheless attainable with moderate-powered equipment.

B. Auroral Zone and Polar Cap Absorption

Absorption events as observed at high latitudes, by riometers monitoring cosmic noise sources, are mainly of two kinds. These are now generally termed "polar cap absorption" and "auroral absorption." The auroral type of absorption is irregular, fluctuating, and well correlated with the occurrence of visible aurora and geomagnetic micropulsations; its onset often accompanies the sudden commencement of a magnetic storm; and its secular variation is not simply related to the solar cycle.[10] There seems little doubt that auroral absorption is due to ionization caused by primary electrons having energies of about 10 kev or more, and secondary bremsstrahlung X-rays.

Polar cap absorption, although only recently identified and relatively little studied, is probably a less complicated phenomenon than auroral absorption. The absorption in a polar cap event occurs over much of the polar regions. The onset is usually within a few hours after the occurrence of a large solar flare, and on riometer records the absorption is represented (after an initial large pulse and before the sudden commencement phase) by a smooth, persistent variation, more pronounced (because of photodetachment effects) by day than by night. It is generally agreed that the origin of a polar cap absorption is in high energy (10-100 Mev) protons which are emitted during large solar flares. There is probably a simultaneous generation of a plasma cloud in which widely differing energies are represented, but the higher energy particles escape ahead in an expansion during the travel through interplanetary space.[11] The density of the high-energy proton flux is small so that there is little modification to the existing geomagnetic field, but calculations[12] show that a flux of 10-Mev protons of only 90 cm^{-2} sec^{-1}, or a density of 2×10^{-8} cm^{-3} in an incoming stream, is sufficient to explain the absorption events.

It would be anticipated that since the protons of highest energies should arrive first of all, and because the momentum cutoff relation for cosmic rays (momentum $\approx 15 \cos^4 \lambda$ Bev/c, where λ is the latitude and c the velocity of light) is operative, then initially effects should be observed at the lower latitudes, subsequently receding towards the magnetic poles. However, the evidence is insufficiently complete for any general pattern in polar cap events to have been established. Protons of the energies indicated above are sufficiently energetic to penetrate to heights of 70 km and lower. They are thus able to produce ionization at levels where the electron collisional frequency is large; in consequence, the absorption is intense.

To calculate the ionization created by the high energy particle flux it is necessary to know:

1. The particle species flux
2. Their energy spectra and entrance angle
3. The composition of the upper atmosphere
4. The rate of energy loss of the particles
5. The energy required to produce an ion pair
6. The equilibrium density of the electrons created in the upper atmosphere.

The species of the high energy flux have not yet been adequately determined.[13] They are assumed to be dominantly protons,[14] however, some He^+ and other ions known to exist in the solar gas have been observed.[14,15,16] (Anderson et al.[16] determined the upper limit to abundances for neutrons, alphas, protons, photons, and electrons in the high energy solar flux for the flare of 23 August 1958). Undoubtedly it is true that the composition of the high energy particle flux will depend strongly upon the ion production and acceleration mechanism associated with each individual flare; thus, relative species concentrations should vary widely for different classes of flares.[13,15]

Obayashi and Hakura[11] have reviewed the state of our knowledge of polar ionospheric disturbances and solar corpuscular emissions. Their

plot of the observed integral spectrum of interplanetary protons is presented in Fig. II-1. Additional data reported by Winckler et al. have been added to the figure (as discussed in the figure caption). Except in a few cases, the integral spectra for polar cap proton fluxes are not known for the low energies (< 10 Mev) for strong flares. A linear extrapolation of the high energy spectrum observed at surface or near the surface of the earth undoubtedly overestimates the low energy flux. Satellite experiments, being conducted by Van Allen et al. in his Injun satellite will aid in determining the characteristic shapes of the integral energy spectra for auroral particles.[13] (See, for example, Astronautics, August 1961, page 8.) The S-3 satellite has measured the spectra of higher energy particles.

The composition of the upper atmosphere is still poorly known as a function of altitude. A model that should be satisfactory for the calculations outlined has been presented by Cook and Lorents[18] in their study of the "Electron Collision Frequencies and Scattering Cross Sections in the Ionosphere." This same report discusses the effective collision frequency and conductivity of the ionosphere.

Knowing (1), (2), and (3), the electron production rate, q(H), can be calculated as a function of height, (H), from the expression

$$q(H)\ \frac{\text{electrons}}{\text{cm}^3\text{-sec}} = \frac{1}{W(H)} \int_{\Omega} \int_{E_{min}}^{D} Y(E,H)\ \frac{dE}{dx}(H)\ \rho(H)\,dE\,d\Omega.$$

where

Ω = entrance angle of a given particle

$W(H)$ = energy required to create an ion pair

$Y(E,H)$ = differential energy spectra of the incident particle (proton) flux at H

$\frac{dE}{dx}(H)$ = rate of energy loss of the particles in the atmosphere at height H

$\rho(H)$ = density of the atmosphere at H

The electron equilibrium density can next be calculated using the usual ionospheric reaction rate equations for day or night conditions. (Bowhill's

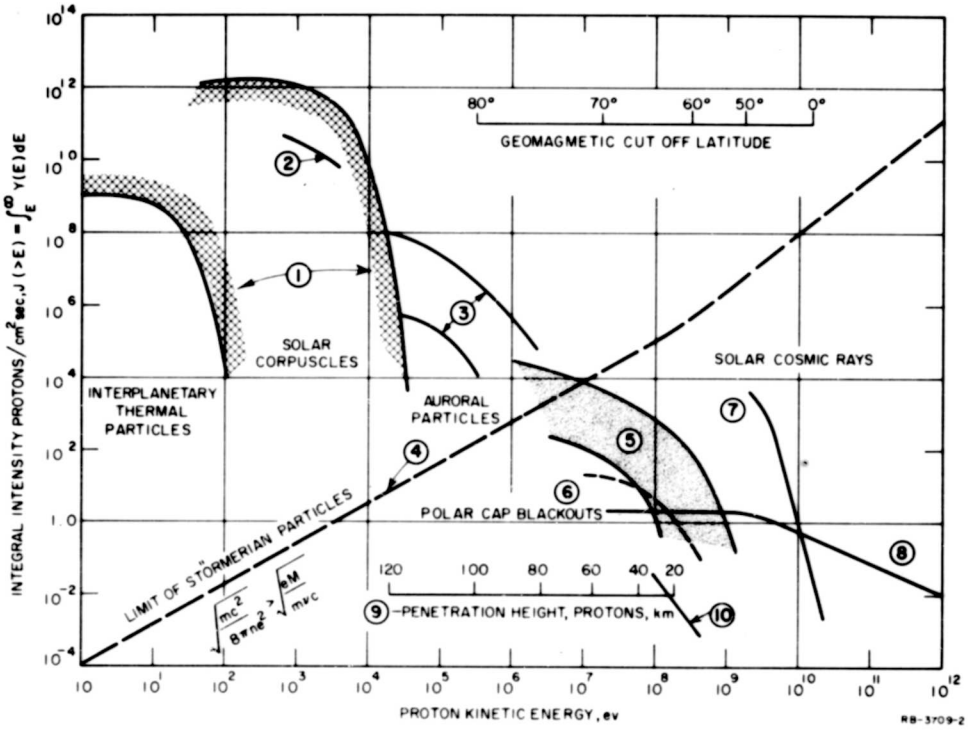


FIG. II-1 INTEGRAL SPECTRUM OF INTERPLANETARY PARTICLES

Figure II-1, Integral Spectrum of Interplanetary Particles; curve references are as follows:

1. Solar corpuscles, discussed by Obayashi and Hakura. Upper curve, $T = 10^7\,^\circ K$, $n = 10^5$, lower curve $T = 10^5\,^\circ K$, $n = 10^3$. A solar flare point was presented at an integral intensity of 10^{14} protons/cm^2 sec, $T = 10^7\,^\circ K$, $n = 10^7$.

2. Electrons estimated from aurora.

3. Auroral particles. See:
   C. E. McIlwain, J.G.R. 65, 2727 (1960)
   Proton and electron fluxes measured by rockets
   J. W. Chamberlain, Astrophys. J. 120, 360 (1954)
   Dappler shift measured for incoming particles.
   J. A. Van Allen, I.G.Y. Rept. 1, 159 (1958)
   Rocket measurements

4. Störmerian limit, Obayashi and Hakura.

5. Polar Cap blackouts.
   E. P. Ney, J. R. Winckler and P. S. Freier, Phys. Rev. Letters, 3, 183 (1959).
   Ion chambers, Geiger and scintillation counters and emulsions exposed above Minneapolis at a pressure altitude of $10 g/cm^2$, March 26, 1958.
   J. R. Winckler, Bull. Am. Phys. Soc. 4, 238 (1959). Further balloon measurements.

6. J. R. Winckler, P. D. Bhavsar, A. J. Masley, T. C. May, Phys. Rev. Letters 6, 488 (1961).
   Discusses measurements made on Sept. 3, 1960 flare by balloons and terrestrial equipment at various geographical locations.

7. R. Lüst and J. A. Simpson, Phys. Rev. 108, 1563 (1957)
   The great solar flare 23 Feb. 1956 was discussed in detail.

8. Normal cosmic rays.

9. D. K. Bailey, Proc. Inst. Radio Engrs. NY, 47, 255 (1959).
   Rectilinear proton paths for vertically incident protons were calculated by
   A. Dalgarno, Annales de Geophysique, 17, 16 (1961) and are in sharp contrast to Baileys calculations. However, Dalgarno obtains only the minimum possible penetration depth.

10. P. S. Freier, S. Biswas and W. Stein, J.G.R. 66, 2529 (1961).
    Measured the content of α's in the Sept. 3, 1960 flare to be about 1/30 the proton intensity.

    P. Meyer, JGR 65, 3881 (1960)
    In contrast to Freier et al, Meyer measured that on 16 May 1959 and for $E > 560$ Kev, there were up to 2 α's for each incoming proton.
    S. Biswas and P. S. Freier, J.G.R. 66, 1029 (1961) did not measure any α's in the fare of May 4, 1960. See also
    C. E. Fichtel and D. E. Guss, J.G.R. 66, 2527 (1961)
    K. A. Anderson, R. Arnoldy, R. Hoffman, L. Peterson and J. R. Winckler, J.G.R. 64, 1133 (1959)
    estimated upper limits for neutrons, photons electrons, protons and alpha particles in the flare radiation of Aug. 22, 1958.

expressions for a two-ion system is preferred.)[14]

The interaction of charged particles with various gases has been extensively studied in the past. Pertinent parameters, such as $\frac{dE}{dx}$, W, charge transfer, total scattering and ionization cross sections, for protons, electrons, and alpha particles traversing N_2, O_2, and air have been collected. (These are shown in Figs. III-1, III-2, and III-3 and discussed briefly in the figure captions.) It is evident that further work must be done to establish an adequate foundation for calculations of the interaction of the entire range of solar particles presented in Fig. II-1.

However, assuming that the incident flux consists essentially of protons, sufficient data are available to roughly calculate q for the D-layer (below 100 km). $\frac{dE}{dx}$ must be estimated from ionization cross sections for protons in O and N for altitudes above 100 km. W, which is essentially constant at about 35 ev/ion pair for all high energy radiations in gases, would not be expected to be significantly different for gas mixtures containing O and N. The reasons for this are discussed by Herring and Merzbacher.[20]

Detailed calculations along the lines described here have been initiated by R. A. Weir,[21] University of California, Berkeley. Assuming that $Y(E) = KE^{-p}$; p = 5, 6, or 7; and that the entire upper atmosphere has the composition of air, Weir tentatively calculates a riometer absorption that is more than an order of magnitude greater than the observed absorption. This high value can be "explained" if it is assumed, as evidence indicates, that $Y(E) = KE^{-p}$ overestimates the intensity of the low energy protons.

In conclusion, experiments could and should be established that will adequately determine all those basic parameters required to calculate polar cap events with regard to electromagnetic wave communications. A detailed investigation should be made as to the applicability of calculation schemes concerning polar cap events for calculating effects of selected high altitude nuclear bursts.

C. Sudden Ionospheric Disturbances

It has long been known that so-called sudden ionospheric disturbances

(SID), such as short wave fade-out, sudden cosmic noise absorption, sudden enhancement of atmospherics, etc., are manifestations of enhanced ionization in the D-region which in turn is associated with the occurrence of a solar flare. Until relatively recently it was generally thought that very large increases in the intensity of Lyman α emitted by the flare region was responsible. Rocket observations by Friedman's group at NRL[22,23,24] have, however, disclosed that copious quantities of hard X-rays are emitted during flares. The total intensity, as well as the spectral form of this radiation, is sufficient to account for all the phenomena associated with SID's.[25,26] Several high altitude balloon-borne experiments[27,28] have measured γ-rays of 10 to 500 kev coincident with the observations of a flare. Satellite-borne Lyman α sensors have detected no increase in Lyman α during small flares.[24]

Rocket observations made during the NRL Sunflare II program[23] have resulted in quite accurate determinations of the flare X-ray spectra (see Section IB 1.b.); they do not approximate a black body spectrum. The radiation penetrates to quite low altitudes, the 2A X-rays being attenuated by about 0.5 at an altitude of 70 km. During a typical importance 2 flare the electron production rate varies from $\sim 10^3$ cm^{-3} sec^{-1} at 90 km altitude to ~ 1 cm^{-3} sec^{-1} at 60 km.[26] The resulting electron density profile at the time of peak X-ray intensity is such that almost all of the high frequency signal absorption occurs in the altitude interval 75 to 85 km.

Whitten and Poppoff[26] have used 18 mc cosmic noise absorption data, in conjunction with flare X-ray data obtained during an importance 2+ flare,[23] to deduce a model of the time variation of X-ray intensity. For the flare considered, the intensity was found to increase rapidly during the first few minutes following commencement of the emission, after which it slowly decreased with a concurrent softening of the spectrum. Of course, not all flares have identical characteristics; examination of cosmic noise absorption data obtained during some flares indicates a rather slow rise in X-ray intensity. The Sunflare II data yielded a value for an "effective" dissociative recombination coefficient of $\alpha_D = (3^{+3}_{-2}) \times 10^{-7}$ cm^3/sec, using the ARDC 1959 model atmosphere.[29] Sudden ionospheric disturbances and their associated solar flares occur very frequently during periods of sunspot

maxima (of the order of 60 to 360 per solar rotation) and very rarely during sunspot minima (of the order of 0 to 2 per solar rotation).[25] Flares of importance ≥ 2 are of course considerably less frequent. In general SID's are much more pronounced when the solar zenith angle is $< 60^{\circ}$. The usefulness of SID's for deducing D-region relaxation constants is steadily decreasing as we approach the sunspot minimum predicted for 1964.

D. Normal D-Region

The origin of the normal D-region has not yet been definitely settled. In 1946 Nicolet[30] proposed that the D-region is formed by the ionization by solar Lyman α of nitric oxide believed to be normally present in minute concentrations. More recently, Inn[31] suggested that the region results from ionization by Lyman α of vibrationally excited oxygen molecules. Consideration of background solar X-ray intensities observed during the Sunflare II program in 1959[23] led Whitten and Poppoff[32] to suggest that, at least during periods of sunspot maxima, solar X-rays may be adequate to account for the formation of the normal D-region. Available data are insufficient to definitely confirm the latter suggestion. It is anticipated that solar X-ray spectra obtained by satellites will permit its confirmation or rejection. Effective D-region recombination coefficients have been obtained by various methods such as the sunrise effect and observations during eclipses, but they are quite unreliable--due, mainly, to inadequate interpretive theory.

E. Geophysical Effects of the Solar Wind

The solar wind is visualized as being a neutral hydrogen plasma, moving at about 10^8 cm/sec across the earth's orbit, and having a density of 200 to 1000 protons and electrons per cm^3. Being a plasma, it is a highly conducting medium, and cannot penetrate the geomagnetic field without dissipating its energy. Consequently, the physical effects it can have at the earth's surface depend only upon its geomagnetic effects or possibly upon slight leakage of the plasma along field lines to the top of the atmosphere.

The surface in space at which the geomagnetic field intensity just balances the pressure of the solar wind is where the magnetic pressure

equals the momentum deposition of the wind,

$$\frac{B^2}{8\pi} = \frac{1}{2}\rho v^2 \quad .$$

This can be looked upon as being where the magnetic energy density equals the kinetic energy density of the wind. This "stagnation surface" can only exist on the day side of the earth; on this side the geomagnetic field will be compressed (increasing the field strength) and on the night side the geomagnetic field can expand into the magnetic shadow cast in the solar wind.[33] The existence of this asymmetric geomagnetic field is supported by observations of the shape of the Van Allen radiation belts and by the diurnal variation in lowest latitude in which auroras are observed.[34]

It is thought highly probable that the ionizing protons observed above auroras[35] and responsible for some of them leak into the magnetically turbulent region at the stagnation surface of the solar wind. These protons could then be accelerated to Mev energies by the Fermi acceleration mechanism (bouncing from magnetic inhomogeneities) and would find their way along field lines to the auroral zones. This does not explain the fact that some auroras have no proton flux associated with them and appear to be caused by electrons.

Another picture of the solar wind's role in auroras is that the plasma leaks into the geomagnetic field at the neutral points where the geomagnetic field is just cancelled by the steady state interplanetary field.[36] This picture requires no role to be played by the turbulent boundary layer next to the solar wind's stagnation surface, and supplies a neat answer to how particles of solar origin can become trapped in the geomagnetic field.

Solar wind protons are not energetic enough to cause observable ionizing effects in the atmosphere. However, the disordered magnetic fields existing at the interface with the solar wind are capable of accelerating protons and electrons which have leaked into the earth's field,[37] thus making the solar wind into a possible source of ionizing particles which would be observable at auroral latitudes.

REFERENCES

1. Bates, D. R. Physics of the Upper Atmosphere, Chapters 6 and 7, pp 269-353, Academic Press, New York, N.Y., Edited by J. A. Ratcliffe (1960).

2. Bates, D. R. The Earth as a Planet, Chapter 12, pp 576-643, The University of Chicago Press, Chicago, Illinois, edited by G. P. Kuiper (1954).

3. Chamberlain, J. W. and A. B. Meinel. The Earth as a Planet, Chapter 11, pp 514-575, The University of Chicago Press, Chicago, Illinois, edited by G. P. Kuiper (1954).

4. Little, C. G., W. M. Rayton, and R. B. Roof. Ionospheric Effects at VHF and UHF, Proc. IRE, 44, 8, pp 992-1018 (August 1956).

5. Booker, H. G., C. W. Gartlein, and B. Nichols. Interpretations of Radio Reflections from the Aurora, J. Geophys. Res. 60, pp 1-22 (March 1955).

6. Dyce, R. B. Auroral Echoes Observed North of the Auroral Zone on 51.9 Mc/sec, J. Geophys. Res. 60, 3, pp 317-323 (September 1955).

7. Leadabrand, R. L., R. I. Presnell, M. R Berg, and R. B. Dyce. Doppler Investigations of the Radar Aurora at 400 Mc, J. Geophys. Res. .64, 9, pp 1197-1204 (September 1959).

   Leadabrand, R. L., L. Dolphin, A. M. Peterson. Preliminary Results of 400-Mc Radar Investigations of Auroral Echoes at College, Alaska, IRE Trans, PGAP-7, 2, pp 127-136 (April 1959).

   Presnell, R. I., R. L. Leadabrand, A. M. Peterson, R. B. Dyce, J. C. Schlobohm, and M. R. Berg. VHF and UHF Radar Observations of the Aurora at College, Alaska, J. Geophys. Res. 64, pp 1179-1190 (September 1959).

8. James, J. C., et al. Observed Characteristics of an Ultra-High-Frequency Signal Traversing an Auroral Disturbance, Nature 185, 4712, pp 510-512 (20 February 1960).

9. Little, C. G. and H. Leinbach. The Riometer--A Device for the Continuous Measurement of Ionospheric Absorption, Proc. IRE 47, pp 315-319 (February 1959).

10. Collins, C., D. H. Jelly, and A. G. Matthews. High-frequency Radio-wave Blackouts at Medium and High Latitudes During a Solar Cycle, Canad. J. Phys., 39, 35-52 (1961).

REFERENCES

11. Obayashi, T. and Y. Hakura. Solar Corpuscular Radiation and Polar Ionospheric Disturbances, J. Geophys. Res., 65, 3131-3142 (1960).

12. Reid, G. C. and C. Collins. Observation of Abnormal VHF Radiowave Adsorption at Medium and High Latitudes, J. Atmos. Terr. Phys. 14, 63-81 (1959).

13. Van Allen, J. A., State University of Iowa. Private conversation.

14. See references in caption to Figure II-1.

15. Yagoda, H. Observations On Heavy Primary Cosmic Ray Nuclei Above the Atmosphere, AFCRC-TR-58-241 (July 1958).

16. Anderson, K. A., R. Arnoldy, R. Hoffman, L. Peterson, and J. R. Winkler. Observations of Low-Energy Solar Cosmic Rays from the Flare of 22 August 1958, J. Geophys. Res. 64, 1133 (1959).

17. Obayashi, T. and Y. Hakura. Polar Ionospheric Disturbances and Solar Corpuscular Emissions, Planet. Space Sci. 5, 59 (1961).

18. Cook, C. J. and D. C. Lorents. Electron Collision Frequencies and Scattering Cross Sections in the Ionosphere. Final Tech. Report No. 6, USASRPA, Fort Monmouth, N.J., Contract No. DA-36-039 SC-85052, Aug. 15, 1961.

19. Bowhill, S. A. Effective Recombination Coefficient of an Ionosphere Containing a Mixture of Ions, J. Atmos. Terr. Phys. 20, 19 (1961).

20. Herring, J. R. and E. Merzbacher. Statistical Problems in Energy Loss and Ionization Processes, J. of the Elisha Mitchell Scientific Soc. 73, 267 (1957).

21. Weir, R. A., University of Calif., Berkeley, Calif. Private conversation.

22. Friedman, H., T. A. Chubb, J. E. Kupperian and J. C. Lindsay. X-ray Emission of Solar Flares, IGY Rocket Report Series No. 1, 183 (30 July 1958).

23. Chubb, T. A., H. Friedman, and R. W. Kreplin. Measurements Made of High Energy X-rays Accompanying Three Class 2+ Solar Flares, J. Geophys. Res. 65, 1831 (1960); X-ray Emission Accompanying Solar Flares, Liege Symposium (1960).

24. Chubb, T. A., et al. IGY Bull. No. 42, Trans. Am. Geophys. Union 41, 717 (1960).

REFERENCES

25. Poppoff, I. G., R. C. Whitten, and F. L. Ludwig. The Determination of Ionospheric Recombination Coefficients; Phase I, Feasibility of Utilizing Solar Flare Sudden Ionospheric Disturbance Relationships, Final Report, prepared for Ionospheric Physics Laboratory, GRD, Air Force Research Division, under Contract No. AF 29(601)-1994 (May 26, 1960).

26. Whitten, R. C. and I. G. Poppoff. A Model of Solar Flare Induced Ionization in the D-Region. J. Geophys. Res., 66, 2779 (1961)

27. Peterson, L. E. and J. R. Winckler. Gamma Ray Burst from a Solar Flare, J. Geophys. Res. 64, 697 (1959).

28. Gordon, I. M. Nature of Gamma Emission in Solar Flares and the Formation of Cosmic Particles in Active Solar Regions. Soviet Astronomy (AJ) 4, 873 (1961).

29. Minzner, R. A., K.S.W. Champion, and H. L. Pond. The ARDC Model Atmosphere, 1959, Air Force Surveys in Geophysics No. 115, GRD, Air Force Cambridge Research Center, ARDC (August 1959).

30. Nicolet, M. Contribution a Etude de la Structure de l'ionosphere, Mem. Inst. Meteor. Belg. No. 19, 83 (1945).

31. Inn, E.C.Y. Origin of the D-Region. Planet.Space Sci. 5, 76 (1961).

32. Whitten, R. C. and I. G. Poppoff. The Possible Roles of Solar X-rays in the Formation of the Normal D-Region. (To be published)

33. Johnson, F. S. The Gross Character of the Geomagnetic Field in the Solar Wind, J. Geophys. Res. 65, 3049 (1960).

34. Liemohn, H. The Outer Radiation Belt and Aurora, Nature 188, 394 (1960).

35. Korff, S. A. and R. C. Haymes. High Neutron and Radiation Intensities at Balloon Altitudes During Auroral Display, J. Geophys. Res. 65, 3163 (1960).

36. Dungey, J. W. Interplanetary Magnetic Field and the Auroral Zones, Phys. Rev. Lett. 6, 47 (1961).

37. Dungey, J. W. Cosmic Electrodynamics, Cambridge Univ. Press (1958).

III ATMOSPHERIC IONIZATION AND RELAXATION PROCESSES

A. Ionization Processes

Ionization of the constituents present in air, principally N_2, O_2, and NO, at the altitudes of interest is caused by collisions of the molecules with energetic charged particles, i.e., electrons, protons, singly and doubly charged helium ions, etc., and with photons having energies ranging from the order of 10 ev to 1 Mev.

Ionization of a medium such as air by electrons occurs through a rather complicated series of processes.[1] The collision of an energetic electron with the bound electrons present in N_2 and O_2 molecules will cause excitation to another bound state of higher energy (excitation) or to the continuum (ionization). If the energy transfer from the incident to the scattered particle is large, the latter can be treated as a free particle (hard collision); this process is generally referred to in the literature as Moller scattering, after the investigator who developed a general formula for the collision cross section. On the other hand, if the energy transfer is small, the struck particle must be considered as bound (soft collision). A general formula for the energy loss per unit path length by soft collisions has been developed by Bethe. An energetic electron may also lose energy by the production of bremsstrahlung when it is scattered by the electric field of the nucleus. The photons so produced will also produce ionization; this will be considered below. Figure III-1 contains a compilation of electron cross section and stopping power data in air.

Ionization by heavy charged particles occurs primarily by soft collisions with the bound electrons. Bethe's equation[1] for the energy loss per unit path length is applicable to this case. Figures III-2 and III-3 contain a compilation of proton and alpha particle cross sections and stopping power data in air. In addition to ionization by soft collisions, energetic heavy charged particles can produce nuclear reactions with

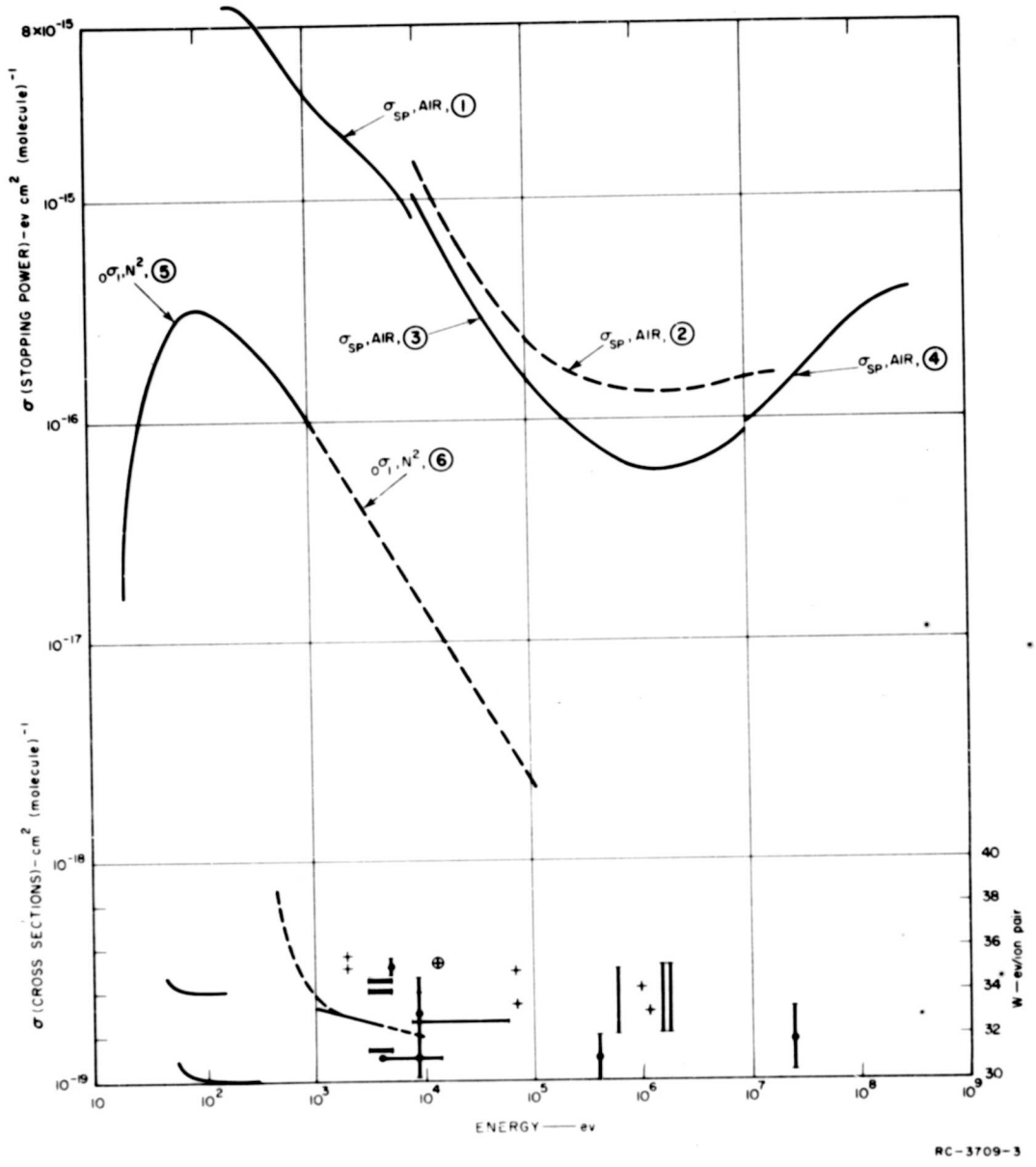


FIG. III-1 INTERACTIONS OF ELECTRONS WITH AIR, N_2 AND O_2.

Figure III-1, Interactions of Electrons with Air, N_2 and O_2. Curve references are as follows:

1. A. Dalgarno, Annales de Geophysique 17, 16 (1961)

2. L. V. Spencer, Phys Rev 98, 1597 (1955)
   Spencer's results seem too high.

3. A. T. Nelms, Nat. Bureau Stds. Circular 577, July 26 (1956)
   Nat. Bureau Std. Circular Supplement 577, July 39 (1958)
   This is an extensive calculation and literature review.

4. H. A. Bethe and J. Ashkin, Exp. Nuclear Phys. Vol I, 188 (1953)
   Edited by Segre, Wiley

5. J. T. Tate and P. T. Smith, Phys. Rev. 39, 270 (1932)
   These measurements are considered to be very precise. Ionization cross sections to 750 ev were determined for electrons colliding with six gases.

6. L. Marton and L. I. Schiff, J. Appl. Phys. 12, 759 (1941)
   The values shown for W were taken from the most comprehensive survey by
   I. T. Myers, Doctorial Thesis, State College of Washington, "The Measurement of the Electron Energy Required to Produce an Ion Pair in Various Gases," (1958)
   Myers also reviews W for α's protons and X-rays in various gases.

Figure III-2, Interactions of Protons with Air, N_2 and O_2; curve references are as follows:

1. C. J. Cook, E. Jones and T. Jorgensen, Phys. Rev. 91, 1417 (1953)
   The range was measured as a function of E (2-250 kev) and σ_{SP} calculated. σ_{SP} was extrapolated below 2 kev by an empirical expression.

2. S. K. Allison and S. D. Warshaw, Rev. Mod. Phys., 25, 779 (1953)
   (dE/dx) was measured directly by several investigators for 20 kev $\leq$ E $\leq$ 1,000 kev., of review.

3. J. E. Brolley, Jr. and F. L. Ribe, Phys. Rev. 98, 1112 (1955)
   σ_{SP} determined for 4.43 Mev protons.

4. H. A. Bethe and J. Askin, Exp. Nuclear Phys. Vol I, 188 (1953)
   edited by Segre, Wiley, σ_{SP} calculated but R has been experimentally checked to 340 Mev.

5. See also American Institute of Physics Handbook 826 (1957)
   H. A. Bethe, Brookhaven National Laboratory Report BNL-T-7 (1949)
   H. A. Bethe, Rev. Mod. Phys., 22, 213 (1950)

6. C. Ramsauer, R. Kollath and D. Lilienthal, Ann. der Physik, 8, 709 (1931). Perhaps others have measured the total scattering cross section for protons.

7. Estimated.

8. P. M. Stier and C. F. Barnett, Phys. Rev. 103, 896 (1956)
   Charge exchange cross sections were measured from 3 to 200 kev. The nomenclature is as follows: If $A^+ + B \rightarrow A + B^+$ we have ${}_{10}\sigma_{01}$
   $A + B \rightarrow A^+ + B$, we have ${}_{00}\sigma_{10}$
   $A^{2+} + B^+ \rightarrow A + B^{3+}$, we have ${}_{21}\sigma_{03}$, etc.

9. J. W. Hooper, E. W. McDaniel, D. W. Martin and D. S. Hammer, 2nd International Conference on the Physics of Electronic and Atomic Collisions, Univ. of Colorado, Boulder, Colo., June 12-15 (1961).
   Ionization cross sections for protons incident on many gases were measured in the energy range 0.15 to 1.10 Mev.

10. R. N. Il'in, V. V. Afrisinov and N. V. Fedorenko, JETP, 9, 29 (1959)
    The ionization cross section for protons in air was measured, 5 $\geq$ E $\leq$ 180 kev. Their curve was extrapolated to low energies, thus may be misleading below 5 kev.

11. Estimated assuming that ${}_{10}\sigma_{11}$ = constant σ_{SP}

12. R. A. Lowry and G. H. Miller, Phys. Rev., 109, 826 (1958)
    W was determined in N_2 and A.

13. H. V. Larson, Phys. Rev. 112, 1927 (1958).
    W was determined in N_2, air and other gases.

14. J. M. Valentine and S. C. Curran, Rep. Prog. Phys. XXI, 1 (1958)
    A review on the average energy expended per ion pair in gases and gas mixtures.

15. H. A. Bethe and J. Askin, Exp. Nuclear Phys. Vol. I, 233 (1953).
    Edited by Segre, Wiley. A review.
    See also I. T. Meyers, The Measurement of the Electron Energy Required to Produce an Ion Pair in Gases, Thesis, State College of Washington (1958).

Figure III-1, Interactions of Electrons with Air, N_2 and O_2. Curve references are as follows:

1. A. Dalgarno, Annales de Geophysique 17, 16 (1961)

2. L. V. Spencer, Phys Rev 98, 1597 (1955)
   Spencer's results seem too high.

3. A. T. Nelms, Nat. Bureau Stds. Circular 577, July 26 (1956)
   Nat. Bureau Std. Circular Supplement 577, July 39 (1958)
   This is an extensive calculation and literature review.

4. H. A. Bethe and J. Ashkin, Exp. Nuclear Phys. Vol I, 188 (1953)
   Edited by Segre, Wiley

5. J. T. Tate and P. T. Smith, Phys. Rev. 39, 270 (1932)
   These measurements are considered to be very precise. Ionization cross sections to 750 ev were determined for electrons colliding with six gases.

6. L. Marton and L. I. Schiff, J. Appl. Phys. 12, 759 (1941)
   The values shown for W were taken from the most comprehensive survey by
   I. T. Myers, Doctorial Thesis, State College of Washington, "The Measurement of the Electron Energy Required to Produce an Ion Pair in Various Gases," (1958)
   Myers also reviews W for α's protons and X-rays in various gases.

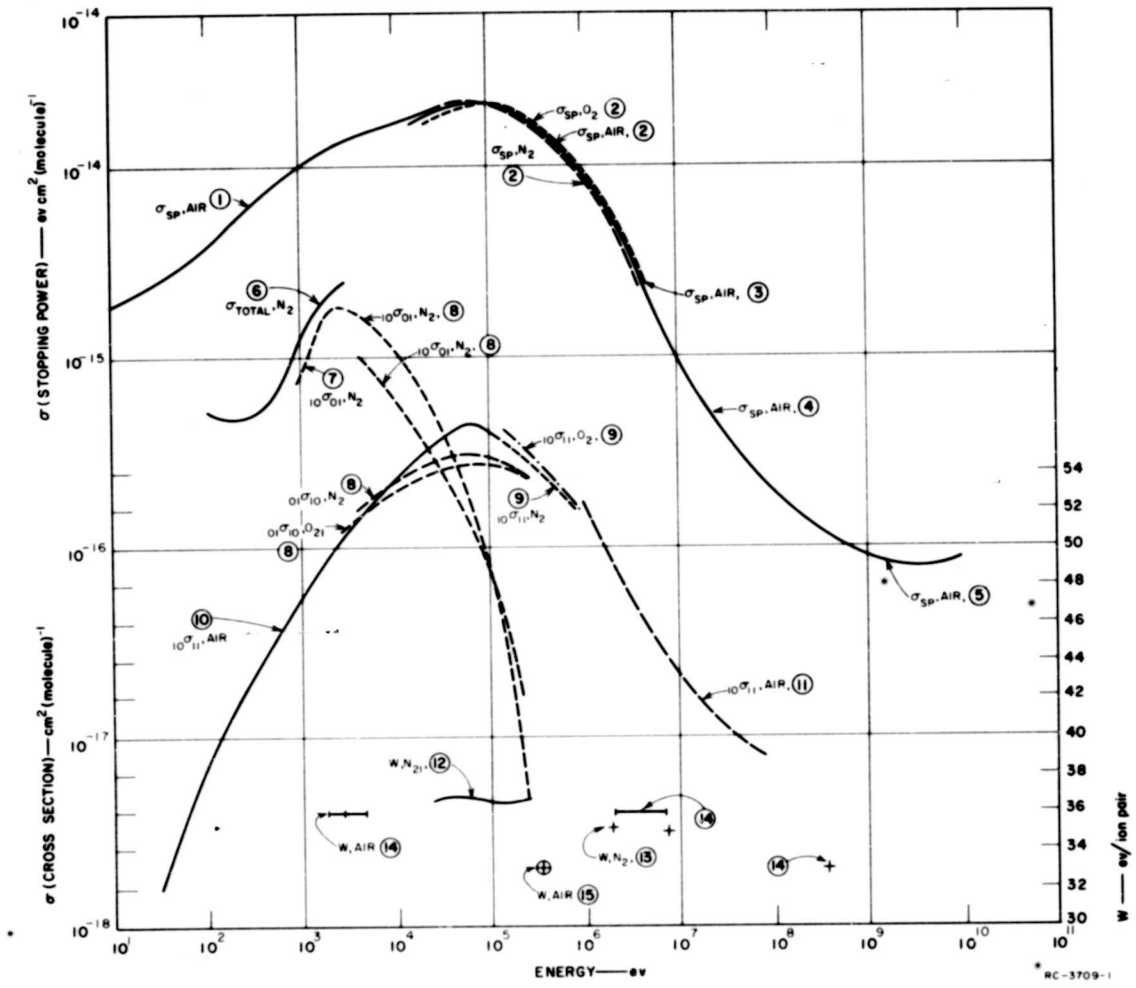


FIG. III-2 INTERACTIONS OF PROTONS WITH AIR, N_2 AND O_2

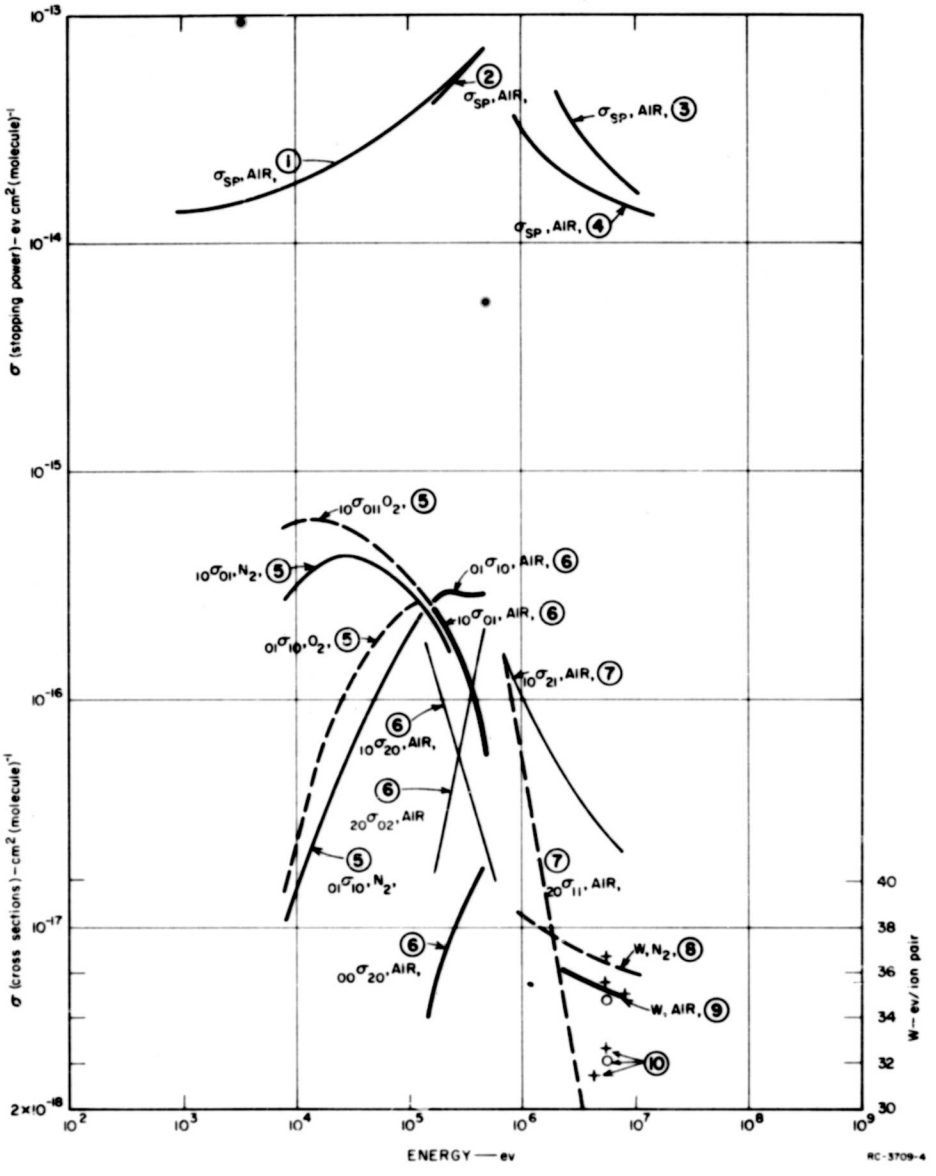


FIG. III-3 INTERACTIONS OF ALPHA PARTICLES WITH AIR, O_2 AND N_2

Figure III-3, Interactions of Alpha Particles with Air, O_2 and N_2; curve references are as follows:

1. C. J. Cook, E. Jones and T. Jorgensen, Phys. Rev. 91, 1417 (1953)
   The range was measured as a function of E (2-250 kev) and σ_{SP} calculated.
   σ_{SP} was extrapolated below 2 kev by an empirical expression.

2. S. K. Allison and S. D. Warshaw, Rev. Mod. Phys. 25, 779 (1953)
   (dE/dx) was measured directly from 150 to 400 kev.

3. G. Mano, Ann de Physique 1, 408 (1934)

4. H. A. Bethe, Brookhaven Nat. Lab. Rept. BNL T-7 (1949)

5. C. F. Barnett and P. M. Stier, Phys. Rev. 109, 385 (1958).
   Charge exchange cross sections were measured for 4 to 200 kev helium ions in various gases.

6. S. K. Allison, Phys. Rev. 109, 76 (1958)

7. S. K. Allison and S. D. Warshaw, Rev. Mod. Phys. 25, 779 (1953)

8. W. P. Jesse, Phys. Rev. 122, 1195 (1961)
   W was determined for alpha particles in N_2.

9. Estimated W for air (from 8)

10. W. P. Jesse and J. Sadauskis, Phys. Rev. 90, 1120 (1953)
    (Observed values are crosses). See also
    J. M. Valentine and S. C. Curran, Rep. Prog. Phys. XXI, 1 (1958)
    A review, circles are reported values.
    See also I. T. Meyers, The Measurement of the Electron Energy Required to Produce an Ion Pair in Gases, Thesis, State College of Washington (1958)
    An additional curve for σ_{SP} can be calculated from the range-energy curves by W. P. Jesse and J. Sadauskis, Phys. Rev. 78, 1 (1950)

the N^{14} and O^{16} which in turn can result in the emission of energetic photons (γ rays), heavy charged particles (protons, alpha particles), neutrons, and pi mesons. Neutrons cannot ionize air directly but can produce more nuclear reactions, the products of which may cause ionization. Pi mesons (π^+, π^-, π^0) are produced only by collisions of protons with energies in the Bev range, and hence are not expected to be an important ionization source in the phenomena of interest. Ionization by the products of nuclear reactions is an extremely difficult problem to solve quantitatively. For this reason no data for these processes are presented here, although they should certainly be included in an ionization model in which heavy charged particles are important.

Ionization by electromagnetic radiation (photons) can occur by means of three different physical processes, photo-ionization, Compton scattering, and pair formation. Photo-ionization consists of the absorption of a photon by a bound electron and a simultaneous transition of the electron from a bound to a continuum state. For incident photons with energies in the X-ray range (100 ev to 50 kev) photo-ionization and secondary ionization by the emitted electrons constitute the principal mode of ionization. Approximately one free electron is produced for each 35 ev of incident photon energy. The photo-ionization cross sections for air[2] are shown in Fig. III-4. Photons in the low and medium energy γ-ray range (50 kev to 5 Mev) ionize N_2 and O_2 principally by Compton absorption. This mode is a two-step process in which the incident photon is absorbed by a bound electron and then re-emitted with a different energy, the difference in energy being taken up by the freed electron. The corrections for the initial bound state of the electron are small and can be neglected in computing the cross section. For photon energies above 10 Mev, pair formation is important. This process is expected to be neglible in the phenomena of interest. Figure III-5 shows the mass attenuation coefficients corresponding to each process for photons in air for energies of 10 kev to 100 Mev. Photons (bremsstrahlung) in the energy range 10 to 500 kev frequently accompany the passage of energetic electrons through matter.

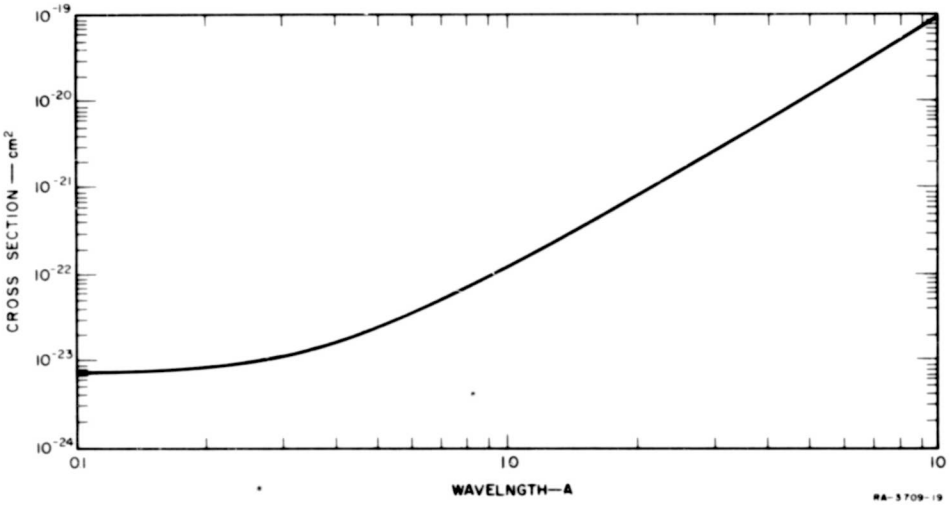
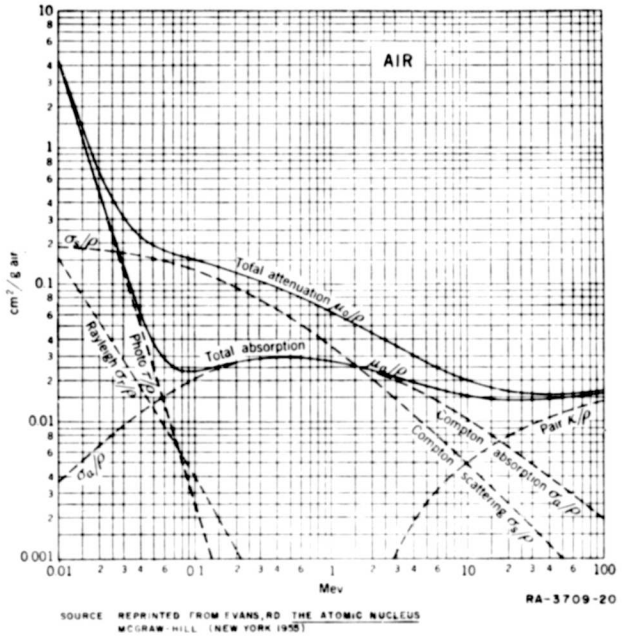


FIG. III-4 ABSORPTION CROSS SECTION FOR X-RAYS IN AIR AS A FUNCTION OF WAVELENGTH



SOURCE: REPRINTED FROM EVANS, R.D. THE ATOMIC NUCLEUS MCGRAW-HILL (NEW YORK 1955)

FIG. III-5 MASS ATTENUATION COEFFICIENTS FOR PHOTONS IN AIR, COMPUTED FROM THE TABLES OF ATOMIC CROSS SECTIONS PREPARED BY G. R. WHITE. THE CURVE MARKED "TOTAL ABSORPTION" IS $(\mu_a/\rho) = (\sigma_a/\rho) + (\tau/\rho) + (\kappa/\rho)$, WHERE σ_a, τ, AND κ ARE THE CORRESPONDING LINEAR COEFFICIENTS FOR COMPTON ABSORPTION, PHOTOELECTRIC ABSORPTION, AND PAIR PRODUCTION. WHEN THE COMPTON SCATTERING COEFFICIENT σ_s IS ADDED TO μ_a, WE OBTAIN THE CURVE MARKED "TOTAL ATTENUATION," WHICH IS $(\mu_0/\rho) = (\mu_a/\rho) + (\sigma_s/\rho)$. THE TOTAL RAYLEIGH SCATTERING CROSS SECTION (σ_r/ρ) IS SHOWN SEPARATELY. BECAUSE THE RAYLEIGH SCATTERING IS ELASTIC AND IS CONFINED TO SMALL ANGLES, IT HAS NOT BEEN INCLUDED IN μ_0/ρ. IN COMPUTING THESE CURVES, THE COMPOSITION OF "AIR" WAS TAKEN AS 78.04 VOLUME PER CENT NITROGEN, 21.02 VOLUME PER CENT OXYGEN, AND 0.94 VOLUME PER CENT ARGON. AT 0°C AND 760 mm Hg PRESSURE, THE DENSITY OF AIR IS $\rho = 0.001\,293$ g/cm^3.

Another type of ionization process, chemionization, has recently received much attention, and may be of considerable importance in atmospheric processes, although its over-all significance cannot yet be fully assessed. Chemionization has recently come to be considered the predominant general ionization mechanism in high temperature air. Calculations of electron density, for example, have customarily been made essentially on the basis of thermal ionization of NO. Studies by S. C. Lin (AVCO Everett Research Laboratory), however, indicate that the predominant source of electrons and NO^+ is the reaction $N + O \leftrightarrows NO^+ + e$. K. Wray (same laboratory) quotes a rate constant for this reaction (to the right) $k \cong 1 \times 10^{-14}\ T^{1/2} \exp(-3.2 \times 10^4\ T^{-1})\ cm^3\ ion^{-1}\ sec^{-1}$, with T in ^oK. This leads to a very fast ionization reaction in the presence of N and O, both of which would be produced in the atmosphere near a nuclear explosion. Two other, two-body reactions which may be of importance are $N + N \leftrightarrows N_2^+ + e$ and $O + O \rightleftarrows O_2^+ + e$. The above reactions are all endothermic and require fairly high temperatures to be important. Some exothermic reactions may conceivably be of significance for either low or high temperatures. For cases where the product molecule increases in complexity the probability of auto-ionization increases. There is some evidence that the following reactions occur $CH + O \rightarrow CHO^+ + e$, $N_2^* + N \rightarrow N_3^+ + e$ and $N_2^* + N_2 \rightarrow N_4^* + e$. A three-body reaction which appears to have an unusually high rate constant ($k \cong 1 \times 10^{-27}\ cm^6\ ion^{-1}\ sec^{-1}$) may be of importance, $N + N + NO \rightarrow N_2 + NO^+ + e$. Further consideration of chemionization would require consideration of the chemical reactions resulting in dissociation and excitation as well as possible competing reactions.

The relative importance of chemionization during geophysical events or at great distances from nuclear explosions is probably low. However, for ionization near explosions or in the D-region, especially at night, chemionization may, conceivably, be important.

B. Relaxation Processes

Chemical reactions and ion-atom interchanges following or accompanying ionization are important in determining which species must be considered

in the subsequent electron removal processes, which are of direct interest to this study. The general electron removal processes to be considered are: electron attachment to neutral species, electron detachment from negative ions, recombination of positive ions with electrons, and the ionic neutralization through ion-ion recombination.

Any selection of pertinent atmospheric relaxation processes is bound to be controversial because of the lack of actual knowledge of atmospheric constituents (species, energy states, etc.) and recombination processes. The following discussion covers the topics that the authors, as well as the many others, feel are important considerations. The details may well be modified in the light of future atmospheric and laboratory investigations.

1. Chemical Reactions

Chemical reactions may be of importance during and following a high altitude nuclear burst because the radiation may dissociate the oxygen and nitrogen sufficiently to result in a change in the ion composition, and hence the electron removal rates, from that expected if there were no dissociation. Within the fireball, there is virtually complete dissociation as well as ionization of the nitrogen and oxygen present. Outside the fireball, the ultraviolet radiation responsible for the dissociation of O_2 (λ 1200 to 1800 A) will be almost entirely absorbed[3] within a distance of 100 meters from the fireball at an altitude of 60 km. Hence one would find a layer of highly dissociated oxygen in a relatively thin region surrounding the fireball. Outside this region, dissociation of oxygen and nitrogen would be caused principally by X-rays from the initial radiation, and beta particles and their associated bremsstrahlung from the fission product decays. The rate of dissociation is expected to be approximately equal (i.e., in order of magnitude) to the electron production rate. Using the reaction rate[4] constants $k \approx 10^{-32}$ cm^6/sec for the reactions $O + O + M \rightarrow O_2 + M$, and $N + N + M \rightarrow N_2 + M$, one obtains a typical equilibrium concentration of $\sim 10^{11}$ cm^{-3} for the atomic oxygen and nitrogen concentrations at an altitude of 60 km. The

atomic oxygen concentration is therefore, at most, of the same order of magnitude as the ambient O concentration at this altitude[4,5] ($\sim 10^{11}$ cm^{-3}) and, consequently, the increased concentration of atomic oxygen is of little importance.

The atomic nitrogen is another story, however, since it is not normally present in the atmosphere. This species can react with atomic oxygen to produce nitric oxide: $N + O + M \rightarrow NO + M$, which can in turn react with atomic oxygen to produce nitrogen dioxide: $NO + O + M \rightarrow NO_2 + M$. The reaction rates[4] are such that one would expect equilibrium concentrations of $< 10^7$ cm^{-3} for nitric oxide and $< 10^3$ cm^{-3} for NO_2 (at night); in the daytime, NO_2 is rapidly decomposed into NO and O by sunlight. The principal importance of the nitric oxide is twofold: it can undergo charge exchange with other ions, thus "shuffling" the ion composition and it can be ionized (during daylight only) by solar Lyman α at altitudes above 65 km, thus perhaps materially increasing the electron production rate in the altitude interval 65 to 80 km (in which the diffusion rate is small). This aspect should be further investigated. While it is true that NO_2 can act as an electron attaching agent in such processes[6] as $e^- + NO_2 \rightarrow NO + O^-$, and $O^- + NO_2 \rightarrow O + NO_2^-$, the fact that NO_2 is present only in minute concentrations is expected to render it unimportant in this respect compared with O_2. The large concentrations of NO_2^- observed with rocketborne spectrometers have not yet been adequately explained.

2. Ion-Atom Interchange

It seems clear that N_2^+ is lost rapidly through charge exchange with O_2 thus, $N_2^+ + O_2 \rightarrow O_2^+ + N_2$, although at the higher altitudes of the D-region NO^+ may be formed via $N_2^+ + O \rightarrow NO^+ + N$. The lack of N_2^+ in the ion spectrum[7] at 100 km is good evidence that these reactions are indeed important.

Consider then what can happen to O_2^+. The dissociative recombination rate constant[8,9] is probably about 10^{-7} cm^3/sec. At an O_2^+ density of $\sim 10^4/cm^3$ the reaction rate will be about 10^{-3} sec^{-1}. The ion-ion

recombination rate will probably be lower. O_2^+ may be lost via $O_2^+ + N \rightarrow NO^+ + O$, or $O_2^+ + N_2 \rightarrow NO^+ + NO$. At 80 km, n(N) is about 10^{10} so that a rate constant of 10^{-13} cm^3/sec makes the first reaction competitive with dissociative recombination. Bates[10,11] believes the second reaction ($O_2^+ + N_2 \rightarrow NO^+ + NO$) is negligible because of activation energy considerations. Due to the high concentration of N_2 ($3 \times 10^{14}/cm^3$ at 80 km) the rate constant of this reaction, however, need be only 10^{-17} or 10^{-18} cm^3/sec to be significant. Thus, this reaction probably is important if it has an activation energy less than 0.3 ev.

Assuming negligible concentrations of excited species, there are no reactions which can remove NO^+ since it has the lowest ionization potential. Therefore NO^+ will accumulate and may become as important as O_2^+. If such is the case, the recombination will be influenced both because the dissociative recombination of NO^+ may not have the same rate constant as O_2^+ and because the ion-ion recombination rates may be changed.

By assuming the estimated order of magnitude value for the rate constant of 10^{-10} cm^3/sec for typical interchange reactions, Hertzberg[12] also finds that the predominant positive ion is NO^+; the other positive ionic species very quickly undergo charge exchange and atomic rearrangement to form NO^+ with a characteristic lifetime of 1 μsec at an altitude of 60 km.

Mass spectrometric methods have been used to measure[7] relative ion concentrations at altitudes above 100 km. These observations indicated daytime relative concentrations at 100 km of $NO^+/O^+ \approx 1$. This yields an interchange rate constant of $\sim 10^{-16}$ cm^3/sec, a value considerably smaller than one would expect for ion-atom/molecule reactions.

The technical difficulties of laboratory measurements of these reactions have caused most experimentalists to look for easier experiments. The only measurement of an ion-atom interchange process[13] at thermal energies has been carried out on $O^+ + O_2 \rightarrow O_2^+ + O$ which was found to have a rate of about 2×10^{-11} cm^3/sec. It is not known, however, whether the dominant mechanism in this reaction is charge exchange or

ion-atom interchange. The need for these rate constants would seem to justify a search for new and novel techniques to accomplish their measurement. One such technique has already been suggested by Cook[14] and a feasibility study determined that the technique could indeed be used for ion-atom interchange reactions. Other techniques should also be investigated, particularly those which might apply to ion-ion recombination.

3. Electron Attachment

Electron attachment to atomic and molecular oxygen is an important electron removal process in the lower ionosphere. These processes are of the types:[15] $O + e^- \rightarrow O^- + \gamma$, $O + O_2 + e^- \rightarrow O^- + O_2^*$, and $O_2 + O_2 + e^- \rightarrow O_2^- + O_2^*$. Different methods of measuring the electron affinity of O_2 have resulted in three different values,[16,17,18] namely, 0.15 ev, 0.46 ev, and 0.74 ev, possibly indicating that excited vibrational states of O_2 may be important. Johnson *et al.*[8] have reportedly detected NO_2^- at altitudes above 100 km by mass spectrometric measurements, but the reliability of their results is questionable. In any event, the importance of this ion in the lower ionosphere is expected to be negligible since it cannot undergo charge exchange with O_2.

Radiative attachment coefficients for atomic oxygen have been obtained by Branscomb *et al.*:[19] $\beta_r = 1.3 \times 10^{-15}$ cm^3/sec at a temperature of 250°K. When one considers the small concentration of atomic oxygen compared with that of O_2 present in the altitude interval 60 to 75 km, it becomes evident that attachment of electrons to atomic oxygen is unimportant. On the other hand, attachment of electrons to molecular oxygen is a very important electron removal process in the lower ionosphere. There are actually three processes by which attachment to O_2 proceeds: $e^- + O_2 \rightarrow O_2^- + \gamma$ (radiative attachment); $e^- + O_2 \rightarrow O^- + O$ (dissociative attachment); and $e^- + O_2 + M \rightarrow O_2^- + M^*$ (three-body attachment). The radiative attachment coefficient has never been measured but is estimated to be $< 10^{-15}$ cm^3/sec; this may be large enough to make the radiative process of some importance between 60 and 80 km. The dissociative process is unimportant except at very high temperatures ($> 10^3$ °K) and is therefore of no consequence.[20] The most important electron attachment process

is the last one. Chanin et al.[20] have found a value for the three-body coefficient of $K = 2 \times 10^{-30}$ cm^6/sec at a temperature of 250°K; their investigation also revealed that only molecular oxygen has the necessary stabilizing characteristics to act as an efficient third body.

4. Electron Detachment

Electrons can be detached from, as well as attached to, oxygen atoms and molecules. The processes by which this is done are photodetachment: $O^- + \gamma \rightarrow O + e^-$, $O_2^- + \gamma \rightarrow O_2 + e^-$; collisional detachment: $O^- + M \rightarrow O + M + e^-$, $O_2^- + M \rightarrow O_2 + M + e^-$; and associative detachment: $O^- + O \rightarrow O_2 + e^-$, $O^- + N_2 \rightarrow N_2O + e^-$, $O_2^- + O \rightarrow O_3 + e^-$. Branscomb and coworkers[16,19] have measured the photodetachment cross sections for O^- and O_2^-. Computation of the reciprocal mean lifetime for solar radiation using these data leads to values of $\rho(O^-) = 1$ sec^{-1}; $\rho(O_2^-) = 0.4$ sec^{-1}.

Collisional detachment from O^- and O_2^- is of little importance at normal temperatures due to the large electron affinity of atomic oxygen[19] (~1.5 ev) and molecular oxygen[17,21] compared with the mean kinetic energy of thermal molecules. Bailey and Branscomb[22] have, however, obtained a value for the apparent D-region collisional detachment coefficient of $\gamma_b = 2 \times 10^{-17}$ cm^3/sec--using data from ionospheric observations during polar cap events.

Preliminary calculations indicate that associative detachment may be of considerable importance. Sufficient atomic oxygen is present at night in the D-region between 70 and 80 km to allow processes such as $O_2^- + O \rightarrow O_3 + e^-$ to proceed; not only are such processes possible but they seem to be the only processes possible. Unfortunately, the rate constant is estimated only to within 3 orders of magnitude and the atomic oxygen to within 2 orders of magnitude. Further investigation needs to be carried out since associative detachment seems to be very important in the relaxation of the D-region after a high altitude nuclear burst at night.

5. Dissociative Recombination

Dissociative recombination, i.e., $O_2^+ + e^- \rightarrow O^* + O^{**}$, $N_2^+ + e^- \rightarrow N^* + N^{**}$, and $NO^+ + e^- \rightarrow N^* + O^{**}$, is one of the most important relaxation processes in the lower ionosphere. Although there is some reason to believe that NO^+ may be the predominant ion in the lower D-region, it is not definitely known that N_2^+ and O_2^+ are not also important. If they are, we can compute an "effective" dissociative recombination coefficient[23]

$$\alpha_D^e = \frac{\Sigma_{ij} \alpha_D^{ij} M^{ij}}{\Sigma_{ij} M^{ij}}$$

where α_D^{ij} is the dissociative recombination coefficient of the ith species in the jth excited state and M^{ij} is the concentration of the ith species in the jth excited state.

The dissociative recombination coefficients of N_2^+ and O_2^+ have been measured with considerable precision;[24] at pressures $\lesssim 0.01$ mm of Hg Biondi and coworkers found that $\alpha_D\ (N_2^+) = (5.9 \pm 1) \times 10^{-7}$ cm^3/sec and $\alpha_D(O_2^+) = (3.8 \pm 1) \times 10^{-7}$ cm^3/sec. At pressures above 0.1 mm of Hg it was found that $\alpha_D(N_2^+) = 2 \times 10^{-6}$ cm^3/sec. Mass spectrometric investigation of the positive ion species revealed that N_2^+ and O_2^+ are the only important species at the low pressures, but, that at the higher gas pressures (i.e., $\lesssim 0.1$ mm of Hg) N_3^+, N_4^+, and O_3^+ apparently dominate the recombination processes. The low pressure values of the dissociative recombination coefficient agree quite well with previous determinations by Faire and Champion[25] ($\alpha_D\ (N_2^+) = 4 \times 10^{-7}$ cm^3/sec); Biondi and Brown[9] ($\alpha_D\ (O_2^+) = 2.8 \times 10^{-7}$ cm^3/sec), and Holt[10] ($\alpha_D\ (O_2^+) = 3 \times 10^{-7}$ cm^3/sec). Measurements of the dissociative recombination of NO^+ at low temperatures has never been attempted. Lin[26] has measured this coefficient at a temperature of 5000°K ($\alpha_D\ (NO^+) = 10^{-9}$ cm^3/sec) but the significance of this value for temperature of the order of 300°K is doubtful. A laboratory experiment to measure $\alpha_D\ (NO^+)$ at this temperature appears to us to have considerable merit.

Bowhill[23] has employed nocturnal, diurnal, and eclipse relaxation data to obtain a value of $\alpha_D(NO^+) = 5 \times 10^{-9}$ cm^3/sec, but this must be treated with caution.

6. Ion-Ion Recombination

Ion-ion recombination is probably of negligible importance in the upper D-region,[27] but in the altitude range 60 to 75 km it may have considerable effect on ionic relaxation. Such a process will involve the mutual neutralization of positive ions O_2^+, N_2^+, NO^+, N^+, O^+, and negative ions O_2^-, O^-, O_3^-, NO_2^-. Mutual neutralization can proceed via two-body, e.g., $O_2^+ + O_2^- \rightarrow O_2^* + O_2^{**}$, or via three-body (Thomson), e.g., $O_2^+ + O_2^- + M \rightarrow O_2^* + O_2^{**} + M$, collisions. Ratcliffe[28] gives the Thomson coefficient for the D-region as $\alpha_T = 6.65 \times 10^{-9} \left(\frac{273}{T}\right)^{3/2} \rho$ cm^3/sec, where ρ is pressure in mm of Hg and T is temperature in ^oK. Loeb[29] states that this value may level off at $\sim 3 \times 10^{-9}$ cm^3/sec. The effective two-body coefficient probably lies somewhere in the range 10^{-9} to 3×10^{-8} cm^3/sec. The bare facts are, however, that we really know little about this very important process. If it should be definitely determined that NO^+ and O_2^- are the predominant positive and negative ions in the altitude range of interest, it may be possible to make laboratory measurements of the ion-ion recombination coefficient. The difficulties involved are obviously very great. It may be preferable to conduct <u>in situ</u> measurements (as proposed in Section VI) to obtain the effective ion-ion recombination coefficient as a function of altitude.

7. Radiative Recombination

Radiative recombination processes are those of the type $O^+ + e^- \rightarrow O + \gamma$. The associated recombination coefficients[30] are of the order 10^{-12} cm^3/sec. These values are much too small for the coefficients to be of interest in the D-region.

8. Temperature Effects

It is known that the various relaxation parameters are functions of the electron temperature. For example, the dissociative recombination coefficient has the functional form[31] $\alpha_D \sim kT^{-M}$ where $1/2 \leq M \leq \frac{3}{2}$. Hence one must be careful in applying the results of geophysical experiments to nuclear blackout conditions until more is learned about (a) electron temperatures in the blacked-out ionosphere, and (b) the temperature dependence of the relaxation coefficients.

REFERENCES

1. Evans, R. C. The Atomic Nucleus (McGraw-Hill, New York, 1955).

2. Handbook of Chemistry and Physics, (Chemical Rubber Publishing Co., Cleveland, 1955).

3. Watanabe, K. Ultraviolet Absorption Processes in the Upper Atmosphere, Advances in Geophysics 5, 153 (Academic Press, New York, 1958).

4. Barth, C. A. Nitrogen and Oxygen Atomic Reactions in the Chemosphere. International Symposium on Chemical Reactions in the Lower and Upper Atmosphere. Interscience Publishers 1961.

5. Handbook of Geophysics (Rev. Ed.), GRD, Air Force Research Division, ARDC (Macmillan Co., New York, 1960). Figure 8-2.

6. Fox, R. E. (Private communication).

7. Johnson, C. Y., J. P. Heppner, J. C. Holmes, and E. B. Meadows. Results Obtained with Rocket-Borne Ion Spectrometers. IGY Rocket Report Series No. 1, 123, (30 July 1958); Townsend, J. W., C. Y. Johnson, J. C. Holmes, E. B. Meadows. Atmospheric Composition at Arctic High Altitudes. IGY Rocket Report Series No. 1, 131, (30 July 1958).

8. Biondi, M. A. and S. C. Brown. Measurement of Electron-Ion Recombination. Phys. Rev. 76, 1697 (1949).

9. Holt, E. H. Electron Loss Processes in the Oxygen Afterglow. Bull. Amer. Phys. Soc. 4, 112 (1959).

10. Bates, D. R. Solar Eclipses and the Ionosphere, Sect. V, p. 191 (Pergamon Press, London, 1955).

11. Bates, D. R. and M. Nicolet. Ion-Atom Interchange, J. Atmos. and Terr. Phys. 18, 65 (1960).

12. Hertzberg, M. Ion-Neutral Reactions, J. Atmos. Terr. Phys. 20, 177 (1961).

13. Dickinsen, P. H. G., and J. Sayers. Ion Charge Exchange Reactions in Oxygen Afterglows, Proc. Phys. Soc. 76, 137 (1960).

14. Cook, C. J. and C. M. Ablow, (1959), A Feasibility Study: Superimposed Beams--A Technique for Determining Two-Body Reaction Cross Sections, Scientific Report No. 1, Contract No. AF19(604)-3475, AFCRC-TN-59-472.

15. Biondi, M. A. Measurements of Electron Attachment, Recombination, Elastic and Inelastic Collisions in Atmospheric Gases. Planet. Space Sci. 5, 104 (1961).

16. Burch, D. A., S. J. Smith, and L. M. Branscomb. Photodetachment of O_2^-, Phys. Rev. 112, 171 (1958).

17. Phelps, A. V. and J. L. Pack. Collisional Detachment in Molecular Oxygen. Phys. Rev. Lett. 6, 111 (1961).

18. Jortner, J. and U. Sokolov. Spectrophotometric Determination of the Electron Affinities of Some Diatomic Molecules. Nature 190, 1003 (1961)

19. Branscomb, L. M., D. S. Burch, S. J. Smith and S. Geltman. Photodetachment Cross Section and Electron Affinity of Atomic Oxygen. Phys. Rev. 111, 504 (1958).

20. Chanin, L. M., A. V. Phelps, and M. A. Biondi. Measurement of the Attachment of Slow Electrons in Oxygen. Phys. Rev. Lett. 2, 344 (1959).

21. Biondi, M. A. Atomic Collision Processes Involving Electrons and Ions in Atmospheric Gases. International Symposium on Chemical Reactions in the Lower and Upper Atmosphere. Interscience Publishers, 1961.

22. Bailey, D. K. and L. M. Branscomb. Rate Coefficient for O_2 Collisional Detachment. Bull. Amer. Phys. Soc. 5, 123 (1960)

23. Bowhill, S. A. The Effective Recombination Coefficient of an Ionosphere Containing a Mixture of Ions. J. Atmos. Terr. Phys. 20, 9 (1961).

24. Kasner, W. H., W. A. Rogers, and M. A. Biondi. Electron-Ion Recombination Coefficients in Nitrogen and Oxygen. Phys. Rev. Lett. 7, 321 (1961)

25. Faire, A. C. and K. S. W. Champion. Measurements of Dissociative Recombination and Diffusion in Nitrogen at Low Pressures. Phys. Rev. 113, 1 (1959)

26. Lin, S. C., AVCO Research Note No. 210 (1960)

27. Crain, C. M. Ionization Loss Rates Below 90 km. J. Geophys. Res. 66, 1117 (1961).

28. Ratcliffe, J. A., Ed. The Physics of the Upper Atmosphere (Academic Press, New York, 1958), p. 385.

29. Loeb, L. B. The Basic Processes of Gaseous Electronics (University of California Press, Berkeley, 1955).

30. Mitra, S. K. The Upper Atmosphere (2nd Ed. The Asiatic Society, Calcutta, 1952), p. 308.

31. Bortner, C. W., M. H. Baulknight. Deionization Kinetics. Scientific Report. Contract No. AF 19(604)-8820. Space Sciences Laboratory, Missile and Space Vehicle Department, General Electric Co. Philadelphia, Pennsylvania, July, 1961.

IV PERTINENCE TO NUCLEAR DETONATION EVENTS

A. Auroral and Bomb Events

1. Ionization

Because the primary source of auroral radiation (protons, electrons) persists for a long time and because of the long range of the secondary source of radiation (bremsstrahlung photons) the auroral events are somewhat similar to the ionization effects of the high altitude fission product cloud. The decay of the radioactive cloud does, however, follow a definite decay law while the auroral ionization generally fluctuates before decaying. Electron production rates are also larger in the fission product cloud than in the auroral ionization region. In general the auroral electrons and γ rays are of lower energy (about 1 order of magnitude) than the corresponding radiations from fission products.

Although the general level of ionization may persist for periods of hours, the short individual brehmsstrahlung bursts may have rise times substantially less than one second and thus may be similar in time characteristics to the pulses of prompt radiations from nuclear events. The properties of nuclear burst-induced ionization and auroral events are summarized in Table IV-1 for ready comparison.

Polar cap absorption is a manifestation of high energy protons (5 Mev to 1 Bev) and perhaps other high energy ions striking the polar upper atmosphere and producing considerable ionization. These events, which usually commence about half-hour to several hours after a solar flare, are generally confined to polar regions because of the influence of the geomagnetic field. However, some polar cap events do spread to and south of the auroral zone during the associated magnetic storm. Since protons of energy 10 Mev have a horizontal range of 10 km at altitudes of 60 km, they can penetrate quite deeply into the ionosphere (e.g., to altitudes of less than 40 km at a geomagnetic latitude of 65°). Hence their ionization effects are in many ways similar to those of fission products, although the electron production rates are

much less than those within the fission product cloud. The time variation of a polar cap event is also somewhat similar to the decay of the fission product cloud; it is characterized by a rapid initial increase followed by a short period of high, fluctuating particle flux. This is followed by a long period of gradually decreasing flux which may last as long as several days. The comparative simplicity of the polar cap absorption phenomenon during the latter phase would make interpretation of the experimental data relatively easy.

Both the proton events and the auroral bremsstrahlung are known to penetrate to the 30-50 km region where ionization from fission gammas is also expected to occur.

2. Radio Effects

Generally speaking, we are able to present a detailed account of the emissions from a typical nuclear detonation, but we do not necessarily know the details of the reaction of these emissions with the atmosphere. The process of understanding is reversed, however, in the case of the natural aurora. The reactions in the atmosphere (visible light of the aurora) are well known, but only recently have we begun to learn what incoming radiations are incident on the upper atmosphere to create the phenomenon of the aurora.

Let us consider four types of radiations and their general nature in the case of a high-altitude nuclear detonation, making comparisons, where possible, with the case of a natural aurora.

A. Prompt X-ray, γ-ray and Neutron Radiation

The prompt uncharged radiation effects from nuclear detonations show up mainly as radio-wave absorption. The X-rays are stopped in the atmosphere when they have penetrated to about 80-km height. This is in the vicinity of the upper ionospheric D-region where long ionization lifetimes enable the effect to far outlast the required formation time (on the order of seconds to minutes) and where electron collision frequencies are comparable to radio wave frequencies.

The gamma and neutron radiations are stopped at altitudes on the order of 25 km, where ionization lifetimes are extremely short. Thus, the X-ray radiations give rise to radio wave attenuation at least 10^4 more severe than that caused by the gamma and neutron radiation, and lasting much longer. Above about 60 km, absorption measured in decibels is inversely proportional to the square of the radio frequency.

These prompt radiations are comparable to the solar radiations responsible for the sudden ionospheric disturbances (SID) which are discussed elsewhere. There is evidence that X-rays are associated with auroras occurring at auroral and sub-auroral latitudes from balloon flights made at altitudes up to 30 km. These X-rays are undoubtedly bremsstrahlung from high-speed electrons impinging on the atmosphere at higher altitudes.

b. Prompt Charged-particle Radiation

Prompt charged-particle radiations from nuclear detonations are believed to be responsible for the ARGUS shell excitation. At radio wavelengths, there is the possibility of weak synchrotron radiation, but none has been positively identified from past tests. The electromagnetic pulse emitted by the detonation may be initiated by the unbalanced electron emission at the time of detonation.

For a discussion of charged-particle excitation of the natural aurora, see the comparison with delayed beta emissions of the fission debris in (d) below.

c. Delayed X-ray and γ-ray Radiation

The delayed, uncharged emissions of the fission debris give important radio effects. The main problem in estimating the degree of this effect is in charting the motion and divergence of the fission cloud itself. For example, a multi-megaton detonation at sea level is capable of pushing debris above about 20-km height so that gamma-shine upwards produces measurable absorption on 30 Mc. In this case, no radio effects (aside from the electromagnetic pulse emission) are noted at all until about 5 min after the detonation. For detonation heights

above 25 km, the effects of prompt emissions generally exceed the effects of delayed emissions to an extent that is partially dependent upon geometry of the observing station with respect to the burst (grouping the charged and uncharged fission debris emissions together because the distinction is not always clear experimentally). The smoke-ring-like rise of fission products from shots such as YUCCA, ORANGE, and TEAK is an important feature which must be taken into account in estimating the radio effects. Long after the shot, these same fission debris apparently take the form of a large flat invisible cloud, several thousand kilometers in lateral extent, resting at an altitude on the order of 150 to 200 km. Points beneath such a cloud would be bombarded by long-lasting γ-ray radiation. For detonation heights exceeding several hundred km, the "pancake" shaped debris cloud is predicted to form immediately over a large area. From a radio point of view, this would replace a large radio effect in a small region with a milder radio effect over an extensive geographical area.

As with prompt radiation (a) these effects may be analogous in some limited ways to auroral bremsstrahlung. However, radio effects of auroral bremsstrahlung have not been studied sufficiently to allow comparions.

d. Delayed Charged-particle Radiation

Delayed, charged emissions from the fission debris of high-altitude nuclear detonations have important radio effects. For a distant observer beyond line-of-sight of the detonation, these are comparable to or may exceed the prompt effects.

Fission nuclear detonations in the atmosphere at altitudes exceeding $\sim$ 40 km give clear indication of charged particle emissions that are confined by the earth's magnetic field. The charged particle energies are such that the particles are stopped chiefly at altitudes on the order of 50 to 100 km. This is adequately described by the early beta energy spectrum from fission debris but positively charged fission debris must also be present. Our information on location of

the important stopping region comes from observations and photographs of visible "nuclear" aurora, although there is also some information from radio-echo data.

It would be well at this point to dwell on the similarities exhibited by nuclear and natural aurora:

(1) Both forms are aligned along the earth's magnetic field (which is oriented at a gentle slope in the Johnston Island area but tilted at a steep angle in the Arctic).

(2) There is fine structure within both auroral forms, which changes with time. This change might be called "undulation" or "motion of a drapery viewed edge-on." Since the motion of charged particles in a constraining magnetic field is diamagnetic, instability theory might well provide a useful basis for discussion of this and related structural phenomena. (The undulating phenomena, although familiar in the natural aurora, are not well documented for nuclear aurora.)

(3) At radio wavelengths, both types of aurora are accompanied by absorption (presumably at the bottom of the formation) and are capable of scattering or reflecting radio waves, particularly at HF but also at VHF and even UHF. The echoes from both types of aurora tend to occur at heights from ~ 100 km to ~ 150 km and are strongest when observed at right angles to the earth's magnetic field. When nuclear aurora is observed by high resolution radar, fine structure as small as 10 km is noted, which is not unlike the ray structure typical of one kind (discrete) of natural aurora.

(4) Both types of aurora are accompanied by disturbance of the earth's magnetic field, which is readily observable with standard slow-response instruments at the earth's surface.

(5) Although the main portion of the visible light generated by both kinds of aurora occurs below ~ 150 km, fainter auroral light has been observed at heights up to ~ 600 km and might be observed even higher.

Although the aurora created by a nuclear detonation closely resembles the natural aurora, it has the following distinctive features:

(1) Nuclear aurora can extend to heights below 50 km whereas the natural aurora seldom is seen below about 80 km. This is undoubtedly a consequence of the differing energies of the source particles approximately 1 Mev electrons for nuclear aurora, but primarily 10 kev electrons for natural aurora).

(2) Since nuclear detonations originate from relatively small points, the extent of the nuclear aurora at right angles to the field is less than 100 km for the first 5 minutes (for the tests which have been made so far). The natural aurora, on the other hand, has been documented to extend in arcs across almost the entire North American continent, or, in the case of glows and extreme activity, can cover at least the entire sky observable from one station. It is this difference that has made some of the wide-angle-radar data on nuclear aurora difficult to compare with natural aurora.

(3) Based on the author's visual observations, the nuclear aurora is more intensely multi-hued than even the most remarkable natural aurora. This may be a result of its lower height (different excitation particles) or may be the result of bombardment by positively-charged fission debris.

It should be remembered, however, that the nuclear aurora and the natural aurora are remarkably similar in their properties, at least according to our present limited and inadequate observations.

B. Sudden Ionospheric Disturbances (SID) and Bomb Events

1. Ionization

As stated earlier, the enhanced ionization present during an SID results in severe high frequency signal absorption predominantly in the altitude range 75 to 85 km. Because the nuclear radiation penetrates to lower altitudes, the absorption associated with "nuclear blackout" may occur at somewhat lower altitudes depending on the altitude of burst. The SID also varies fairly rapidly in time, at least compared with auroral absorption and fission product decay, although not nearly so rapidly as the ionization produced by the initial radiation from a nuclear explosion. The ionic species present during an SID are expected to be quite similar to the species present during "nuclear blackout":

NO^+, N_2^+, O_2^+, N^+, O^+, O_2^-, O^-, although the proportion of N^+ and O^+ present may be lower in the former case. This is due to the fact that in the ionization of a diatomic gas the ratio of atomic to molecular ions rises with increasing energy of the ionizing particles. The nature of the ionizing particles present during an SID is, of course, quite different from those present in a fission product cloud.

2. Radio Effects

a. Natural Origin

The natural SID is due to a pulse of solar X-rays which enhances the ionization particularly in the height range of 60-100 km. The radio effects are the result of the establishment and decay of the enhanced ionization, and could be accurately predicted if the ionization distribution were well known. However, since this is not the case, the observed radio effects are often used in the converse sense to deduce information regarding the extra ionization.

The ionizing X-ray flux from the sun rises to a maximum in a few minutes and subsequently decays over a time of perhaps ten minutes. The maximum electron density produced--and therefore the resulting radio effects--tends to lag slightly behind the maximum of the ionizing flux. Subsequently, the rate of decay of ionization by attachment and recombination processes depends upon the exact height in the ionosphere that is concerned. Generally speaking, since the major radio effects result from the ionization between 60 and 100 km, the radio phenomena have their peak some ten minutes after the start of a strong SID and take about an hour to return to the normal undisturbed state.

The radio effects may be conveniently divided according to whether they are dominantly due to absorption or not; this, in turn, implies a subdivision according to frequency. Frequencies exceeding some 2 Mc/s will have to penetrate the D-region during their propagation. This applies both to communcation between a transmitter and receiver on the earth's surface, in which case the propagation link is usually by reflection from

the E and F layers at heights of about 120 and 220-320 km, respectively, and also to the reception, normally at a frequency exceeding 15 Mc/s, of noise from a cosmic source. The waves suffer considerable absorption during their passage through the enhanced D-region ionization.

On the other hand for frequencies in the VLF and LF bands (3-300 kc/s), the electron density is sufficient for reflection before a wave, incident from below, has penetrated greatly into the normal D-layer. The increased ionization acts to some extent to improve the reflecting properties of the lower D-region, and can therefore lead to better propagation at VLF.

b. Absorption Effects

Suppose a wave of frequency f is propagating vertically through the ionosphere. Then for nondeviative absorption in which the refractive index is effectively unity, the absorption coefficient k may be written[1] as

$$k(h) \approx 4.6 \times 10^4 \frac{N_e \nu}{4\pi^2 f^2 + \nu^2} \text{ db/km} \qquad (1)$$

where ν is the electron collisional frequency, f the operating frequency, and N_e the electron concentration per cm^3. N_e, ν, and therefore k, are all functions of height, h.

Several profiles of N_e against h, both under quiet daytime and SID conditions, appear in the literature. There are considerable discrepancies between these individual profiles and indeed great variations undoubtedly actually occur; standard models are of limited applicability. However, mainly for illustrative purposes, two profiles under normal daytime and SID conditions, respectively, are shown in Figure IV-1. Using these profiles, the collisional frequencies given by Nicolet,[2] and relation (1), the absorption coefficient has been plotted in Figure IV-2 as a function of height; the two frequencies of 20 Mc/s and 50 Mc/s are considered and both SID and normal conditions are included. It can be seen that absorption is less pronounced at the higher frequency, and

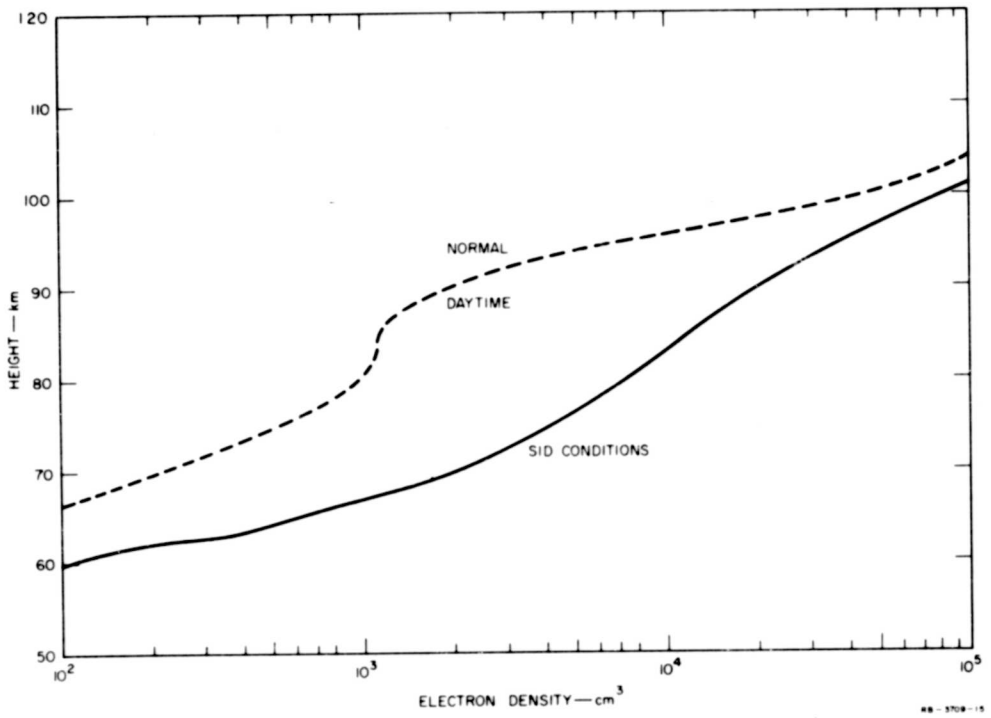


FIG. IV-1 ELECTRON DENSITY PROFILES FOR SID AND NORMAL CONDITIONS

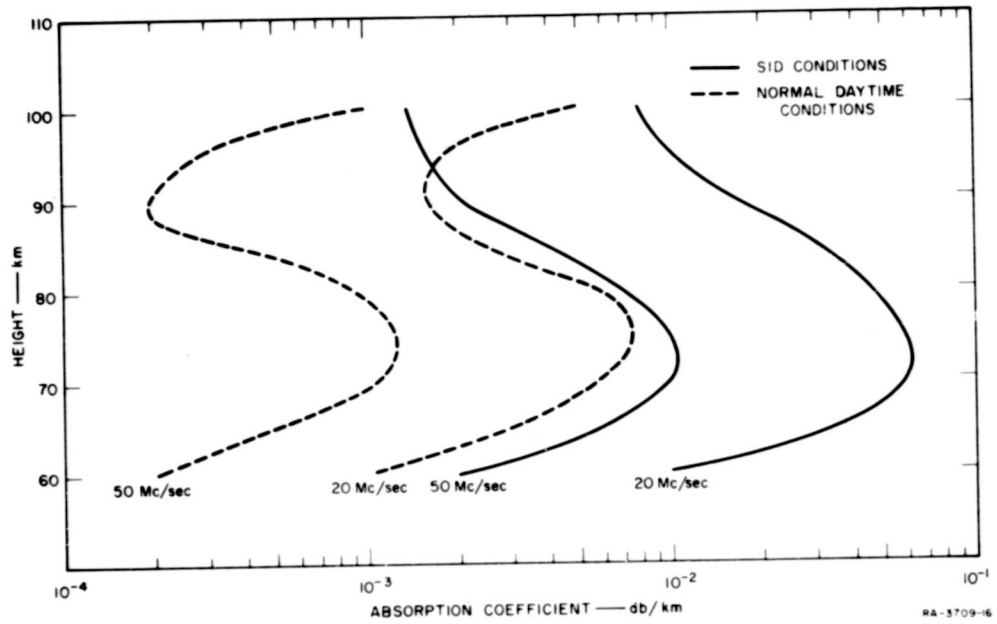


FIG. IV-2 ABSCRPTION COEFFICIENTS FOR SID AND NORMAL CONDITIONS

that an SID increases the absorption coefficient by about an order of magnitude.

The absorption associated with an SID is commonly detected in two ways. Cosmic noise sources may be monitored by riometers; the increase in absorption is termed a sudden cosmic noise absorption (SCNA). The absorption is of course observed for a one-way path, and at frequencies that completely penetrate the ionosphere, that is exceeding some 15 Mc/s. The other absorption effect is on frequencies normally reflected from the E and F layers. Here, since there is both an upward and a downward path, and the frequency is less than 15 Mc/s the absorption can be very great. Indeed, there is often an early and complete disappearance of signal so that the details of the phenomenon cannot be studied. The effect is known as a sudden short wave fadeout (SWF).

c. Effects at VLF

Radio frequencies in the VLF and ELF bands (< 30 kc/s) are normally propagated in the wave-guide formed by the earth and the lower edge of the ionosphere.[3] There is little penetration into the D-region and consequently little absorption. The increased D-region ionization associated with an SID causes a lowering of the upper boundary of the wave-guide, typically from a height of 70 km to 65 km or less, and a consequent narrowing of the guide. At the same time there is a modification of the conductivity at the upper edge. The influence of these effects is somewhat complicated but the modification to the propagational attenuation coefficient for long horizontal distances is depicted on Figure IV-3. A frequency of 27 kc/s, for instance, is less attenuated during an SID than under normal circumstances. This leads to the effect known as the sudden enhancement of atmospherics (SEA), which is merely the increase, accompanying an SID, in noise, at certain frequencies, due to atmospherics of distant origin.

A very sensitive indicator of enchanced ionization in the lower D-layer is the phase change detectable when a VLF transmitter is being received. The effect is known as a sudden phase anomally (SPA). The SPA

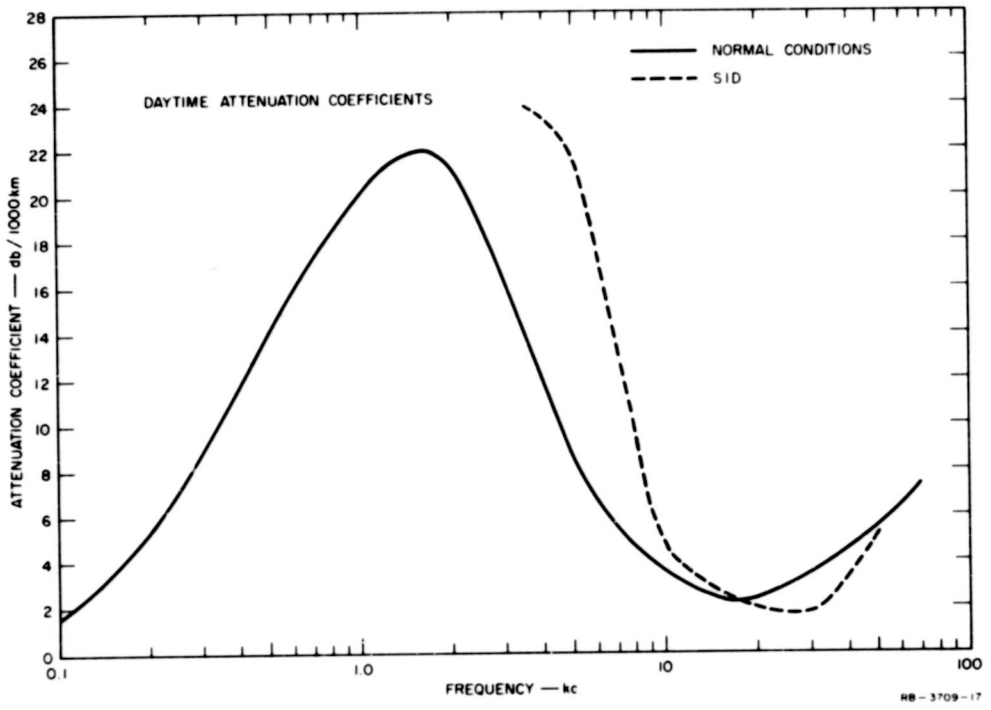


FIG. IV-3 ATTENUATION COEFFICIENTS FOR SID AND NORMAL CONDITIONS

is detectable even for frequencies between 15 and 20 kc/s where there is little change in amplitude for long distance propagation. This is because phase changes are primarily due to alterations in the width of the waveguide; the change in conductivity at the upper boundary is of secondary importance. At vertical incidence an SID may give, at a frequency of 16 kc/s, an alteration in reflection height of 5 km in 5 minutes; that is, a rate of change of phase of some 40° per minute or a Doppler frequency variation exceeding 1 in 10^7. Path lengths of up to 500 km give similar results, but for paths of some 4000 km the peak Doppler effect that has been observed is about 8 in 10^8.

d. Radio Effects Not Due to D-Region Ionization

Solar flares do not produce increased ionization solely in the D-layer, but also in the E-region[4] and even in F.[5] The observation of the effects is difficult because of the masking influence of the enhanced D-layer ionization. However, it seems that a strong SID will have associated radiation effective in ionizing E-region levels, with a significant flux persisting for 25 to 120 minutes. Typically, the resultant ionization is sufficient an hour after the onset of the SID to raise the ordinary critical frequency of the E-layer by some 5%.

Flare effects in the F-region are less frequent, but drops of 18 km in the reflection height at 20 Mc/s have been observed. Only the rare flares that give large outbursts of solar cosmic rays seem to be effective in increasing F-layer ionization; it is probable that these flares, besides being unusual in their cosmic ray output, are also unusual in their photon emission, and that it is the latter factor that is responsible for the F-layer phenomena.

e. Nuclear Origin

Most of the radiation and particles emitted by a nuclear explosion have properties that result in the production of ionization in the D-region. For an explosion occurring in space, X-rays and β particles deposit most of their energy at D-layer heights, although

γ rays and neutrons penetrate considerably more deeply. An explosion at ground level can also produce D-layer ionization. The fireballs due to megaton shots only stabilize within the lower or intermediate stratosphere.[6] Although X-rays and β particles are quickly absorbed in the lower atmosphere, it has been shown[7] that γ rays from fission products at heights of some 30 km generate ionization at all altitudes above. Although the rate of production decreases with height so does the rate of loss, and a situation arises in which a maximum of persistent ionization occurs at a height of about 75 km. For explosions intermediate between the troposphere and space the phenomena are complicated in that all the ionizing constituents may produce significant effects. However, it again appears that the most important ionizing results will be in the D-region.

Since both natural SID's and nuclear explosions have the effect of enhancing D-layer ionization, their radio effects are very similar in many respects. There are distinctions, however. The most important of these is that the ionizing flux from the sun takes a few minutes to reach its maximum, whereas in the case of most nuclear explosions the prompt flux will be greatest and there will be a steady decay thereafter. Thus the radio effects should have a far more sudden onset for the nuclear event than for the natural SID. For instance, the VLF phase change has been quoted as 40° per minute for a natural disturbance; in a typical nuclear incident the same phase change would occur in a fraction of a second.

It should be pointed out that this onset criterion is not infallible. For instance it is conceivable that a tropospheric explosion in which the prompt ionizing influences are quickly absorbed in the lower atmosphere, can produce D-layer ionization as the radioactive products are carried upwards on the ascending fireball, and that the resulting time variation of the rate of production could be very similar to that associated with a normal SID. It cannot be over-emphasized that the radio effects resulting from a nuclear explosion are very sensitive functions of the altitude and charcteristics of the shot.

C. "Quiescent" Conditions and Bomb Events

1. Ionization

Ionization in the quiescent D-region probably results from ionization of nitric oxide by solar Lyman-α, although ionization of nitrogen and oxygen by solar X-rays may be an important contributor. The dominant initial positive ion species formed during SID's, auroral events, PCA events, and during and after nuclear explosions are N_2^+ and O_2^+. If ion-atom interchange processes of the type

$$O_2 + N_2^+ \rightarrow NO^+ + NO$$

are sufficiently rapid, the N_2^+ and O_2^+ will soon disappear, however, and NO^+ will become the dominant positive ionic species. This point is not yet clear. If NO^+ is dominant under all conditions of ionization, the exact nature of the ionizing radiation is irrelevant and the important ionic species present are similar to those occurring in the disturbed D-region as well as in the fission product cloud. The properties of nuclear burst-induced ionization and of the normal D-region are summarized in Table IV-1 for ready comparison.

2. Radio Effects

Any radio effects associated with nuclear explosions are principally due to increased ionization in the D-region. The influence of this enhanced electron content is best detected by absorption studies and by the modifications to VLF propagation. As nuclear weapons will tend to produce sudden changes, the natural events where the rate of variation in D-layer ionization is large are most likely to prove instructive in predicting the behavior under conditions of nuclear warfare. The natural variations may be conveniently subdivided into two categories--systematic and transient. Diurnal and seasonal changes are characteristic of the first category; sudden ionospheric disturbances, magnetic storm effects, and so on, represent transient influences.

C. "Quiescent" Conditions and Bomb Events

1. Ionization

Ionization in the quiescent D-region probably results from ionization of nitric oxide by solar Lyman-α, although ionization of nitrogen and oxygen by solar X-rays may be an important contributor. The dominant initial positive ion species formed during SID's, auroral events, PCA events, and during and after nuclear explosions are N_2^+ and O_2^+. If ion-atom interchange processes of the type

$$O_2 + N_2^+ \rightarrow NO^+ + NO$$

are sufficiently rapid, the N_2^+ and O_2^+ will soon disappear, however, and NO^+ will become the dominant positive ionic species. This point is not yet clear. If NO^+ is dominant under all conditions of ionization, the exact nature of the ionizing radiation is irrelevant and the important ionic species present are similar to those occurring in the disturbed D-region as well as in the fission product cloud. The properties of nuclear burst-induced ionization and of the normal D-region are summarized in Table IV-1 for ready comparison.

2. Radio Effects

Any radio effects associated with nuclear explosions are principally due to increased ionization in the D-region. The influence of this enhanced electron content is best detected by absorption studies and by the modifications to VLF propagation. As nuclear weapons will tend to produce sudden changes, the natural events where the rate of variation in D-layer ionization is large are most likely to prove instructive in predicting the behavior under conditions of nuclear warfare. The natural variations may be conveniently subdivided into two categories--systematic and transient. Diurnal and seasonal changes are characteristic of the first category; sudden ionospheric disturbances, magnetic storm effects, and so on, represent transient influences.

Table IV-1

PERTINENT IONIZING EVENTS

Type Event	Energy of Emitted Radiation	Energy Fluxes of Emitted Radiation	Ionization Processes	Ionization Rates	Penetration Into Atmosphere	Time-Intensity Characteristics
Nuclear Burst (1 MT)	Prompt rad. 1. Thermal X-rays temp ~ 1 kev initially; fireball cools rapidly	Initial flux ~ 10^{33} ev/sr	Photo-ionization of N_2, O_2 to yield N_2^+, O_2^+, N^+, O^+	Causes complete ionization within and just outside fireball	1 kev X-ray penetrates horiz. dist. of ~10 m at 60 km alt. ~100 m at 80 km alt. 3 kev X-ray: ~ 200 m at 60 km ~ 2 km at 80 km	Almost all emission within 1 μs Intensity decreases rapidly after burst (radiation ceases within ~10 sec after burst).
	2. γ rays* $\bar{E} \approx 1$ Mev	Initial flux ~10^{30}ev/sr	Ionization of N_2, O_2 by Compton scattering & Moller scattering by secondary electrons	At horiz. dist. of 100 km from burst: ~10^{12}/cm^3 sec at 60 km alt.	Horiz. range at 60 km alt. ~500 km	These radiations are emitted within a few μsec. after burst
	3. Neutrons* $\bar{E}$ ~ 10 Mev	Same as 2. above	Produces 10 Mev protons by reaction $N^{14}(n,p)C^{14}$; protons ionize N_2, O_2; secondary electrons ionize by Moller scattering	At horiz. dist. of 100 km from burst: ~10^3/cm^3 sec	Horiz. mean free path for (n,p) reaction at 60 km alt.: ~10^4 km	
	*Energy fluxes and ionization rates are estimated to within 2 orders of magnitude					
	Delayed (β & γ emission by fission products 1 hour after burst). 1. β-particles $\bar{E}$ ~ 2 Mev	~2 ergs/cm^2 sec at edge of fission product cloud**	Moller scattering; production of bremsstrahlung which ionizes N_2, O_2 by Compton scattering, photo ionization	~10^8/cm^3 sec within and just outside fission product cloud	Horiz. range of 1 Mev electrons: ~10 km at 60 km alt.	Decay of fission products follows a ~ $t^{-5/4}$ law
	2. γ rays $\bar{E}$ ~ 100 kev to 1 Mev	0.5 ergs/cm^2 sec	Compton scattering	10^2 cm^3/sec outside fission product cloud	Horizontal range of 1 Mev γ-rays: ~500 km at 60 km alt.	
	**Fission product cloud dimensions assumed to be 200 km horiz. diameter, 30 km thick.					

Type Event	Energy of Emitted Radiation	Energy Fluxes of Emitted Radiation	Ionization Processes	Ionization Rates	Penetration Into Atmosphere	Time-Intensity Characteristics
Auroral	1. Electrons $\bar{E}$ = 10 to 250 kev	0.01 to 1 erg/cm^2 sec	Moller scattering of bound electrons in O_2, N_2	~10^4/cm^3 sec at 80 km alt.	~75 km	Fairly steady, lasting as long as several days; time variation follows no simple pattern.
	2. X-rays (bremsstrahlung) E = 10 to 100 kev	10^3 to 10^5 photons/cm^2 sec	Largely photo-ionization; some Compton scattering of bound electrons in O_2, N_2	~10/cm^3 sec at 40 km alt	< 40 km alt	
	3. Protons E ~ same as 2. above	--	--	--	Above 100 km	
	4. Lyman α resulting from electron attachment to protons λ = 1216A	unknown	Photo ionizes nitric oxide	unknown	~70 km	
Polar Cap	1. Protons and heavy ions E = 10 Mev to 1 Bev or more	Flux ~ 500/cm^3 sec for E = 30 to 100 Mev ~2/cm^3 sec for E = 100 to 400 Mev	Stripping of electrons from N_2, O_2	At geomagnetic latitudes > 65°: ~3 x 10^2/cm^3 sec at altitudes of 40 to 80 km	< 40 km alt	Increases rapidly about 1/2 to 1 hour after solar flare; gradually decreases over period of several hours
	2. γ rays from (p,γ) reactions	See Section IB2e				
SID (class 2 flare)	X-rays λ = 2 to 8A	~0.1 ergs/cm^2 sec	Photo ionization of N_2, O_2	~10^3/cm^3 sec at 80 km alt; ~1/cm^3 sec at 65 km alt.	70 to 90 km alt	In general characterized by a rapid increase followed by a slow decrease and softening of spectrum. Typical 2+ flare X-ray pulse ~ 40 to 30 min.
	λ = 1 to 2A	~10^{-3} ergs/cm^2 sec			~65 km alt	
Quiet D-region	1. X-rays λ = 2 to 8A (high sunspot activity)	≲10^{-2} erg/cm^2 sec	Photo ionization of N_2, O_2	≲10/cm^3 sec at 80 km alt	70 to 90 km	Fairly regular dirunal variations; maximum ionization occurs shortly after noon
	λ = 2 to 8A (low sunspot activity)	≲10^{-6} erg/cm^2 sec		~10^{-2}/cm^3 sec at 80 km alt	70 to 90 km	
	2. Lyman α λ = 1216A	~6 ergs/cm^2 sec	Probably photo ionization of NO	~0.1/cm^3 sec at 80 km alt	~70 km	

The D-region is formed by the ionizing action of cosmic rays, and of Lyman α and X-ray emissions. Since the latter two are of solar origin, it is not surprising that the D-layer shows a marked diurnal variation; indeed, it may be said practically to disappear at night, the absence of photodetachment being then an important contributory factor. Diurnal alterations in VLF phase[8] and in absorption[9] both show a regular dependence upon solar zenith angle; the absorption is never strong and consequently can be conveniently studied in terms of f_{min}, the minimum frequency at which a signal can be obtained using conventional ionosondes. The most rapid D-layer variations occur at sunset and sunrise, for instance a VLF phase change of 4° per minute is typical for these times of day. Seasonal and solar cycle effects are other examples of systematic D-region behavior, but the time-scale bears little relation to that of nuclear events.

Regarding transient incidents the most important--the sudden ionospheric disturbance (SID)--have already been considered. Effects associated with magnetic storms may last for several days; they are intimately related with auroras and can be extremely complicated. Both absorption and VLF propagation are subject to changes, rapidly fluctuating spatially and temporally; this kind of turbulent component is often superimposed upon a variation of much longer period, one aspect of which is a partial elimination of the normal diurnal changes. At VLF a typical frequency deviation over a long distance path during a magnetic storm is 2 parts in 10^{8}. Meteors produce sudden sporadic ionization in the D-layer. They thus give transient absorption and VLF[10] effects, for which the rates of change are comparable with those during magnetic storms. There is some evidence that thunderstorms can generate local D-region ionization. Finally, the influence of fluctuations in incoming cosmic rays should be mentioned. The changed flux could be due to an increased solar output of energetic particles--the mechanism responsible for the polar cap absorption. Alternatively, distortions of the field distribution accompanying magnetic storms entail a modification of the latitudinal energy cutoff;[11] thus although the original radiation may have unchanged characteristics, the flux and mean energy of the particles reaching a particular latitude will alter as a result of a magnetic perturbation basically of solar origin.

REFERENCES

1. See for instance J. A. Ratcliffe, The Magneto-Ionic Theory. Cambridge University Press, Cambridge, England (1959)

2. Nicolet, M. The Collision Frequency of Electrons in the Ionosphere. Phys. Fluids, 2, 95-99 (1959)

3. See for instance J. R. Wait, Terrestrial Propagation of Very-Low-Frequency Radio Waves. J. Research NBS, Vol. 64-D, pp 153-203 (1960)

4. Bazzard, G. H. Enhancement of Ionization in the E-Layer Due to Solar Flares During the IGY. Nature, 189, 47-48 (1961)

5. Knecht, R. W. and K. Davies. Solar Flare Effects in the F-Region of the Ionosphere. Nature, 190, 797-798 (1961)

6. Martell, E. A. Atmospheric Aspects of Sr-90 Fallout. Science, 129, 1197-1205 (1959)

7. Pierce, E. T. Ionization Below 100 km Due to Radioactive Clouds. Technical Memorandum, SRI Project No. 3097 (1961)

8. Bracewell, R. N., K. G. Budden, J. A. Ratcliffe, T. W. Struker, and K. Weekes. The Ionospheric Propagation of Low and Very-Low-Frequency Radio Waves Over Distances less than 100 km. Proc. Inst. Elect. Engrs., 98(III), 221-236 (1951)

9. Appleton, E. V. and W. R. Piggott. J. Atmosph. Terr. Phys., 5, 141 (1954)

10. Chilton, C. J. VLF Phase Perturbation Associated with Meteor Shower Ionization. J. Geophys. Res., 66, 379-384 (1961)

11. Meyer, P. and J. A. Simpson. Changes in the Low-Energy Particles Cutoff and Primary Spectrum of Cosmic Rays. Phys. Rev., 106, 568-571 (1957)

V SOLAR ACTIVITY EXPECTED DURING THE 1963-67 PERIOD

Since the geophysical phenomena of interest to this study are either directly or indirectly caused by solar phenomena, it is obviously necessary to consider solar characteristics very carefully. Solar activity can generally be related to sunspot number, which characteristically varies with a cycle of approximately 11 years. This is illustrated in Figure V-1. The period of interest (1963-67) would be a particularly good period to study solar activity and related terrestrial effects because it begins relatively quiet (sunspot minimum 1963-65), continues through a period (1965-67) of increasing activity, and ends at a relatively active point in the new solar cycle. If we assume that the smoothed sunspot number is an index of activity, the level of activity in 1967 should be well over half of the peak value for that cycle. Thus a research program planned for the period 1963-67 can allow time for the important problems of instrument development and experimental design as well as exploratory measurements of the ionosphere under quiescent solar conditions. This should provide an excellent baseline for the interpretation of results obtained during the more interesting period of increasing solar activity.

It may be useful at this point to discuss some of the parameters of solar activity.

1. Sunspot Number

The sunspot number is defined as follows:

$$R = k(s + 10\,g)$$

where s is the total number of individual spots, g is the number of sunspot groups, and k is a correction factor assigned to observatories. R varies cyclically with an average period of 11.2 years, although periods have varied from 7.5 to 16 years[1]. It has also been noted that although solar activity maxima and minima do correspond to maxima and minima in the sunspot number, the actual level of activity is not necessarily proportional to the sunspot number. Sunspot numbers can be predicted to

first approximation by utilizing the mean value of all previous cycles; however, a more satisfactory prediction can be found in the Monthly Solar-Geophysical Data, Part B, issued by the Central Radio Propagation Laboratory of the National Bureau of Standards.

By using the approximate method and by assuming that the next cycle will begin in June 1964, sunspot numbers predicted for the period 1963-67 would be: June 1963--20, June 1964--12, June 1965--18, June 1966--58, and June 1967--90.

2. Flare Frequency

The frequency of solar flares occurring per solar rotation (27 days) has been related to sunspot number as follows[2]:

$$N_f = a(R - 10)$$

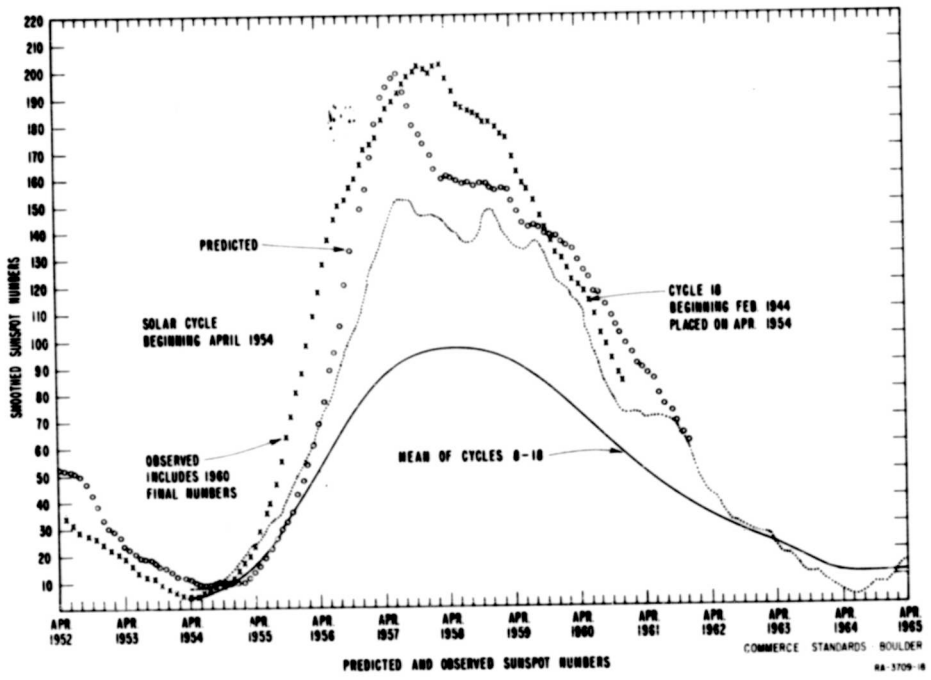
where R is the sunspot number and a is a proportionality factor which has been observed to vary between 1.47 and 1.98.

The frequency of occurrence of flares for the solar cycle whose maximum fell in 1937 was as follows (according to Waldmeier[3]): Importance 1--73%, Importance 2--23%, and Importance 3--4%.

From the above relationship and from the estimated sunspot numbers, predicted flare frequencies (per solar rotation) are as follows: June 1963--15 to 20; June 1964--3 to 4; June 1965--12 to 16; June 1966--72 to 96; and June 1967--120 to 160.

3. Polar Cap Proton Events

Polar cap proton events are directly associated with some, but not all, large flares. Anderson[4] feels that the occurrence of large flares is more closely associated with the occurrence of large geomagnetic storms than with sunspot number. On this basis, he makes the very approximate prediction that the number of proton events per year will vary from 3 at sunspot minimum to 10 at sunspot maximum.



SOURCE Solar-Geophysical Data part B, CRPL-F 203 National Bureau of Standards Central Radio Propagation Laboratory

FIG. V-1 PREDICTED AND OBSERVED SUNSPOT NUMBERS

4. M-Regions

Geomagnetic storm and aurora activity generally increase during sunspot maxima although the frequency of their occurrence is not simply related to sunspot number. Geomagnetic storms and auroras are observed to occur after the central meridian passage of a large sunspot or the occurrence of a flare. However, the converse is not necessarily true; geomagnetic storms and auroras occur in the absence of any visible manifestation of solar activity. Many geomagnetic storms recur with a 27-day cycle (rotation period of the sun) and tend to avoid sunspot groups. The yet unidentified solar areas responsible for this type of storm are called M-regions. The identification of these regions is one of the current solar research problems. The M-region disturbances are expected to persist throughout the solar cycle and thus become important subjects for research during the sunspot minimum.

5. Auroras

The correlation between auroral activity and sunspot cycle is higher at lower latitudes than in the auroral zone. As noted above, although the occurrence of many auroras can be correlated with the passage of large spots or with flare activity, these solar features are not required. The frequency of occurrence of auroras apparently varies with the sunspot cycle, but the maxima and minima aurora activity are not as pronounced as they are for solar flares. There is also evidence[5] that there are differences in auroral forms at different times in the solar cycle. Very little evidence of a 27-day recurrence period has been found for auroras.

REFERENCES

1. Menzel, D. H. Our Sun. Harvard University Press, Cambridge, Mass. (1959)

2. Kuiper, E. G. The Sun. University of Chicago Press, Chicago (1953)

3. Waldmeier, M. Statistische Untersuchungen an Chromospharischen Eruptionen. Astr. Mitt. Zurich, No. 153 (1948)

4. Anderson, K. A. and C. E. Fichtel. Discussions of Solar Proton Events and Manned Space Flight. NASA TN D-671 (March 1961)

5. Bates, D. R. The Auroral Spectrum and Its Interpretation. Physics of the Upper Atmosphere, edited by J. A. Ratcliffe, Academic Press, New York and London (1960)

VI PERTINENT GEOPHYSICAL EXPERIMENTS

A. General

1. Value and Limitations

The obvious value of investigating solar-terrestrial events to obtain a better understanding of nuclear blackout is that these phenomena have much in common, and--in view of weapon test limitations--natural geophysical perturbations provide many more possibilities for *in situ* investigations of atmospheric ionization and recombination processes.

Not so obvious, perhaps, are two other valuable aspects of this area of research: First, solar-terrestrial events can be used to check theoretical predictions regarding the atmospheric conditions that should obtain during nuclear blackout; hence, if a particular theoretical technique is valid for the description of nuclear blackout, it should be capable of describing (with appropriate modifications) solar-terrestrial phenomena. Second, if the number of high altitude nuclear tests should be increased, solar-terrestrial investigations would still be invaluable for the development of experimental techniques for use in nuclear testing and, again, for checking results obtained under the rather tense and restrictive conditions of such tests. The continual, but random, recurrence of natural events is, in a sense, complementary to the limited number of definitely scheduled nuclear events.

The limitations of geophysical experiments must also be considered in planning a research program that will lead to useful information regarding nuclear blackout. Despite the great insight provided by IGY, IGC, and other programs of geophysical exploration, large and important gaps remain in the knowledge of solar-terrestrial relationships. Therefore, any program that seeks to utilize these relationships must also be prepared to expend a reasonable effort to investigate the causal relationships between solar events and atmospheric perturbations even though such effort may not seem to be strictly within the province of the

program. Thus, exploratory geophysical experiments and laboratory investigations of basic processes will undoubtedly be required.

2. Pertinent Areas of Research

The following areas of geophysical research would seem to be pertinent to the nuclear blackout problem and amenable to study during the 1963-67 period.

a. Aurora

Auroral events comprise an area of research that seems quite promising during the period of sunspot minimum, as well as during periods of increasing activity. Although frequency of active aurora decreases with decreasing sunspot number, the decrease is not as drastic as it is for flares. In the auroral zone auroras will continue to appear nightly. Opportunities should exist for the study of both particle and electromagnetic radiation. In fact, auroral zone activity, with or without visible auroras, may well provide the only sources of atmospheric ionization that can be used during the period of low sunspot number. This area should be investigated actively as soon as possible.

b. Polar Cap Events

Polar cap events will become more important toward the end of the 1963-67 period. They make up a particularly interesting area of research because the ionizing events are produced almost entirely by a single class of radiation, protons. Thus, calculations and measurements should be much more straightforward and less ambiguous than for auroral events. Also, the fluxes appear to be relatively steady (though slowly decreasing) for long periods of time which may allow the separation of photo- and collisional-detachment processes by comparing day and night periods. Analysis indicates that experiments in this area would probably be more rewarding (in terms of number of relaxation parameters determined) than any of the other areas.

c. Sudden Ionospheric Disturbances (SID)

At present more is known regarding these events than any of the other events discussed. Although further exploratory research is required in this area, sufficient information exists to start a series of experiments expressly designed to collect specific recombination information. However, these experiments must be delayed until the latter part of the 1963-67 period when the solar flare activity will again be favorable. Meanwhile, as with the polar cap events, planning, theoretical considerations, and instrument development can be pursued profitably.

d. "Quiescent" Solar Conditions

This is an area that requires further study before many recommendations can be made. Measurements by the NRL solar satellite indicate that X-ray emission increases during periods not associated with flares and surges; these conditions conceivably may be utilized during periods of low solar activity. Also, studies of quiescent solar conditions are important in establishing a reference base for the interpretation of experiments made during active conditions.

The relative effects of Lyman α - NO ionization and X-ray-atmosphere ionization in the normal D-region have not been resolved. With adequate support, experiments could be conducted to investigate this important problem. If Lyman α ionization of NO is indeed the dominant process, an excellent opportunity to determine the dissociative recombination rate for the nitric oxide ion would be provided.

3. Research Phases

A research program for the period 1963-67 can be divided into the following one-year phases. Although these phases now seem appropriate (according to estimates of sunspot activity) they should be reviewed periodically to take advantage of additional solar activity information.

1963-64: Exploratory auroral experiments
Initial planning of studies for future experiments
Instrument development for quiescent period explorations

1964-65: Continuation and further development of auroral experiments
Exploratory experiments to determine quiescent solar and ionospheric conditions
Instrument development for SID and polar cap experiments

1965-66: Continuation of auroral experiments
Continuation of background explorations
Exploratory SID and polar cap experiments

1966-67: Continuation of auroral experiments
Further development and continuation of SID and polar cap experiments.

4. Recent and Current Geophysical Investigations

Experience acquired and data obtained during the following recent and current geophysical investigations will be of great value in planning the geophysical experiments of interest to this study. Where possible, therefore, continuation and/or amplification of current pertinent programs should be encouraged.

a. Satellite Observations of Solar X-rays

The U.S. Naval Research Laboratory has been conducting a program of solar observation utilizing X-ray and Lyman α sensors aboard a small satellite. The experiment recently concluded (Solar Radiation I)[1] consisted of an X-ray sensor (sensitive to radiation in the 2-8 A band), two Lyman α radiation detectors, and a solar aspect sensor. The satellite does not store information and therefore observations are only made if a solar event is observed during a particular pass over a telemetry station. Although the information obtained has been limited rather severely by the paucity of telemetry stations, a rather considerable body of data has been obtained regarding long- and short-duration enhancements of the 2-8 A X-radiation (which is responsible for D-region perturbations) during both "quiescent" and active solar periods.

A second satellite was launched early this past summer which contains two X-ray sensors, respectively sensitive to the 2-8 A and the 8-18 A bands. This, theoretically, would allow a crude estimate to be made of the spectrum of X-ray emissions. Although a considerable amount of data is being collected, the data reduction problem has been complicated by the fact that this satellite did not separate from its companion satellite,[2] Injun.

b. Rocket Observations of Solar X-rays

A continuing series of rocket observations of solar flares has been conducted by the Rocket Astronomy group at the U.S. Naval Research Laboratory throughout the present sunspot cycle. All available data regarding X-ray fluxes and spectra emitted by solar flares is that obtained by this group. The most recent series of rocket measurements was Sunflare II, conducted in 1959.

c. Injun Satellite

A satellite recently launched (concurrent with the second solar satellite described above) carried a number of experiments designed to study aurora. The experiments have the following objectives:[3]

1. Detailed plotting of the auroral zone by observation of the intensity of the oxygen green line (5577 A) excited in the atmosphere beneath the satellite; also, study of airglow by the same photometer

2. Simultaneous plotting and monitoring of the intensity structure of the outer radiation zone of the earth with a variety of charged particle detectors

3. Study of the relationship between optically observed auroras and "particle-dumping" from the outer zone

4. Measurement of absolute energy and particle flux of protons and electrons separately and in several selected energy ranges in the lower edge of both the inner and outer radiation zones

5. Monitoring of galactic and solar cosmic rays over a wide range of latitudes.

Unfortunately, the Injun satellite did not separate from the solar radiation satellite. This has altered the planned orientation of the satellite and blocked the photometer.

d. Lockheed Satellite Experiments

A series of experiments to be carried aboard "Discoverer" satellites are being planned by Lockheed Missiles and Space Division.[4] The objective is to measure the characteristics of auroral particles and correlate these measurements with observations of optical auroral events. It is expected that relationships can eventually be established between primary particle fluxes and atmospheric ionization. The first series is planned for the winter 1961--spring 1962 period.

e. Balloon Observations of Auroras

Groups at both the University of Minnesota and the University of California have been conducting balloon flights in the auroral and subauroral regions. The most recent series was conducted at 4 stations along a meridian over Central Canada and the United States by K. A. Anderson of the University of California and J. R. Winckler of the University of Minnesota in the fall of 1961.[5] All the available data regarding bremsstrahlung accompanying auroral events is that gathered by groups at NASA and the above Universities.

f. Solar Proton Experiments

Experiments have been conducted with balloons in the polar regions by K. A. Anderson of the University of California for the determination of solar proton characteristics. Similar experiments have been conducted by J. R. Winckler of the University of Minnesota at lower latitudes.

Rocket probes have been utilized for solar proton measurements by L. R. Davis and C. E. Fichtel of the National Aeronautics and Space Agency.[6]

It is understood that these are continuing programs.

g. Quiescent D-region Experiments

Techniques for measuring D-region electron concentrations are under development at the Goddard Space Flight Center, the Pennsylvania State University, and the University of Michigan. Future experiments by these groups are expected to yield information of direct pertinence to the geophysical experiments suggested in this report.

B. Specific Experiments

1. Design Philosophy

The specific experiments suggested and discussed in this report are designed to take advantage of three different kinds of geophysical events that result in the production of excess ionization in the D-region. These are: Polar Cap Absorption (PCA), Sudden Ionospheric Disturbances (SID), and auroral bremsstrahlung. Measurements would also be made during quiescent conditions.

The experiments are very similar in basic philosophy and over-all concept. The basic philosophy is to make in situ measurements that provide values of electron production rate, free electron concentration, and negative ion-to-electron density ratio simultaneously and as functions of time and altitude. Thus, the following well-known equations describing ionization of the ionosphere can be utilized to compute values of the ionospheric recombination coefficients. With these values the effect of any similar ionizing event (in the lower ionosphere) can be described.

$$\frac{dN_e}{dt} = \frac{q}{1+\lambda} - (\alpha_D + \lambda\,\alpha_i)\,N_e^2 - \frac{N_e}{1+\lambda}\frac{d\lambda}{dt}$$

$$\frac{1}{1+\lambda}\frac{d\lambda}{dt} = \beta - \lambda\left[\rho + \Gamma + N_e\,(\alpha_i - \alpha_D) + N_e\frac{q}{(1+\lambda)}\right] \qquad (1)$$

Where N_e = electron density

q = electron production rate

λ = negative ion to electron density ratio

α_D = dissociative recombination coefficient

α_i = mutual ionic neutralization coefficient

β = electron attachment rate; this parameter is equal to a sum of products of attachment coefficients with attaching species concentrations

ρ = photodetachment reciprocal lifetime

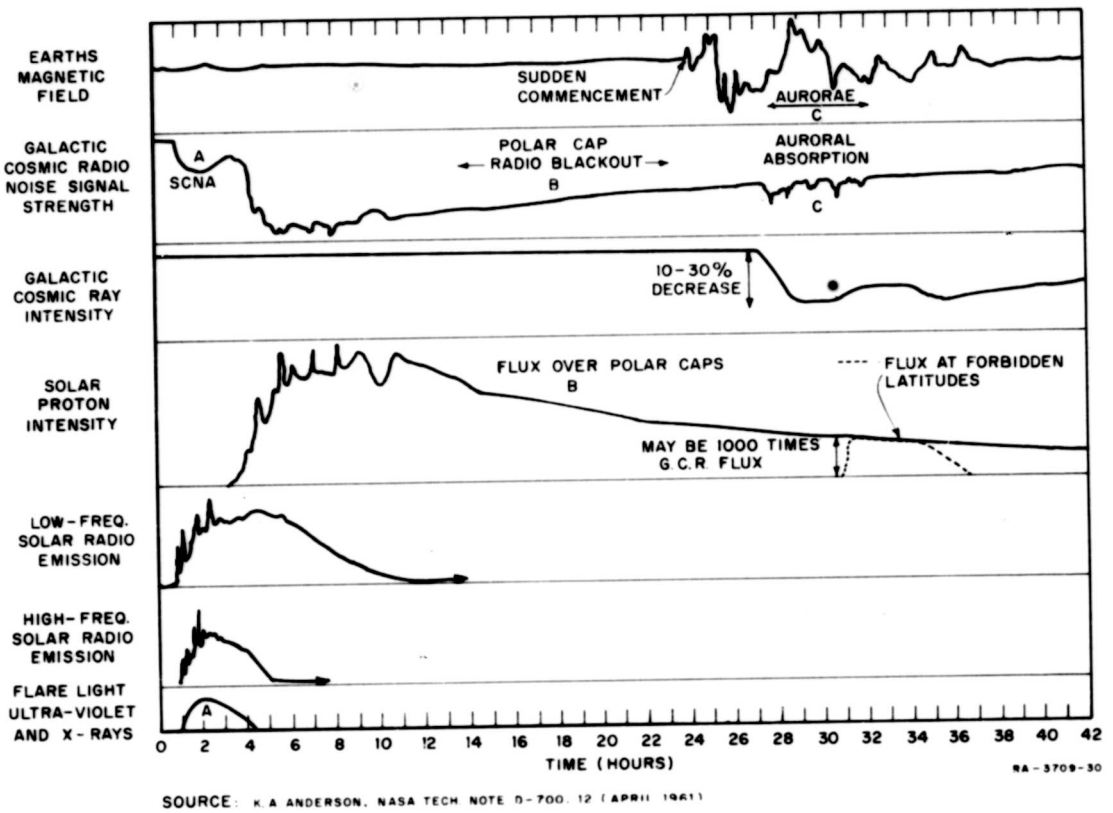
Γ = electron collisional-type detachment reciprocal lifetime; this parameter is equal to the product of a detachment coefficient with the detaching species concentration.

The over-all concept is to probe the ionosphere, during an ionizing event, with an instrumented missile. Measurements would be made of radiation flux, electron concentration, negative ion concentration, electron temperature, and atmospheric density. The probe would move rapidly, making measurements through the D-region, into the E-region, and back through the D-region. The instrumentation would be very similar for all three types of experiments, except for the radiation flux apparatus. The experimental procedure and computations of coefficients would be different in the three experiments. These details are discussed briefly below.

a. Polar Cap Absorption (PCA)

The PCA experiments should be planned to take advantage of the slowly decaying phase of the PCA event. This is the period designated "B" in the accompanying Figure VI-1. During this period the proton flux is decaying slowly and equilibrium conditions can be assumed. Thus terms involving both $\frac{dN_e}{dt}$ and $\frac{d\lambda}{dt}$ can be eliminated from the above equation, greatly simplifying the computations.

Several rocket probes could be made during the desired period, thus increasing the reliability of the experimental results as well as checking the assumption of equilibrium. The measurement of proton flux and energy (or the loss in energy) at several altitudes from 50 to 100 km simultaneously with measurements of electron



SOURCE: K.A. ANDERSON, NASA TECH. NOTE D-700, 12 (APRIL 1961)

FIG. VI-1 TIME SEQUENCE OF MOST OF THE IMPORTANT CHROMOSPHERIC FLARE EFFECTS OBSERVABLE AT THE EARTH

concentration, negative ion concentration, electron temperature, and atmospheric density will provide sufficient information for the calculation of α_D and ρ. By judicious combinations of day and night observations with instrumented probes, α_i, Γ, and β can also be determined.

Ancillary measurements of cosmic radio noise absorption and (from balloons) radiation flux and atmospheric conductivity would aid greatly in correlating these probe measurements with radio effects as well as with the entire event.

Details of the instrumentation and computations are discussed in later sections.

b. Sudden Ionospheric Disturbances (SID)

The procedure would be very similar to that discussed above for PCA's, with two important differences.

The first difference would be that equilibrium conditions cannot be assumed. Thus, in order to determine the time dependence of N_e and λ, two or three measurements must be made during the decay phase of the flare.

The second difference is, of course, that X-ray sensors must be used instead of particle detectors.

Very close cooperation with a solar observatory would also be required.

Balloon level measurements would be very useful but not necessary for SID's; cosmic radio noise records would be useful in correlating the measurements with radio effects.

c. Quiescent D-region

Measurements during quiescent periods will be useful for the establishment of a reference base for comparison with measurements made during disturbed conditions. In addition, something could be learned about ionization and recombination, particularly in the upper D-region. The main problem would be the sensitivity of the electron and ion concentration instrumentation.

For the establishment of background conditions, the same instrumentation would be used as for SID investigations. For possible investigations of low level ionization and recombination processes, measurement of Lyman α radiation and nitric oxide concentrations should be added.

d. Auroral Bremsstrahlung

Successful utilization of auroral bremsstrahlung events will require radiation sensors to measure both X-ray and particle fluxes. Monitoring of high energy components with balloon-borne instrumentation would be necessary in order to determine firing times for rocket probes and to record the time variation of the ionizing flux during the rocket probing operations. The procedure followed would be similar to that suggested for SID's, i.e., firing near the maximum of an X-ray burst and once or twice during the decay period in order to establish dN_e/dt and $d\lambda/dt$.

2. Measurement of Ionizing Radiation

a. Particle Fluxes

It is desired to measure, preferably within 10%, the rate of electron production as a function of altitude in the upper atmosphere (over ca. 50 km) during a polar cap absorption event. It appears to be commonly accepted that the electrons are produced almost entirely by ionization of the atmosphere by protons, under the experimental conditions envisaged (high geomagnetic latitude, more than 1/2 hour after onset of flare), and that the expected flux is from 1 to 10^4 protons/cm^2 sec with energies mostly of 1 to 1000 Mev.

Therefore, the instrument desired would measure dE/dx (energy absorption per unit length of absorption path) of the protons as a function of altitude. The instrument would be designed to be as direct an analog to the layer of atmosphere as is technically possible considering all the problems of information gathering from rocketborne instrumentation.

The information we require, namely the electron production rate as a function of altitude, could be derived if one knew the proton energy spectrum as a function of zenith angle and altitude. However, the more direct approach is recommended. Measuring the electron

production rate in a detector which has a thickness equivalent in stopping power to some acceptably small thickness of the atmosphere is to be preferred because acquiring all the flux parameters for the calculation is a far greater undertaking and one that will be much more difficult to achieve. Knowing the value of energy loss/electron produced for air and the detector material allows direct calculation of the electron production rate in a particular atmospheric layer from a measurement at the layer altitude.

For a detector of a given particle stopping power, the equivalent thickness of atmosphere will vary with altitude. Table VI-1 shows roughly this variation for a semiconducting silicon detector 20 microns thick (4.66 mg/cm^2).

Table VI-1

ATMOSPHERIC LAYER EQUIVALENT IN PROTON STOPPING POWER OF A 20μ SILICON DETECTOR

Altitude (km)	Atmospheric Layer Thickness (km) (assuming uniform density throughout the layer)
50	0.0115
60	0.130
70	0.460
80	2.20
90	16.4*
100	124*

*Uniform density assumption obviously breaks down for these altitudes.

This is adequate resolution in the chief region of interest, namely from 50 to 80 km. It is inadequate in the region above 90 km. A choice of optimum detector thickness would depend upon (1) the allowable uncertainty in the equivalent atmospheric layer thickness, (2) the proton energy range of greatest importance for producing electrons, and (3) the noise and background levels of the detector.

production rate in a detector which has a thickness equivalent in stopping power to some acceptably small thickness of the atmosphere is to be preferred because acquiring all the flux parameters for the calculation is a far greater undertaking and one that will be much more difficult to achieve. Knowing the value of energy loss/electron produced for air and the detector material allows direct calculation of the electron production rate in a particular atmospheric layer from a measurement at the layer altitude.

For a detector of a given particle stopping power, the equivalent thickness of atmosphere will vary with altitude. Table VI-1 shows roughly this variation for a semiconducting silicon detector 20 microns thick (4.66 mg/cm^2).

Table VI-1

ATMOSPHERIC LAYER EQUIVALENT IN PROTON STOPPING POWER OF A 20μ SILICON DETECTOR

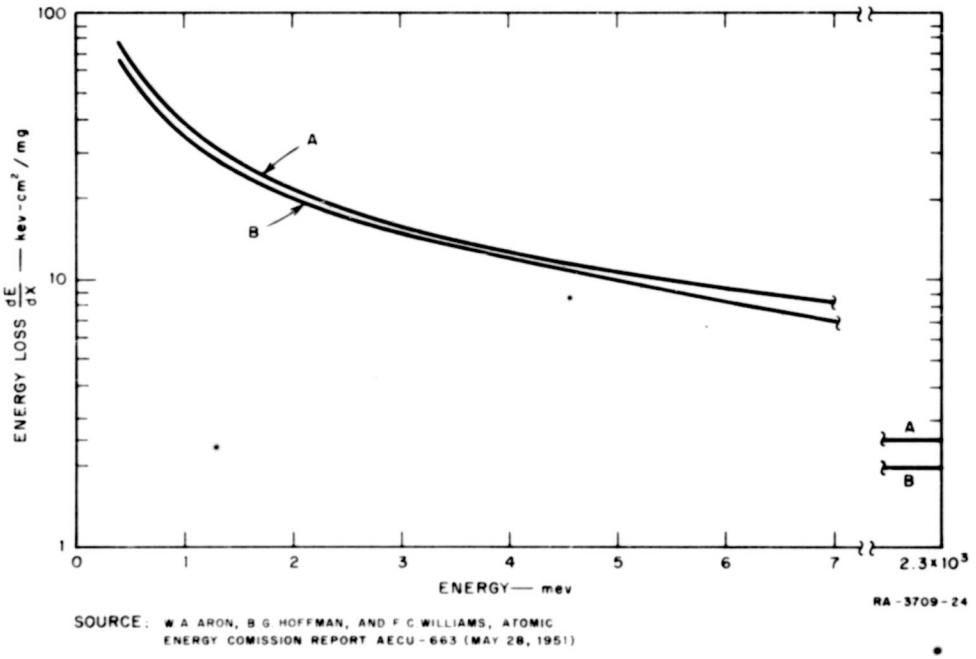
Altitude (km)	Atmospheric Layer Thickness (km) (assuming uniform density throughout the layer)
50	0.0115
60	0.130
70	0.460
80	2.20
90	16.4*
100	124*

*Uniform density assumption obviously breaks down for these altitudes.

This is adequate resolution in the chief region of interest, namely from 50 to 80 km. It is inadequate in the region above 90 km. A choice of optimum detector thickness would depend upon (1) the allowable uncertainty in the equivalent atmospheric layer thickness, (2) the proton energy range of greatest importance for producing electrons, and (3) the noise and background levels of the detector.

Condition (1) is not critical although the layer thickness should probably be kept below 10 km at the highest altitudes of interest. Condition (2) can be inferred to be the lowest energy protons that are present in the spectrum at any given altitude since their value of dE/dx is greatest. For example, dE/dx for 4.0 Mev protons is 10 times that for 70 Mev protons and 34.5 times that for 2.3 Bev (minimum ionizing) protons. (See Fig. VI-2). No matter what the spectrum shape or low energy cutoff, protons in the range 2 to 50 Mev will build up (relative to higher energies) with increasing atmospheric penetration depth. Since essentially every incident proton will eventually degrade to this region, and since it is at these lower energies that dE/dx is greatest, we must choose a detector thickness less than the range of particles in this energy region.

Condition (3) is usually determined by the electronic system used to amplify the detector-generated signal. For most systems the



SOURCE: W A ARON, B G HOFFMAN, AND F C WILLIAMS, ATOMIC ENERGY COMISSION REPORT AECU-663 (MAY 28, 1951)

FIG. VI-2 RANGE-ENERGY CURVES FOR PROTONS IN AIR (A) AND ALUMINUM (B)

noise level of the amplifiers is equivalent to the interception of 10 to 50 kev particles in the detector. This noise level will be most serious at the higher altitudes where low energy protons may be relatively less abundant. It may be avoided by using separate, thicker detectors for the higher altitude measurements. However, the equivalent atmospheric layer will also be increased thereby, although not in direct proportion, because of the increasing atmospheric density with decreasing altitude.

A number of requirements can be formulated for a detector designed to obtain the electron production rate.

1. The detector must have a minimum degree of shielding or dead layer to be traversed by the radiation before it enters the measurement area; otherwise the low energy particles will be stopped in the dead layer. The energy dose rate measured at a given altitude will be representative of that actually existing at a lower altitude, the height difference (in g/cm^2) being equal to the thickness of the dead layer. Hence, at 80 km, a dead layer of 1 mg/cm^2 will represent a level difference of 500 meters.

2. The sensitive layer in which measurement takes place, must also be thin. If it is not, the less energetic particles will be stopped in it, and there may appear to be a marked variation in dose rate through the width of the layer. In other words, the measured average electron production rate would not be constant throughout the atmospheric layer in question.

3. The conversion factor for translating ionization in the device to ionization in the atmosphere must be sufficiently well known.

4. The device must furnish sufficient current for easy measurement; the signal must also be greater than the noise level.

We shall consider three devices and see how they fit these requirements. They are: the semiconductor counter, the scintillation counter, and the gas ionization chamber.

The semiconductor counter is the most recent and sophisticated of these devices, and by the same token is still in an experimental or developmental stage. However, a number of them have been flown in various

satellites and operate satisfactorily as long as the destruction dose--10^{14} 14-Mev neutrons or equivalent per cm^2, or 10^8 rads of Co-60 gammas--is not exceeded. For rocketborne experiments of a few minutes duration possible radiation damage is of no consequence. For long term satellite passage through the Van Allen zones, radiation damage is a limiting factor.

The appropriate commercially available device suitable for this application is conceived to be the standard P-N junction semi-conductor detector. These detectors have essentially no dead layer on the front surface. On the assumption that protons with energies less than 2 Mev are unimportant, a sensitive layer thickness of 20 microns will be considered for discussion purposes. Each unit would be effective to intercept radiation over π steradians, so four units would be adequate to cover 4π steradians.

Although several thin semiconductor counters[7] which could function as a single 4π solid state ionization chamber sufficiently thin to all the protons of interest here have been constructed, such devices would probably be too fragile for this application.

Table VI-2 shows the approximate energy loss of protons of various energies in the assumed 20-micron sensitive layer of silicon. The noise level (due to the solid state preamplifiers and amplifiers) is expected to be equivalent to less than 30 kev energy loss.

Over 90% of the particles at a given altitude will probably be less than 60 Mev.[8] This means that possibly 95% of the energy loss and hence electron production rate at a given altitude will be from protons $<$ 60 Mev. The sensitivity of the silicon detector thus varies directly with the necessity of accurate measurement, i.e., inversely with particle energy. More exact calculations of the portion of the proton spectrum effective in electron production would possibly determine a more appropriate sensitive thickness for the detector.

Table VI-2

ENERGY LOSS IN SENSITIVE LAYER

Proton Energy E (Mev)	Energy Lost by Proton in 20 Microns of Silicon (kev)
2	1000
5	360
10	240
20	120
50	60
100	36

Other characteristics of the semiconductor detector of importance in this application are:

(1) Its requirement of only a few volts bias to obtain a depletion depth (sensitive region) of 20 microns.

(2) Its small size. The volume of detector and its mounting is of the order of 1 cm^3.

(3) Its ability to withstand shocks up to 2000 g.

(4) Its statistical advantage over gas ionization chambers and scintillation systems because only 3.5 ev is required per primary electron collected, whereas the values for the latter instruments are 32 and $\sim$ 1500 ev respectively.

An appropriate circuit for conversion of the pulses from the detector to a voltage proportional to the total charge produced in the detector is shown in block diagram in Figure VI-3. The advantage of this circuit is the fact that noise in the frequency range above 1 kc is filtered out. It may be that an even longer time-constant integrator can be used to further reduce the amplifier noise level.

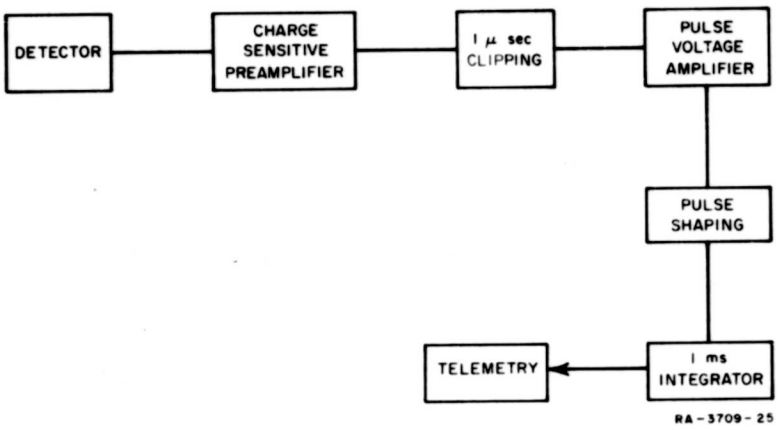


FIG. VI-3 BLOCK DIAGRAMS OF THE CIRCUIT FOR USE WITH THE SEMICONDUCTOR PARTICLE DETECTOR

A thin scintillation counter is another possibility for a dE/dx detector for protons. Thin layers of zinc sulfide, cesium iodide, or potassium iodide are all feasible choices. Such detectors have been widely used for purposes similar to the present objectives.[9]

A basic limitation of the thin scintillation counter as compared with the semiconductor detector is its resolution--20-50% compared with 1-10% for the semiconductor. Since we must provide a value of pulse height times the pulse rate, the accuracy of pulse height vs energy loss is essential to the precision of the result. On this basis alone one would be inclined to favor the use of the semiconductor. In addition, the problem of making a scintillator (CsI, KI, or ZnS) of uniform thickness in the range 20-30 microns is not trivial; a great deal of care is required. Such a thickness in the silicon semiconductor detector is achieved by choosing the appropriate reverse bias voltage across the junction and can be varied continuously over a wide range for the same detector (the thickness varies as $(\rho V)^{1/2}$ where ρ is the resistivity and V the reverse bias voltage).

We next consider the air or gas-filled ionization chamber. Because of the possible low incidence rate of proton pulses, individual counts can be recorded in spite of the slow rise times of 10-100μ sec. The necessity of a fragile, gas-tight thin window plus the somewhat poorer (2-15%) resolution of this device relative to the semiconductor detector, however, tend to weigh heavily against the ionization chamber in this application. Nevertheless, with sufficient care in its design and use, the device is fundamentally capable of achieving the goals set forth above.

Earlier it was stated that the goal was to measure the electron production rate q(e), to $\pm$10% accuracy. Can this be achieved with the measurement system chosen? Assuming the average proton will deposit 0.3 Mev energy in the detector, with an expected uncertainty of pulse height of $\pm$25 kev, the percent uncertainty in pulse height becomes $\sim$ 8%. If 500 pulses are collected for each atmospheric layer the statistical uncertainty is 4%. Since q(e) is proportional to the product of pulse height and pulse frequency, an over-all uncertainty of $\sqrt{8^2 + 4^2}$ or 9% is to be expected. This uncertainty is independent of uncertainty in the number of electrons produced per unit energy loss in air and detector material which might be of the order of 5%. This raises the over-all uncertainty in q(e) to $\sim$ 10%.

Since the pulse height resolution for scintillation detectors is generally 10-30% for 1-10 Mev protons it is obvious that a 1% statistical accuracy in the pulse counted would be required to even approach the desired $\pm$10% limit.

In general, all the other possible devices for detecting protons have lower resolution in pulse height than the semiconductor detector. Its exceptional resolving power is adequate for the purpose outlined here but there is not a wide margin of safety.

Although we have emphasized the direct dE/dx measurement of electron production rate in this discussion, the obvious next step would be to measure simultaneously (and in addition) the proton energy spectrum

and angular distribution incident upon the top of the atmosphere or at one or more levels in the atmosphere. Thus one could have an independent means of calculating the directly measured electron production rate. Even a fairly crude measurement of this spectrum would be of great value if it included the energy region from 1-100 Mev since the electron production rate is particularly sensitive to the intensity at lower energies.[10]

For this measurement we propose a Geiger-Müller counter telescope with interleaved absorbers. The advantage of the simplicity of handling G-M counter pulses is balanced by the high voltage supply requirement. (However, only a crudely regulated supply is necessary.)

Alternatively a semiconductor counter telescope can be used. Such a telescope is currently being designed and built for satellite instrumentation by one of the manufacturers of these detectors.

b. X-rays in the 2-8A Wavelength Range

The system outlined below is intended to measure both the intensity and energy spectrum of X-rays as a function of altitude and time during a solar flare. The instruments are assumed to be telemetering their information continuously during rocket ascent and descent.

Various investigators (see Sect. IB) give spectral irradiances in the wavelength range 1 to 8 A of 10^{-4} to 10^{-1} ergs/cm^2 sec A for a few minutes during a solar flare. With such intensities and intensity ranges, the detectors used must have a wide dynamic range.

Ordinarily, the Geiger-Müller counter does not have a wide usable dynamic range because of the background count rate of one per second and the 100μ sec dead time per pulse. However, coupled with K-edge absorbers of varying thicknesses, a number of G-M counters can be made to cover the dynamic range required.

Table VI-3 lists the transmission window for three thicknesses each of aluminum and copper absorbers proposed for coupling with G-M counters. Other elements such as chlorine (from Saran), titanium, chromium, and iron provide transmission windows in the intermediate energy ranges.

Table VI-3

X-RAY DETECTOR TRANSMISSION WINDOWS

Absorber Element	Thickness (mg/cm^2)	X-Ray Energy at Center of Transmission Window (kev)	Transmission at Peak of Transmission Window (%)	E Full Width at 1/4 Max. (kev)	Wavelength Limits Corresponding to E (A)
Al	5	1.40	25	0.3	8.0 - 9.9
Al	10	1.43	6.2	0.2	8.0 - 9.3
Al	20	1.50	0.4	0.1	8.0 - 8.5
Cu	38	8.2	25	1.6	1.38 - 1.68
Cu	76	8.5	6.2	0.9	1.38 - 1.53
Cu	152	8.7	0.4	0.4	1.38 - 1.46

It will be noted that as the absorber thickness increases, the width, ΔE (full width at 1/4 maximum) of the transmission window decreases. The thicker absorbers are required for the higher intensity portions of the spectrum both as a function of time during flare and of X-ray energy.

In principle, the L_{III} absorption edges of the heavier elements could be used for transmission windows. In cases where the practical problems of obtaining suitable forms of a particular element are difficult the L_{III} edge absorbers may be a useful alternative. For example, a tin-L_{III} edge absorber might be a worthwhile substitute for calcium, an element not well suited for producing thin absorbers. A tin-L_{III} absorber would have a transmission window near 4 kev.

The absorber must not be too near the G-M counter. Otherwise X-rays (or L X-rays in the case of an L_{III} edge absorber) of the absorber element excited by incident X-rays of energy greater than the absorption edge will enter the G-M tube and effectively widen the transmission window.

Since the emission of X-rays characteristic of the element itself is isotropic, the effect can be decreased by arranging the G-M counter to intercept the lowest solid angle (with respect to the absorber) allowable for the expected X-ray intensity range.

The main advantages of a G-M counter system are its simplicity, ruggedness, and low cost, inasmuch as a minimum of electronic pulse handling equipment is required. For rocket shots such a system would allow the buildup of a single module which could serve as a building block for any desired number of information channels. A single, simple dc high voltage source could supply a large number of such modules. Simple plug-in replacements could thus be made during final checkout before firing.

The G-M tube windows must be thin with respect to the absorber used. This will be a limiting factor only at the low energy end of the spectrum. Some development of supported thin windows may thus be in order for counters expected to count 1-2 kev X-rays.

The Solar Radiation Section at the U.S. Naval Research Laboratory have successfully employed "K-edge" counters of both the Geiger-Müller and ion chamber types for the measurement of solar X-ray intensities; Table VI-4 gives the characteristics of some of the counters used by them It should be noted that the energy windows of their counters are somewhat wider than desirable for the experiments suggested in this report.

Table VI-4

SPECTRAL RESPONSE OF G-M COUNTERS

Spectral Range	Window Material	Gas
2-8 A	14.7 mg/cm^2 Be	Neon + quench gas
5-10 A	14.7 mg/cm^2 Be	Argon + quench gas
9-20 A	1.7 mg/cm^2 Al	Neon + ethyl formate

A battery of G-M counters each separately coupled with a selective K-edge absorber via a collimator is envisioned to divide the 2-8 A X-ray wavelength band into several energy channels. Duplicate modules for each energy channel would greatly improve the chances of

obtaining results on rocket flights where there is so little final preparation time because of the short term nature of the flare. Monitoring of each of four angles with respect to the zenith is proposed in order to observe the change in angular distribution with altitude in the 50 - 100 km region.

c. Auroral Brehmsstrahlung

Because of the rapid drop in photon intensity with increasing energy per photon observed in auroral bremsstrahlung events, a simple and rugged X-ray spectrometer can be based upon the combination of K-edge absorbers and a detector. At a photon energy just below the K and L_{III} absorption edges of any element, the mass absorption coefficient reaches a minimum.

By appropriate choice of thickness of that element used as an absorber in the radiation path between source and detector, a transmission window of some width, ΔE, is created. The effective ΔE becomes smaller the thicker the absorber. There must be sufficient source intensity to allow the consequent sacrifice in absolute intensity.

The window ΔE just at the K absorption edge is not the only transmitting region. However, transmission at the $E \gg K$ absorption edge is not serious because of the relative paucity of photons of E much greater than any given energy in the spectrum.

Table VI-5 lists the proposed absorbers for a series of energy windows from 8-80 kev. We estimate the counting efficiency of such a system would be 10^{-4}. This allows a factor of 10 loss at the peak of the transmission window, and another factor of 10 loss because the detector must not subtend more than 10% of the solid angle of the absorber (to avoid detection of the K X-rays of the absorber element itself--produced when photons are absorbed at energies above the K absorption edge). The counting efficiency for the X-rays finally incident upon the detector varies from about 1% for a G-M counter to 100% for a scintillator phototube combination.

Table VI-5

EXAMPLES OF TRANSMISSION WINDOWS FOR ABSORBERS TRANSMITTING 25% RADIATION AT K-EDGE

Absorber Element	Absorber Thickness (mg/cm^2)	E at Midpoint of Transmission Window (kev)	ΔE, Full Width at 1/4 Max of Transmission Window (kev)
Cu	37.6	8.2	1.6
Ag	135	21	8
Ta	448	60	15
Pb	720	78	20

A separate absorber-detector combination would be used for each energy window.

The expected counting rates can be estimated from the reported energy flux $\sim 10^{-5}$ ergs/cm^2-sec

$$\text{photons/cm}^2\text{-sec} = \frac{10^{-5}\ \text{ergs/cm}^2\text{-sec}}{1.6 \times 10^{-9}\ \text{ergs/kev} \times 30\ \text{kev/average photon}}$$

$$= 2 \times 10^{-2} \times 10^{4}$$

$$= 200\ \text{photons/cm}^2\text{-sec}$$

With 10^{-4} counting efficiency (as for a G-M counter) this gives a count rate of 0.2 count/sec, assuming a 10 cm^2 detector area. Compared with expected background counting rates of 0.5-1 count/sec, this is unacceptably low. Even if one were to increase the efficiency by a factor of 10, the count rates would be marginal, i.e., about 1-5 times background.

If the simplicity of the G-M counter is sacrificed in favor of the 100% counting efficiency of a scintillation counter, a factor of 100 can be gained, which brings the count rates to acceptable levels. Although the scintillation counter can be used to differentiate photon energies without selective absorbers, one would not be using that capability in this application.

Nevertheless, the use of scintillation counters and pulse discrimination would be at least as satisfactory as the edge absorber instrument for this application. The advantage to be gained by using the ~ 20% energy resolution capability of the scintillation system without absorbers is the reduction in the number of detection units required. However, a larger number is sometimes an advantage in that one failure does not negate the entire experiment. The scintillation spectrometer has been widely used and hence would require a minimum of development.

The absorber system for resolution of energies is adequate only to ~ 100 kev. This does not appear to be a serious limitation since very little of the total X-radiation lies above 100 kev.

3. Measurements of Electron and Ion Concentrations Electron Temperature, and Collision Frequency

a. General

In this section the various methods that may be used to determine the electron density, ion density, the electron temperature, and collision frequency are briefly reviewed. The advantages and disadvantages of the techniques are also discussed. Following the general discussion, a system suitable for providing the required measurements in the D-region is given. The information used in this section was obtained from published data as well as from discussions with several of the principal investigators currently performing experiments in the ionosphere.

It would appear that the measurement of the plasma characteristics in the D-region during an SID could best be performed with the use of a combination of techniques rather than any single experiment. The measurement schemes selected would include an RF impedance probe, a Langmuir probe, and ion traps. The exact form of the various probes will depend on the results of experiments to be performed in the near future which will provide additional design information. Also, once a specific experimental program is initiated certain tests in a simulated environment would be necessary before an optimum configuration could be evolved.

b. Propagation Experiments

Probably the most widely used propagation technique for determining electron densities is the Seddon-Jackson CW experiment.[11] The method consists of transmitting a CW signal of a few megacycles and its kth harmonic (usually the sixth harmonic) from the rocket during ascent or descent through the ionosphere. The frequencies are chosen so that the low frequency is delayed in propagating through the ionosphere while the higher frequency is virtually unaffected by the ionosphere. At the ground receiving site, the lower frequency is multiplied by the factor k and beat with the high frequency signal. The beat frequency thus obtained is

$$f_b = k \frac{f_L}{c} \left[\frac{dr}{dt} (1 - n) - r \frac{\partial \bar{n}}{\partial t}\right] \qquad (2)$$

where

f_L = transmitted low frequency
c = free space velocity of light
r = vertical distance between rocket and receiver
n = index of refraction at rocket
$\bar{n}$ = average index of refraction between rocket and receiver.

In (2) it is assumed that the rocket is directly above the receiving site, but if this is not the case, corrections can be made for oblique paths.[12] The usual approach is to assume a quiet ionosphere so that $\bar{n}$ is approximately constant and the beat frequency reduces to a function of rocket velocity and local index of refraction only. Thus, from the beat frequency and vertical velocity of the rocket, the local index of refraction can be determined as a function of altitude, and using the Appleton-Hartree formula, the electron density can be determined.

Other factors affecting the measurement are geomagnetic effects which split the signals into ordinary and extraordinary waves, reflections from the upper ionosphere, Doppler shift of both the high and low frequency signals, and frequency shifts of the circularly polarized waves due to rocket roll.

The Seddon-Jackson technique has been quite successful for determining electron densities at altitudes above 75 km where it is permissible to neglect collision frequency terms in the Appleton-Hartree formula. The method has been used to measure electron densities at altitudes from 57 to 75 km, but Kane shows that the results can be in error by as much as a factor of 2.5 in this region unless collision frequencies are accounted for.[13] Even including the collision frequency term in the Appleton-Hartree formula does not provide accurate results because of the idealized nature of the Appleton-Hartree formula (i.e., the assumption that collision frequency is independent of electron energy).

By measuring the relative signal amplitudes as well as the phase (beat frequency), the collision frequency can be determined and the true electron density extracted from a more exact analysis or more direct methods. The mean collision frequency, $\bar{\nu}$, in an altitude interval, Δh, is obtained from the following approximate equation

$$\bar{\nu} \approx 0.138 \frac{\bar{D}}{\Delta h} \frac{c}{\bar{\omega}_p^2} \frac{\omega_1^2 \omega_2^2}{\omega_2^2 - \omega_1^2} \qquad (3)$$

where

c = the velocity of light

$\overline{D}$ = the mean differential absorption (in db) between altitudes h and h + Δh

$\bar{\omega}_p^2$ = mean square of the plasma frequency in the interval Δh

ω_1 and ω_2 = the frequencies of the two radio signals; $\omega_1 \gg \overline{\nu}$

A variation of the Seddon-Jackson experiment has been used by the Pennsylvania State University group in which the transmitters were located on the ground and the receivers and phase comparators were carried by the rocket.[14] A VHF signal of approximately 40 megacycles is frequency divided by a factor of 72 to get a 512 kilocycle signal and both of these are transmitted from the ground to the rocket. In the rocket the 40-megacycle signal is frequency divided by the factor of 72 and compared with the 512-kilocycle signal in a phase comparator. The phase difference and automatic gain control voltages (which are related to the signal amplitudes) are telemetered to the ground site. Data reduction is essentially the same as for the Seddon-Jackson approach.

The principal advantage of this technique is that with the lower frequency, electron density measurements could be made at lower altitudes than with the Seddon-Jackson experiment where the low frequency was usually 4 to 10 megacycles. This advantage is related to the fact that the transmitters are located on the ground so that the low frequency transmitting antenna can be made large enough to be an efficient radiator.

Another technique that is similar to the Seddon-Jackson method is reported by Haycock and applied by Pfister and Ulwick.[15,16] In this method a UHF reference pulse is transmitted from the ground to the rocket followed by a pulse in the HF range somewhat above the critical frequency. Both the UHF pulse, which is virtually unaffected by the ionosphere, and the HF pulse trigger a beacon in the rocket which transmits a UHF pulse back to ground as each pulse arrives. Thus the

retardation of the HF pulse relative to the UHF pulse can be obtained from the known time between the two pulses when they were transmitted and the measured separation when they arrive at the rocket. From the incremental change in retardation time between two consecutive HF pulses and the incremental change in rocket altitude during the time lapse between the pulses, an average index of refraction in the vicinity of the rocket can be obtained provided the ionosphere is quiet and uniformly stratified so that the retardation in the air column between the ground transmitter and the initial radial position of the rocket does not change between pulses.

The system can also be used with pulses transmitted from the rocket and received at the ground, although this approach requires that relatively efficient HF antennas be carried by the rocket. The rocket to ground system has the advantage, however, that amplitudes (as well as retardation times) can be determined.

Another propagation experiment that differs from the Seddon-Jackson approach only in the ratio of the frequencies used consists of using two frequencies in the HF range and observing both magnitude and phase changes.[17] A rocketborne transmitter transmits one frequency and its second harmonic, for example, and the ground receiving site records amplitude and phase of both received signals. The phase difference is due primarily to the change in index of refraction caused by the presence of free electrons, while the difference in amplitudes is due to power loss to electrons through collision processes. Thus, with the relative attenuation and phase of two signals, both electron density and collision frequency can be obtained with the aid of the Appleton-Hartree formula. (The collision frequency is given by equation (2).)

Another propagation phenomenon that can be used to determine electron density is the Faraday rotation of a plane-polarized wave as it passes through the ionosphere.[18] Faraday rotation results from the fact that the index of refraction for right-hand circularly polarized waves is greater than the index of refraction for left-hand circularly

polarized waves when the direction of propagation is anti-parallel to the geomagnetic field. A plane-polarized wave, which may be decomposed into right and left circularly polarized waves, thus suffers a rotation in its plane of polarization as the phase difference between the two circularly polarized waves accumulates. The electron density can be determined from[19]

$$N_e = \frac{2\omega^2 m^2 c\, \epsilon_0 \cos\theta}{e^3 \mu_0 H \cos\phi} \left(\frac{d\Omega}{dz} \right) \qquad (4)$$

where

ω = signal frequency

c = velocity of light

ϵ_0, μ_0 = free space permittivity and permeability

e, m = electronic charge and mass

θ = angle between transmission path and vertical

ϕ = angle between transmission path and geomagnetic field

Ω = Faraday rotation in radians

z = altitude of rocket in meters.

This method has the obvious disadvantages that the angular position of the rocket must be known quite accurately, and the determination of the Faraday rotation angle must be made quite precisely. If the collision frequency is significant, the relative amplitudes of the two circularly polarized waves can be measured in addition to the Faraday rotation.

c. Impedance Probes

When an antenna is operated in an ionized medium, its impedance is altered by a factor that depends on the electron density and collision frequency. If collisions are neglected, the effect of the free electrons is to reduce the effective dielectric constant, thereby reducing the antenna capacitance. Thus a measure of the change in capacitance of a dipole (or similar) antenna on a rocket can be used to determine the

the electron density from

$$C_{\text{ionosphere}} = C_{\substack{\text{free} \\ \text{space}}} \left(1 - \frac{N_e e^2}{\omega^2 m \epsilon_o} \right) = C_{\substack{\text{free} \\ \text{space}}} \left(1 - \frac{81 N_e}{f^2} \right) \quad (5)$$

where

e = electronic charge

m = electronic mass

ϵ_o = permittivity of free space

ω = signal radian frequency = $2\pi f$

f = signal frequency (cycles/s)

N_e = electron density.

Haycock and Baker describe an experiment in which the standing wave pattern on a dipole antenna feed line is measured by means of a tapped artifical line between the RF driving oscillator and the dipole.[20] The taps on the artificial line are commutated to provide the standing wave pattern. In addition, both sides of the dipole are biased with respect to the rocket by a very low frequency saw-tooth voltage so that the effects of the ion sheath about the antenna will be canceled at some point on the saw-tooth voltage wave.

The NASA group has also used impedance probes for electron density measurements on rocket and satellite experiments.[21,22] Their measurement technique consists essentially of determining the amount of external capacitance that must be added or removed to retune the antenna to a given frequency when it has been detuned by the presence of free charge. Jackson and Kane note that the electron density data provided by the RF probe may be in error by a factor of 3 (compared with the results of CW propagation experiments and ionosonde data).[22] They attribute this error to the ion sheath formed about the probe and the high RF voltage applied to the probe (about 200 volts). The experiments were repeated with RF voltages of 2 and 0.2 volts with

better agreement, but the deviation of the impedance probe data from the CW data was still significant.

Severin and Crain proposed a method of measuring the change in dielectric constant in which the capacitance of the probe is made a part of the tuned circuit of a stable oscillator.[23] Changes in probe capacitance thus produce changes in oscillator frequency which can be measured very accurately.

Another impedance probe technique that can be used consists of sweeping the frequency applied to the probe through the plasma frequency. When the applied frequency is equal to the plasma frequency, the effective dielectric constant is zero and the probe impedance becomes purely resistive. The probe thus displays a resonance effect similar to that of a tuned L-C circuit. If collisions are accounted for, however, the effective dielectric constant is complex, and the capacitance of the probe will vanish when the sum of the signal radian frequency and the collision frequency is equal to the plasma radian frequency. It then becomes necessary to determine the collision frequency before the plasma frequency can be determined. The method fails if the collision frequency approaches the plasma radian frequency, as can be seen below.

If the collision frequency is a significant fraction of the signal frequency the previous formula for capacitance must be modified so that

$$C_{\text{ionosphere}} = C_{\substack{\text{free} \\ \text{space}}} \left[\left(1 - \frac{\omega_p^2}{\omega^2 + \nu^2}\right) - j \frac{\nu}{\omega} \frac{\omega_p^2}{\omega^2 + \nu^2} \right] \quad (6)$$

where

$\omega_p^2 = \sqrt{\frac{N_e e^2}{\epsilon_o m}}$ = square of plasma radian frequency

ω = signal radian frequency

ν = electron collision frequency.

It is then necessary to measure the Q of the probe as well as the capacitance to determine either electron density or collision frequency (or both).

d. Conductivity Measurements

Atmospheric conductivity has been measured in the region between 30 and 80 km using a Gerdian condenser.[24] In this region it was assumed that the electron density was negligible compared with the negative ion density so that current due to negative charges was entirely attributable to negative ions.* The conductivity for either positive or negative polarity on the condenser is then

$$\sigma = N_i e k \qquad (7)$$

where N_i is the ion density, e is the ion charge (the ions are assumed to be singly ionized) and k is the mobility of the ions (k_+ for positive ions, k_- for negative ions).

The conductivity measurements reported by Bourdeau, Whipple, and Clark displayed an anomaly between 40 and 60 km for positive conductivity which they attributed to reduced positive ion mobility due to high ratio of electric field to pressure. Their measurements also yielded conductivities much lower than had been expected for both polarities above 50 km, which they suggest is due to the diffusion of ions to dust particles.

For the Gerdian condenser to be effective, the dimensions of the air gap must be large compared with the mean-free-path of the charged particles. This requirement places an altitude limitation on the Gerdian condenser. In addition, it is not known to what extent the condenser perturbs the region where the measurement is being made; hence it seems that more development will be necessary before the Gerdian condenser will become an accurate measurement device for studies of the upper atmosphere.

---

*This assumption is questionable above 50 km.

e. Langmuir Probes

Probe theory dates from the original work by Langmuir and Mott-Smith in 1924. The use of rocketborne Langmuir probes for electron temperature and density measurements in the ionosphere was initiated by Hok and Dow in 1946 with the successful flight of a probe-equipped V-2 rocket.[25] Langmuir probes have since been used extensively on rockets and in experiments in which the probe is ejected from the rocket.[26-28]

The Langmuir probe is a bipolar device which collects electrons (or negative ions) at one pole and positive ions at the other pole when a dc voltage is applied between the poles. If the collecting areas of the poles are about equal and the poles are large compared with sheath thickness,* the positive ion current to the negative pole is sheath-area-limited at high probe voltages and tends to saturate at a current level determined by the ion density. The probe current at high voltages is thus determined by the ion current. At lower voltages the current to the negative pole consists of the positive ions attracted to the pole plus a few electrons that have enough energy to overcome the probe potential. Likewise at the positive pole the current consists primarily of electrons attracted to the pole, with a few positive ions that have enough energy to overcome the positive potential. At low probe voltages the current is primarily due to electron flow and is of the form

$$i = i_0 \exp \frac{-eV}{kT_e} \qquad (8)$$

so that the slope of a plot of log i vs V is inversely proportional to the electron temperature.

If the poles of the probe are unequal in area as they are in some of the rocketborne Langmuir probe experiments where one pole is a small isolated patch of rocket skin (called the probe) and the

*It is assumed that no collisions occur within the sheath.

other pole is the remainder of the rocket, the probe current will tend to saturate at positive potentials at a level determined by the electron density and at negative potentials at a level determined by positive ion density. The slope between saturation levels remains inversely proportional to the electron temperature. Such probes are more difficult to analyze because of the irregularities of the geometry and uncertainties in the behavior of the sheath around the probe. Other factors which may affect probe performance that do not appear to have been adequately investigated are the effects of probe surface condition and rocket outgassing. Photoelectric emission also appears to be an important consideration.

Due to the uncertainties regarding perturbance of the ionosphere by the rocket it seems advisable to remove the probe from the vehicle by placing it on a standoff or similar support so that it is removed from the influence of the rocket. The University of Michigan group has carried this to the extreme of ejecting the probe from the rocket.[29] While it may not be necessary to go this far in attempting to remove the influence of the rocket, the problem of proximity effect certainly warrants thorough investigation.

An interesting probe variation has been described by Takayama et al., in which an RF voltage is placed on the probe as well as a dc voltage.[30] The RF voltage is swept in frequency through the plasma frequency, at which a resonance effect occurs. In addition, because of the rectifying action of the probe, the dc current at frequencies somewhat removed from the plasma frequency is enhanced by a factor involving the electron density and temperature. The maximum current at resonance is a function of collision frequency. This probe thus offers some redundancy in electron temperature and density measurements which would be useful for crosschecking the results of the standard probe measurements.

f. Ion Traps

Ion traps of various forms have been used on satellites and rockets to measure ion currents, ion mass, ion temperature, and electron temperature.[21,27,31] The ion traps consist essentially of a collector behind a grid so arranged that the grid repels particles of one polarity and allows those of the other polarity to pass through and be collected by the collector. The particle energy distribution can be determined from the collector current vs grid voltage characteristic, or if the energy is known from some other experiment, the particle mass can be found. Electron temperature can be determined in much the same way as is done with Langmuir probes. Since the grid provides a means of separating the particles by charge, either electron or ion temperatures can be determined.

Additional grids may be used to suppress photoelectric currents or secondary emission, or to assist in particle segregation.

It appears that the ion traps would suffer most of the uncertainties regarding sheaths, outgassing, etc., that plague the Langmuir probes.

g. Recommended Measurement Techniques

Outlined above are various techniques which investigators have used in rocketborne experiments to study the ionosphere. It is evident from the discussion that two general approaches are used. The first approach is the "ionospheric sampling" technique in which the required probes are carried on the vehicle and measure the desired parameters when they are immersed in the region of interest. Data obtained by the probes are supplied to the telemetry system carried aboard the vehicle. Since the probes in experiments of this sort are influenced only by their immediate surroundings, local perturbations and contaminations resulting from the presence of the vehicle can have a marked effect upon the measurements. For this reason, it is essential that care be exercised in designing and locating probes on the vehicle either to avoid perturbations resulting from the presence of the vehicle or to take these perturbations into account.

The second general approach is the propagation technique in which certain characteristics of the ionosphere are studied by noting the manner in which a radio signal propagating from the ground to the vehicle varies as a function of altitude. Since the received signal is influenced by conditions existing along the entire propagation path, local perturbations caused by the presence of the rocket have very little effect upon measured results. By the same token, however, time changes in ionospheric characteristics occurring anywhere along the propagation path influence the received signal and may be erroneously interpreted as variations with altitude. Errors in determining electron profiles from propagation experiments are also apt to be quite large if the increase in electron content through a given altitude increment is not a significant fraction of the integrated electron content at that altitude. Consequently, propagation techniques were not considered to be suitable.

Several of the sampling methods developed by the experimenters mentioned above are suitable for use in a study of the sort being contemplated.

Discussions with various upper atmosphere investigators indicated that many of the ionosphere sampling techniques are not yet fully developed. It appears, however, that a reassessment of experimental techniques and results is underway, and that experiments are being designed to test the validity and accuracy of the various devices in performing the measurements. It is anticipated, therefore, that, in the near future, the various techniques and their shortcomings will be understood much more thoroughly than they are at present.

Most of the experimenters thus far have been concerned with studying the ionosphere above 100 km. Obviously, care must be exercised in extending their techniques to the D-region--primarily because the high collision frequencies at these low altitudes do not permit the use of the simplified theory employed at high altitudes. However, several experiments are presently being prepared or planned which should shortly yield information regarding the problems associated with D-region studies.

In the ensuing discussion, several measurement techniques will be proposed. An effort will be made to point out the problem areas associated with each method. Preliminary experiments to test the validity of the various methods will be suggested whenever it appears that problem areas are inadequately understood. Mention will be made of applicable investigations currently planned or underway.

(1) Modified Langmuir Probe

The modified Langmuir probe employed by Takayama, et al.,[30] is attractive in that it permits the normal measurements possible with a Langmuir probe (electron density N_e, electron temperature T_e, and ion density N_i) and, with the same probe, offers redundancy in the measurement of electron temperature and electron density. In using the probe--illustrated in the block diagram of Figure VI-4(a)--the RF source is first shorted out and the dc-voltage applied to the probe is swept through its range to yield the normal Langmuir probe curves shown in the lower part of Figure VI-4(b). From the slope of this curve it is possible to determine T_e, while N_e and N_i may be found from the values of the saturation currents.

Next, the RF source is unshorted, and set at some convenient frequency below the plasma frequency. The dc voltage is again swept through its range to yield, this time, the upper curve of Figure VI-4(b). The increased current obtained for a given dc voltage where the RF signal is applied results from the fact that the V-I characteristic of the probe is nonlinear and that rectification of the RF occurs. It can be shown that the ratio of the two currents in Figure VI-4(b) is proportional to the applied RF voltage and T_e.

Finally, the dc voltage is set at a convenient value and the frequency of the RF source is swept over a range including the plasma frequency ω_p to yield the response illustrated in Figure VI-4(c). Since maximum probe current occurs when the frequency of the applied RF signal equals ω_p, this technique provides a method for determining ω_p and, consequently N_e. Unfortunately, as the collision frequency ν approaches

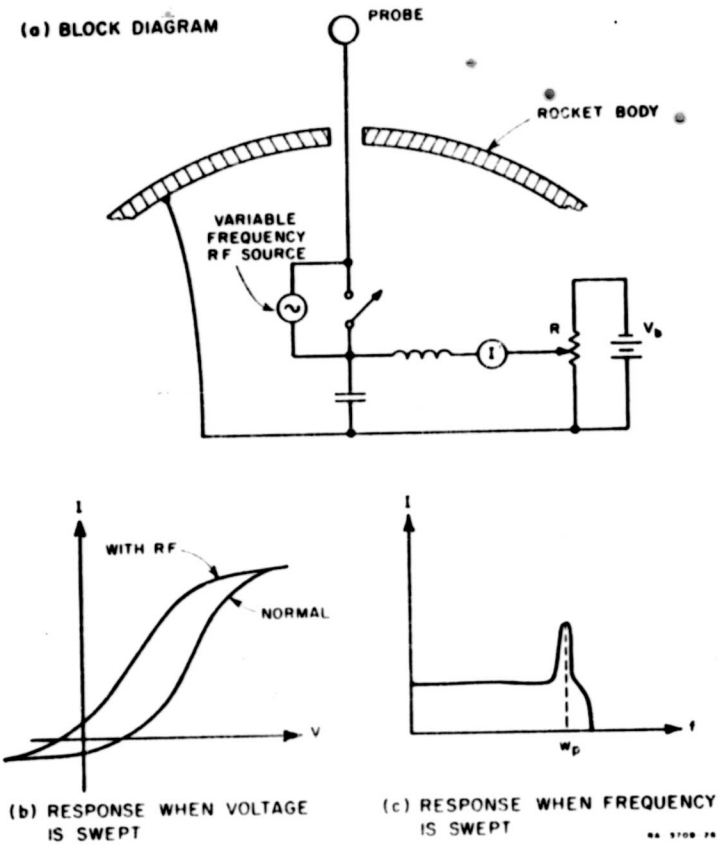


FIG. VI-4 MODIFIED LANGMUIR PROBE

ω_p, the current peak becomes less pronounced. For this reason, experimenters have found that the swept frequency method of determining N_e cannot be used at altitudes of less than about 90 km under normal conditions or 80 km under disturbed conditions. Even though the swept-frequency technique is useless over part of the range of interest, it can be used to check values of N_e at the higher altitudes thereby indicating the degree of accuracy with which N_e is being measured. Thus, unless weight limitations are extremely severe, it is recommended that the swept-frequency instrumentation be included on the rocket.

Careful consideration should be given to the physical configuration selected for the Langmuir probe. Three general types

may be used: (1) planar, (2) cylindrical, and (3) spherical. In selecting a probe type, consideration must be given to its mechanical complexity and reliability, to aerodynamic problems which might preclude its use, to the weight penalty which a particular design imposes, and to the degree to which the details of the ionospheric perturbation produced by a given design can be analyzed. For example, if the probe is to be deployed on a boom, the instrumentation will of necessity be mechanically complicated since timers and mechanisms for extending the boom will be required. Furthermore, measurements cannot be made at low altitudes since aerodynamic forces would destroy the boom if it were deployed. (Experimenters indicate that booms can safely be deployed at altitudes above 60 km.) If on the other hand, the probe is mounted on the skin of the vehicle, readings will be influenced by the space charge sheath surrounding the vehicle and by contaminants released as the vehicle and motors outgas.

A widely used Langmuir probe design, and certainly an ideal design from the mechanical point of view is the plane probe consisting of an isolated patch of skin on the vehicle. It appears, however, that the interpretation and analysis of data obtained from such a simple probe may prove to be extremely difficult. For example, the rocket vehicle acquires a negative charge in flight so that the vehicle and probe will be surrounded by a sheath of positive ions which will undoubtedly affect the characteristics of the probe. Even if a sheath did not exist about the vehicle a sheath will form about the probe itself as is indicated in Figure VI-5. The thickness and extent of the sheath will vary with potential as indicated in the two parts of the figure. If the dimensions of the probe are not large compared with the sheath thickness, the variation in sheath area with changing dc voltage, [compare Fig. VI-5(a) and Fig. VI-5(b)] may amount to a large fraction of the probe area. Since the sheath area must be used in calculating N_e and N_i from the probe data, variations in sheath area can introduce

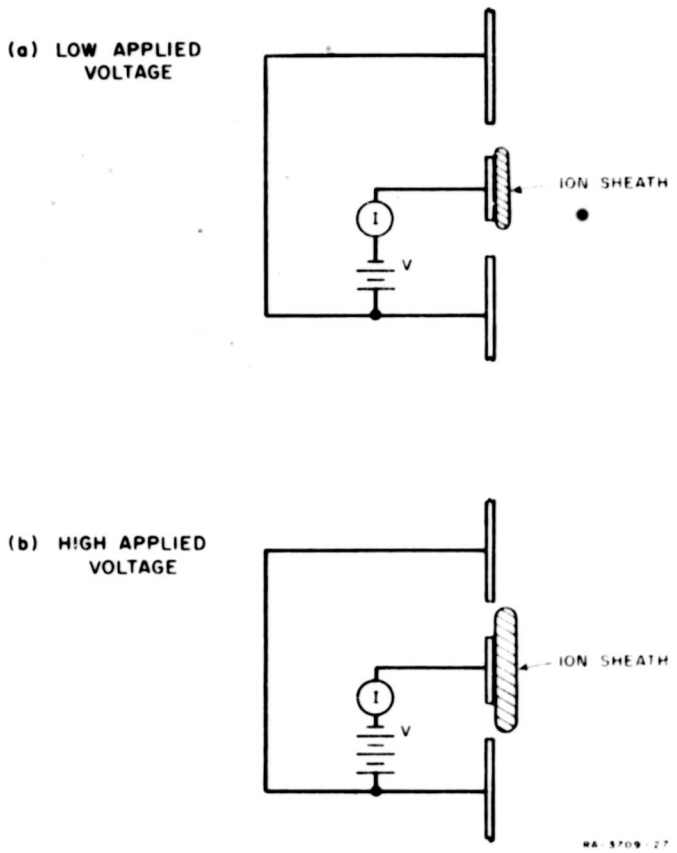
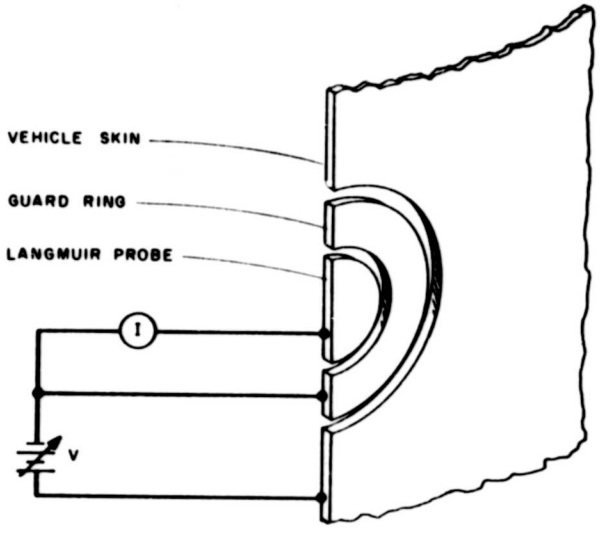


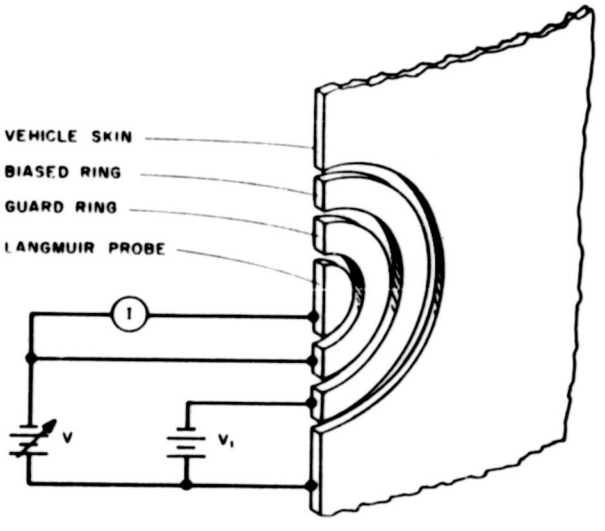
FIG. VI-5 VARIATIONS OF SHEATH STRUCTURE ABOUT PLANE PROBE IN ROCKET SKIN

considerable error into the determination of these two quantities. A possible technique for eliminating this uncertainty regarding probe sheath dimensions is the use of the simple guard ring structure illustrated in Figure VI-6(a). The guard ring is isolated from the skin and driven together with the probe. In this way the fringing of the sheath is confined to the region between the guard ring and the skin. The sheath in the vicinity of the probe varies only in thickness.

A further refinement which might be used to eliminate the effects of the nonzero vehicle potential in producing a sheath about the entire vehicle is illustrated in Figure VI-6(b). A second ring



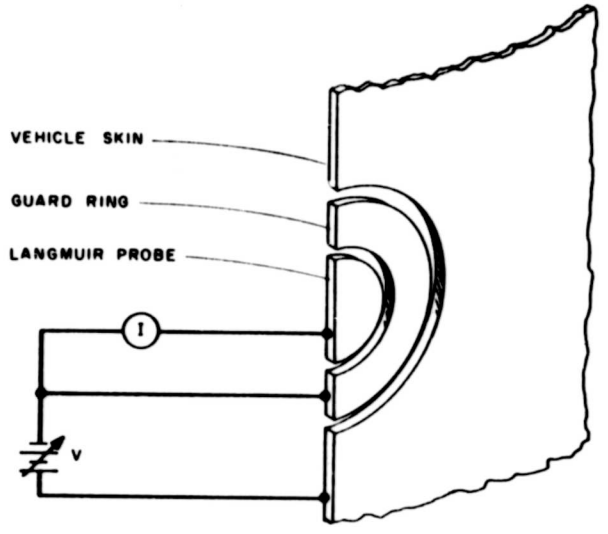
(a) CONTROL OF PROBE SHEATH EXTENT



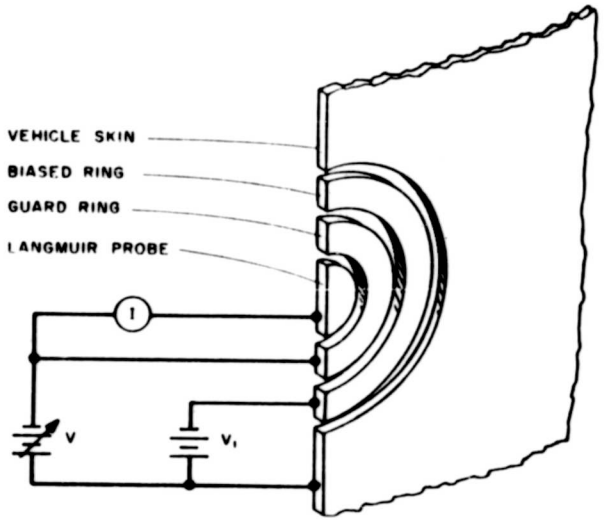
(b) ELIMINATING SHEATH CAUSED BY VEHICLE POTENTIAL

RA-3709-28

FIG. VI-6 POSSIBLE REFINEMENTS OF PLANE PROBE



(a) CONTROL OF PROBE SHEATH EXTENT



(b) ELIMINATING SHEATH CAUSED BY VEHICLE POTENTIAL

RA-3709-28

FIG. VI-6 POSSIBLE REFINEMENTS OF PLANE PROBE

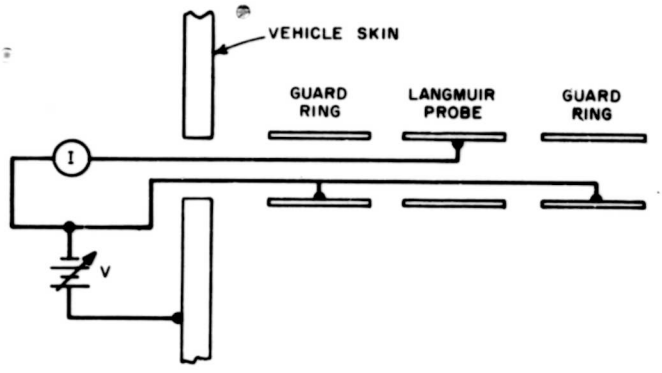
isolated from the skin would be placed around the guard ring and biased to some appropriate potential to eliminate the effects of the vehicle sheath in the region of the Langmuir probe. These probe designs [illustrated in Figs. VI-6(a) and VI-6(b)] should be studied in the laboratory in order to be certain of their characteristics before they are used on a rocket.

A further problem associated with the use of a plane probe in the vehicle skin is that in this location the probe is sampling a region where considerable outgassing can occur. Experimenters endeavor to minimize outgassing by hermetically sealing the instrumentation and using special fuel shutoff valves on liquid fueled motors.

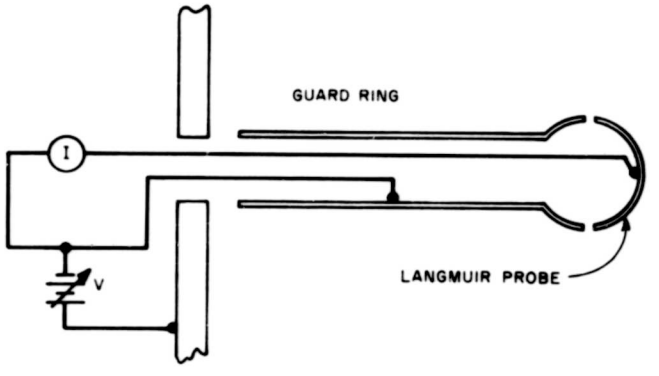
Most of the problems associated with the use of the plane probe are eliminated if the cylindrical or spherical probes illustrated in Figure VI-7 are used. Mounting the probe on a boom removes the probe from the vehicle sheath and from the region where outgassing is occurring. The guard ring structures shown eliminate field fringing so that in the case of both probes, ion sheath thickness variations are amenable to analysis. The outer guard ring in Figure VI-7(a) may be omitted if the sheath thickness is small compared with the length of the Langmuir probe section of the structure.

As was indicated earlier, the use of a boom to support the probe involves additional mechanical complexity and precludes the possibility of obtaining data at very low altitudes. However, unless the fundamental problems associated with the use of a skin-mounted plane probe can be eliminated, a cylindrical or spherical probe should be used.

Associated with the use of any of the Langmuir probe types is the question of how different probe materials and contaminants affect probe performance. This problem is being investigated by L. H. Brace of the University of Michigan who plans to fire a rocket equipped with six Langmuir probes arranged in two sets of three probes each. One set consists of three flush-mounted plane probes, and the second set



(a) CYLINDRICAL PROBE



(b) SPHERICAL PROBE

RA-3709-29

FIG. VI-7 CYLINDRICAL AND SPHERICAL LANGMUIR PROBES

consists of three cylindrical probes. Three different materials will be used in fabricating the probes in each set. Thus, by comparing the results obtained with a set, it will be possible to investigate the importance of probe material in determining performance. By comparing the results between the two sets it will be possible to obtain an indication of the importance of the vehicle sheath and variable probe sheath in degrading the accuracy of the data which can be obtained using a flush-mounted probe. The results of Brace's work, if available in time, should certainly be considered in planning the details of the proposed instrumentation.

(2) Impedance Probe

To provide an independent determination of N_e, it is recommended that an impedance probe be carried on the vehicle. Since the collision frequency, ν, will be significant in the altitude range of interest, it will be necessary to obtain values for both ν and the plasma frequency, ω_p, in order to determine N_e. Thus, as was discussed earlier, a simple capacitance measurement will not suffice; it will be necessary either to measure both the real and imaginary parts of the probe impedance or to measure the change in probe capacitance at two different frequencies.

Several approaches to the measuring problem are possible. It is worth noting in this regard that frequency is generally easier to measure accurately than is impedance. It appears, therefore, that a suitable technique might be to use the probe as part of the frequency-determining tank circuit of an oscillator which can be made to switch between two frequency ranges. By measuring the frequency change at the two frequencies, sufficient information will be obtained to define the capacitance at the two frequencies, thereby permitting the determination of ν and ω_p. Additional information regarding the use of a probe in the tank circuit of an oscillator should be available soon from J. A. Kane of NASA who will shortly perform a rocket experiment of this sort using an oscillator operating in two frequency bands.

Several probe designs may be used. For example, an unfurlable probe protruding from the vehicle in a manner similar to that illustrated in Figure VI-7(a) would be suitable. Alternatively, to avoid the complications associated with unfurling a probe, the rocket vehicle itself may be split at some fuselage station and two halves used to form the elements of the impedance probe. An advantage of using the vehicle as a probe is that the thickness of the plasma sheath formed as the result of nonzero vehicle potential is small compared with the vehicle diameter below 100 km.[27] On the other hand, the sheath thickness may approach the diameter of an unfurlable probe.

(2) Impedance Probe

To provide an independent determination of N_e, it is recommended that an impedance probe be carried on the vehicle. Since the collision frequency, ν, will be significant in the altitude range of interest, it will be necessary to obtain values for both ν and the plasma frequency, ω_p, in order to determine N_e. Thus, as was discussed earlier, a simple capacitance measurement will not suffice; it will be necessary either to measure both the real and imaginary parts of the probe impedance or to measure the change in probe capacitance at two different frequencies.

Several approaches to the measuring problem are possible. It is worth noting in this regard that frequency is generally easier to measure accurately than is impedance. It appears, therefore, that a suitable technique might be to use the probe as part of the frequency-determining tank circuit of an oscillator which can be made to switch between two frequency ranges. By measuring the frequency change at the two frequencies, sufficient information will be obtained to define the capacitance at the two frequencies, thereby permitting the determination of ν and ω_p. Additional information regarding the use of a probe in the tank circuit of an oscillator should be available soon from J. A. Kane of NASA who will shortly perform a rocket experiment of this sort using an oscillator operating in two frequency bands.

Several probe designs may be used. For example, an unfurlable probe protruding from the vehicle in a manner similar to that illustrated in Figure VI-7(a) would be suitable. Alternatively, to avoid the complications associated with unfurling a probe, the rocket vehicle itself may be split at some fuselage station and two halves used to form the elements of the impedance probe. An advantage of using the vehicle as a probe is that the thickness of the plasma sheath formed as the result of nonzero vehicle potential is small compared with the vehicle diameter below 100 km.[27] On the other hand, the sheath thickness may approach the diameter of an unfurlable probe.

Thus the presence of the sheath about the probe will introduce more error in the case of the unfurlable probe. It should be possible, however, to apply a dc bias between the unfurlable probe and the vehicle to eliminate the plasma sheath. Kane, in his experiment, plans to study this problem by applying a variable dc voltage to his probe and observing the effect of this voltage upon probe impedance.

(3) Ion Trap

To provide a second method for determining N_i, it is recommended that an ion trap be installed on the vehicle. Many of the problems associated with the use of Langmuir probes on rocket vehicles also apply to ion traps. Flush-mounting the trap places it within the ion sheath surrounding the vehicle, and, at the same time, increases the possibility of erroneous measurements resulting from vehicle outgassing. The use of a boom mounting for the trap, on the other hand, removes the trap from the vehicle sheath and the region of outgassing, but increases the mechanical complexity and weight of the instrumentation.

As in the case of the Langmuir probe, three general ion trap geometries are possible: plane, cylindrical, and spherical. The arguments regarding the use of guard rings also apply to the ion trap. Various grid arrangements and sweeping techniques have been used. Suitable arrangements can be chosen to study particle energy and to eliminate photo-electric currents which often cause confusion. Another type of ion trap is presently being investigated by Kane of NASA. In this design a plane collector plate is recessed in the vehicle and a dc magnetic field is established across the face of the trap to deflect electrons into the walls of the recess so that only ions reach the collector plate. This technique does not lend itself to use in cylindrical or spherical geometries.

Much ion trap work is currently under way, and the final design determination should be based in part upon the results of current experiments. Of particular interest will be a comparison of the results

Thus the presence of the sheath about the probe will introduce more error in the case of the unfurlable probe. It should be possible, however, to apply a dc bias between the unfurlable probe and the vehicle to eliminate the plasma sheath. Kane, in his experiment, plans to study this problem by applying a variable dc voltage to his probe and observing the effect of this voltage upon probe impedance.

(3) Ion Trap

To provide a second method for determining N_i, it is recommended that an ion trap be installed on the vehicle. Many of the problems associated with the use of Langmuir probes on rocket vehicles also apply to ion traps. Flush-mounting the trap places it within the ion sheath surrounding the vehicle, and, at the same time, increases the possibility of erroneous measurements resulting from vehicle outgassing. The use of a boom mounting for the trap, on the other hand, removes the trap from the vehicle sheath and the region of outgassing, but increases the mechanical complexity and weight of the instrumentation.

As in the case of the Langmuir probe, three general ion trap geometries are possible: plane, cylindrical, and spherical. The arguments regarding the use of guard rings also apply to the ion trap. Various grid arrangements and sweeping techniques have been used. Suitable arrangements can be chosen to study particle energy and to eliminate photo-electric currents which often cause confusion. Another type of ion trap is presently being investigated by Kane of NASA. In this design a plane collector plate is recessed in the vehicle and a dc magnetic field is established across the face of the trap to deflect electrons into the walls of the recess so that only ions reach the collector plate. This technique does not lend itself to use in cylindrical or spherical geometries.

Much ion trap work is currently under way, and the final design determination should be based in part upon the results of current experiments. Of particular interest will be a comparison of the results

obtained by R. Sagalyn of AFCRL who is using spherical traps mounted on booms with the results of J. A. Kane of NASA who is using flush-mounted traps.

h. Conclusions

Discussions of the capabilities of various methods for obtaining electron and ion density with several groups currently performing experiments indicated that within specific ranges of charged particle densities and collision frequencies, a relative precision of 10% is claimed. To obtain comparable accuracy in the D-region where the conditions may change rapidly and the collision frequency may become comparable to the plasma frequency, requires one to utilize a combination of measuring techniques as proposed in Section g. rather than a single measurement.

Unfortunately, since very few measurements have actually been accomplished in the D-region and very little testing has been performed in simulated environments, the precise accuracy limitations of the various methods are not yet determined. In the near future, however, further flight test data should be available (Kane, Brace, and Sagalyn), which may provide a basis for comparing the various methods of measurement.

Another factor which complicates the assessment of system precision is the fact that the density data obtained from the up and down legs of missile flights differ by as much as a factor of two below 100 km. Since the horizontal distance between the up and down paths may be on the order of 30 to 40 km, the inhomogeneity in the D-region can be at least partially responsible for such a variation with an additional component supplied by the short-term variation of the entire layer density.

Final design of an instrumentation system should depend on the outcome of a suitable testing program. The principal aim of such a program would be the subjecting of the various probes and sensing elements

to a simulated environment to determine exactly what their characteristics are rather than relying on a strictly theoretical approach. This will give a more realistic basis for specifying the accuracy of the measurement.

4. Measurement of Density

Atmospheric density is required to obtain the neutral particle concentration. It can be determined by measuring the missile altitude and referring to a standard atmosphere. It would be much more satisfactory, however, to measure it directly.

If density is measured directly, no need theoretically exists for the measurement of altitude. However, in order not to lose valuable experimental results because of possible malfunction of the density instrumentation, radar tracking should be provided. Several systems have been developed for density measurements in the past, such as the pitot tube technique (up to $\sim$ 80 km) or an analysis of the pressure variations of a flush-mounted gauge as the missile rolls (80 - 120 km). Radioactive ionization gauges under development seem capable of simplifying density measurement techniques.

5. Ancillary Measurements and Observations

a. Riometers

Riometer measurements would be useful, though not essential in all of the experiments except, possibly, those conducted during quiescent conditions. They would serve as a check on the values obtained during the experiments. Also, if some of the rocketborne equipment malfunctions, riometer records may aid in interpreting data from the operating instruments. For SID, PCA, and auroral bremsstrahlung experiments, riometer data can aid in choosing appropriate firing times for the probes.

b. Solar Patrol

The value of a close liaison with a solar observatory during SID experiments canot be overemphasized. Close cooperation would also be valuable during PCA experiments. For SID experiments, local solar patrol should be established in addition to the observatory participation. The local solar patrol should be established well in advance of the experiments so that the observers can be trained to provide the visual (Hα) observations required to alert the missile launching crew.

c. Auroral Features

Observations of auroral features during both the PCA and auroral bremsstrahlung experiments may prove to be of value in interpreting results. The presence of auroral features could explain anomalous results from PCA experiments. The observation of characteristic moving, red auroral features may be of considerable value in alerting balloon and missile launching crews for auroral bremsstrahlung experiments.

6. Solar Aspect Measurements

Response characteristics of collimated sensors depend upon their orientation relative to the direction of the ionizing beam. Variation of sensor response with solar aspect angle must therefore be determined to correct the data. Electro-optical solar aspect systems can be easily incorporated into the rocket configurations and are capable of higher accuracy than is warranted by the solar radiation flux measurements.

An accurate description of the rocket's orientation in space is provided by the Naval Research Laboratory two-cell optical aspect system which utilizes photocells, each oriented with its axis of maximum sensitivity perpendicular to the roll axis of the rocket. One photocell is narrowly collimated and sweeps out a plane as the rocket rolls, seeing the earth for half of each roll and dark sky for the other half. The companion photocell is of low sensitivity and wide field of view. A relationship exists between rocket orientation, and the relation of the

horizon signals generated by the collimated (earth) cell, to the time and amplitude of the maximum response generated by the sun cell.

A single photocell can also be employed to determine the solar aspect. Signal amplitude is directly proportional to the amount of radiant energy falling upon the sensing surface. At constant illumination, the photocell response varies with relative aspect angle between the sensing surface normal and the sun. The crux of this method is, of course, knowing the photocell response for zero-incidence (i.e., direct viewing of the sun) at all points along the flight path. Since the overhead air mass will change continuously with altitude, the total radiant energy will also change accordingly. Thus the maximum response of the photocell at the particular altitude will correspond to direct viewing of the sun; any deviation from the maximum can be related to the angle of incidence by reference to preflight calibration information. It should be noted that this same information is necessary for solution of the expressions used with the two-cell aspect system.

7. Data Reduction

a. Ionizing Flux: Protons

Polar cap proton events are, in the slowly decaying phase, quite uniform in character; they vary slowly with time and are produced by measurable fluxes of ions, dominantly protons. Since they do not perturb the earth's field during this phase and apparently follow Störmer orbits, calculations of the electron production rates, q(h), in the ionosphere caused by a given proton influx should be straightforward. The initial considerations were presented in Sections IIB and IIIA.

Initially it was felt that if protons were incident in a given layer of the ionosphere from a random direction, then there could be a strong influence on the Störmer orbits at particular incident angles due to the energy loss (dE/dx) of the particles in the ionosphere. Recently it was found that this problem has been considered in detail by Weir[32] (he has also calculated ionospheric effects of solar protons).[33]

Inclusion of dE/dx in orbit calculations was found not to perturb the lossless orbit significantly: the electron production rate q(h) can thus be calculated without this complicating effect. The major uncertainty in calculating q(h) rests in our sketchy knowledge of the differential kinetic energy spectra of the protons (or other ions in the polar flux). Studies now underway in various laboratories should resolve this uncertainty. Factors such as dE/dx, the average energy per ion pair, W, etc., were summarized in Section IIIA and are believed to be of adequate accuracy for the calculation of q(h). Weir's calculations should be carefully studied when they become available. When adequate knowledge of the ion flux creating PCA's is obtained, experiments to test the validity of the calculations should be performed, particularly near the geomagnetic pole where perturbations due to geomagnetic cutoffs are negligible.

b. Ionizing Flux: X-rays

When X-rays are observed in the ionosphere, they produce primary ionization by photoelectric "stripping" of electrons from neutral molecules and secondary ionization by the stripped electrons. The time rate of electron production per unit volume q is obtained from the relation

$$q = \int \sigma^{air}_{X\text{-ray}}(\lambda) \frac{d\,Q(\lambda)}{d\lambda} \frac{n(N_2,\ O_2)}{W} d\lambda \qquad (10)$$

where

$\sigma^{air}_{X\text{-ray}}(\lambda)$ is the X-ray absorption cross section as a function of X-ray wavelength λ

$\frac{dQ(\lambda)}{d\lambda}$ is the spectral radiance (erg/cm^2-sec-A) of incident X-radiation

$n(N_2,\ O_2)$ is the particle number density of air

W is the average energy lost by a photon in removing an electron from a molecule of air (35 ev).

Of these parameters the X-ray absorption cross section $\sigma^{air}_{X\text{-ray}}$ and the average energy required to produce a free electron, W, are quite well known (i.e., to within a few percent). The uncertainties in $n(N_2,\ O_2)$

and $\frac{dQ(\lambda)}{d\lambda}$ are, on the other hand, expected to be much larger than those in $\sigma^{air}_{X\text{-}ray}$ and W; hence the latter two uncertainties may be neglected in our treatment. Determination of $n(N_2, O_2)$ is considered elsewhere.

Since the values of $Q(\lambda, h)$ are not measured simultaneously at the different altitudes, one must standarize to a given time by estimating the time rate of change of R (defined below) at each altitude from the values measured at the same altitudes during the descent phase of the flight and during subsequent flights. By numerical methods we can compute

$$R_{standard} = R_{observed} + \int_{t_{obs}}^{t_{stand}} \left(\frac{dR}{dt}\right) dt \qquad (11)$$

In order to obtain the X-ray spectrum at any altitude, one must find the mean measured spectral radiance $R(\lambda)$ in each wavelength interval at a given altitude and divide by the mean spectral counting efficiency $\bar{\epsilon}(\lambda)$ of the corresponding sensor:

$$\left(\overline{\frac{dQ}{d\lambda}}\right)_{\frac{\lambda_1+\lambda_2}{2}} = \frac{1}{\lambda_2 - \lambda_1} \int_{\lambda_1}^{\lambda_2} \frac{R(\lambda)}{\epsilon(\lambda)}\, d\lambda = \frac{\bar{R}(\lambda)}{\bar{\epsilon}(\lambda)} \qquad (12)$$

A histogram of the $\left(\overline{\frac{dQ}{d\lambda}}\right)$ for each wavelength interval is plotted as in Figure VI-8. A smooth curve drawn through the blocks as shown in the figure represents the trial spectrum at altitude h_1. This spectrum is extrapolated to an altitude above the absorbing region $(h = \infty)$ of the atmosphere by use of the equation

$$\frac{dQ}{d\lambda}(\lambda, \infty) = \frac{dQ}{d\lambda}(\lambda, h_1) \exp -\int_{h_1}^{\infty} \sigma^{air}_{X\text{-}ray}(\lambda) n(N_2, O_2)\, dh \qquad (13)$$

The shape of the spectrum is varied until one finds a $\frac{dQ(\lambda, \infty)}{d\lambda}$ which best agrees with all the extrapolated spectra. This is selected as the spectrum used in the computation of q.

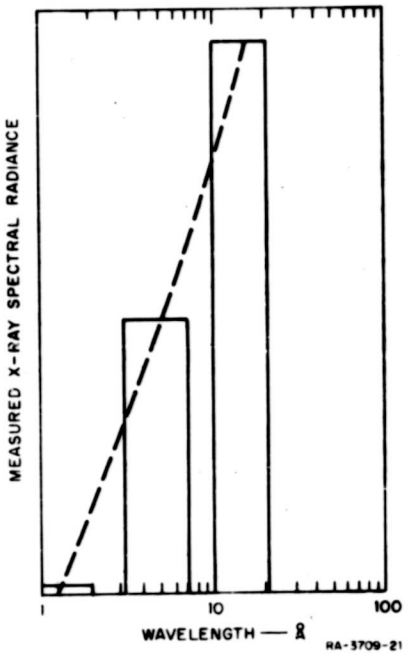


FIG. VI-8 OBSERVED X-RAY SPECTRUM. THE BLOCKS REPRESENT THE MEAN SPECTRAL RADIANCE IN THE APPROPRIATE WAVELENGTH INTERVAL. THE BROKEN LINE REPRESENTS THE ESTIMATED X-RAY SPECTRUM

The degree of precision present in the determination of the X-ray spectral radiance $\frac{dQ(\lambda)}{d\lambda}$ is dependent upon the width of the spectral "windows" of the sensors (see Section VI B 2 for a discussion). It is believed that q(h) can be obtained to within, possibly well within, a factor of 1.5 by this method of approach. Most of the uncertainty in q is expected to be a systematic one.

c. Measured Electron Concentration and Time Rate of Change of Electron Concentration

The electron concentration profiles obtained during the course of an SID or a PCA must be analyzed for probable error and for the time rate of change of electron concentration. Estimates of the former are based on the methods employed in measurement as well as on the dispersion of the data about smooth curves faired through them. It is anticipated that our previously described measurement of electron concentration will yield a dispersion of less than ten percent at altitudes above 70 km. The time rate of change of electron concentration at a given altitude and given time can be obtained by plotting the concentration as a function of time for each altitude considered. The data establish three points through which a smooth curve can be faired. The slope of the curve is equal to the time rate of change of the electron concentration. Numerous smooth curves can of course, be faired through these points; limiting curves of this type can be used to estimate the probable error in dN_e/dt. Since the values of N_e are not measured simultaneously at the different altitudes, one must standardize each N_e profile to a given time by estimating the time rate of change of N_e at each altitude. By numerical integration we can compute

$$N_e(\text{standard}) = N_e(\text{observed}) + \int_{\text{obs}}^{\text{stand}} \left(\frac{dN_e}{dt}\right) dt \qquad (14)$$

It is believed that after the initial phase of PCA events the ionosphere is sufficiently close to a steady state that $\frac{dN_e}{dt}$ can be neglected in computations of the various relaxation parameters.

d. Measured Negative Ion-Electron Concentration Ratio and Its Time Rate of Change

The negative ion-electron concentration ratio $\lambda = \frac{N^-}{N_e}$ is not measured directly; it is derived from measurements of electron and negative ion concentrations. The time rate of change of λ is obtained from N_e and N_i^- and their time rates of change:

$$\frac{d\lambda}{dt} = \frac{1}{N_e}\frac{dN_i^-}{dt} - \frac{N_i^-}{N_e^2}\frac{dN_e}{dt} \qquad (15)$$

It is expected that $\frac{d\lambda}{dt}$ will be a small quantity, even during the initial phases of SID's. Hence the uncertainties arising from the dispersion in N_e, N_i^-, $\frac{dN_e}{dt}$, and $\frac{dN_i^-}{dt}$ will probably prevent the observation of a nonvanishing $\frac{d\lambda}{dt}$. This speculation can only be decided by experiment.

In the determination of λ the adjustment of the negative ion concentration to a standard time (equation (14)) must be applied.

8. Interpretation

In the foregoing, methods of measuring various physical quantities associated with the D-region during PCA events, SID's, and under quiet conditions have been considered. In order to construct, from the measurements, a model of the D-region which can be used for prediction purposes during various types of disturbances one must derive as many relaxation parameters as possible, as well as electron collision frequencies.

a. Relaxation Parameters

(1) Dissociative Recombination Coefficient α_D

α_D can be determined from the electron concentration N_e and electron production rate profiles made in the quiet D-region and during PCA and SID's and possibly during auroral events. One must be cautious in the interpretation of the quiet D-region α_D since it may

correspond to a different positive ion (possibly NO^+) than the α_D representative of a disturbed D-layer (N_2^+ and O_2^+ are probably the dominant ions here). Under steady state conditions (quiet D-layer and the steady portion of PCA events) the dissociative and ion-ion recombination coefficients, α_D and α_i, are related to N_e and q by the expression

$$\frac{q}{1+\lambda} = (\alpha_D + \lambda\, \alpha_i)\, N_e^2 \qquad (16)$$

where λ is the ratio of negative ion to electron concentration. At high altitudes (i.e., > 75 km), $\lambda \ll 1$ during the daytime and equation (16) reduces to

$$q \approx \alpha_D\, N_e^2 \qquad (16a)$$

Thus daytime measurements of q and N_e between altitudes of 75 and 90 km immediately yield the dissociative recombination coefficient profile in this interval. This profile coupled with electron temperature measurements should yield the temperature dependence of α_D. Because of the very low electron concentrations present in the normal D-region, α_D corresponding to quiet conditions cannot be determined below 75 km altitude. At altitudes of ~ 50 to 65 km measurements of λ, q, and N_e are made during PCA events just before and just after sunrise or sunset and substituted in the equation

$$\alpha_D = \left[\frac{\lambda^D}{(N_e^N)^2} \left(\frac{q^N}{1+\lambda^N} \right) - \frac{\lambda^N}{(N_e^D)^2} \left(\frac{q^D}{1+\lambda^D} \right) \right] \frac{1}{\lambda^N - \lambda^D} \qquad (17)$$

(in which the superscripts D and N in the right hand member denote day and night respectively) in order to find α_D. Hence one can, if the ionospheric measurements are sufficiently accurate, determine the dissociative recombination coefficient for altitudes between 50 and 90 km. Biondi's laboratory measurements[34] of α_D for N_2 and O_2 at pressures greater than 0.1 mm of Hg revealed that the ions N_3^+, N_4^+, and O_3^+ are very important at these relatively high pressures. These ions may therefore be of considerable importance at altitudes below 65 km; if so,

the effect will be manifested as a much larger α_D than one would expect from N_2^+ and O_2^+ ions. At high altitudes (> 75 km) α_D can be determined to an accuracy of about 10 percent if N_e and q are known to within 10 and 20 percent, respectively. At low altitudes α_D can be determined to an accuracy of about 25 percent if N_e, N_i^- and q are known to within 10, 10, and 20 percent respectively.

During SID's steady state conditions do not prevail and one must replace equation (1) by the time-dependent form

$$\frac{dN_e}{dt} = \frac{q}{1+\lambda} - (\alpha_D + \lambda \alpha_i) N_e^2 \qquad (18)$$

At altitudes above 75 km this relation simplifies to

$$\frac{dN_e}{dt} \approx q - \alpha_D N_e^2 \qquad (18a)$$

and one can readily find α_D from the measurements of $\frac{dN_e}{dt}$, q, and N_e. It is doubtful that the α_D profile can be extended to altitudes below 75 km by this method because of lack of knowledge of the role played by the ion-ion recombination coefficient below this altitude. If $\frac{dN_e}{dt}$, q, and N_e can be found to within uncertainties of 20, 20, and 10 percent, respectively, α_D can be determined to an accuracy of about 40 percent.

The dissociative recombination coefficient may also be determined in auroral events if the ionized columns are sufficiently homogeneous and either steady or smoothly varying in time. The method is essentially that used in PCA events.

(2) Ion-Ion Recombination Coefficient α_i

This parameter cannot be determined from experiments in the quiet D-region. It was once considered feasible by the authors to find α_i for altitudes of 65 to 75 km by use of the equation

$$\alpha_i = \frac{\alpha_{eff} - \alpha_D}{\lambda}$$

where α_{eff} is the effective recombination coefficient obtained during SID's. The extrapolation of α_D to lower altitudes would be based on its observed temperature dependence at altitudes above 75 km. However, as discussed in the preceding section, recent laboratory work by Biondi and coworkers[34] on the dissociative recombination coefficients of N_2^+ and O_2^+ at pressures above 0.1 mm of Hg indicates that such an extrapolation is not justified. Hence one is limited to PCA or auroral experiments for the determination of the ion-ion recombination coefficient.

A feasible PCA experiment was briefly discussed in the preceding section. It consists of the measurement of the electron production rate q, the electron concentration N_e, and the negative ion concentration N_i^- before and after sunset or sunrise. The coefficient α_i is obtained from the equation

$$\alpha_i = \frac{1}{\lambda^N - \lambda^D} \left[\frac{q^N}{(1+\lambda^N)(N_e^N)^2} - \frac{q^D}{(1+\lambda^D)(N_e^D)^2} \right] \qquad (19)$$

where the superscripts N and D refer to nighttime and daytime. Assuming that one can measure N_i^-, N_e, and q to accuracies of 10, 10, and 20 percent, respectively, one can find α_i to within a factor of two. This method can also be used with auroral events in which the ionization is produced by bremsstrahlung if the columns are sufficiently steady or smoothly varying in time.

(3) Nighttime Detachment Coefficient

This parameter can, of course, be investigated only by means of PCA or auroral experiments. The authors consider the most important nighttime electron detachment process to be associative detachment by atomic oxygen[35]

$$O_2^- + O + O \rightarrow O_2 + O_2 + e \qquad (20)$$

rather than collisional detachment by molecular oxygen

$$O_2^- + O_2 \rightarrow O_2 + O_2 + e \qquad (21)$$

Which of these is the important mode of nighttime detachment at various altitudes can be determined by the ratio of negative ion concentration to electron concentration, λ, at night at altitudes of 70 to 90 km. The λ profile is given by the equation

$$\lambda = \frac{\kappa[n(O_2)]^2 + \beta_r(O)n(O) + \beta_r(O_2)n(O_2)}{\delta} \qquad (22)$$

where δ is the detachment parameter given by

$$\delta = \gamma_a n(O) \quad \text{(process (20))} \qquad (23a)$$

$$\delta = \gamma_c n(O_2) \quad \text{(process (21))} \qquad (23b)$$

The other parameters are

κ - three body attachment coefficient for O_2[36]

$n(O_2)$ - molecular oxygen concentration

$n(O)$ - atomic oxygen concentration

γ_a - coefficient of associative detachment

γ_c - coefficient of collisional detachment

$\beta_r(O)$ - coefficient of radiative attachment to atomic oxygen

$\beta_r(O_2)$ - coefficient of radiative attachment to molecular oxygen.

Due to the relative magnitudes of κ and β_r, radiative attachment is probably considerably less important than 3-body attachment in the altitude interval 70 to 85 km. Also, it is well known that the nighttime concentration of atomic oxygen increases with increasing altitude between 70 and 90 km. It is apparent from equations (22) and (23) that if process (2) is the important nighttime detaching mechanism, the ratio $\frac{\lambda}{[n(O_2)]^2}$ decreases with increasing altitude. On the other hand if the dominant detachment mechanism is given by process (21), the ratio $\frac{\lambda}{n(O_2)}$ will be almost constant with respect to increasing altitude. The functional relationship of λ to altitude may thus be used as a means of determining which process, (20) or (21), is dominant. Assuming that the controlling detachment process is the associative mode, one can compute the corresponding coefficient γ_a if the n(O) profile is known. This profile can be determined down to ~ 85 km by airglow intensity measurements.[37] A method for extrapolating it to lower altitudes will be discussed in Section VI B 8a(5).

The principal sources of error in γ_a and γ_c are uncertainties in the molecular and atomic oxygen concentrations. If λ, $n(O_2)$, and n(O) can be determined to within 50, 50, and 100 percent, respectively, the uncertainties in γ_a and γ_c will be about 150 and 70 percent, respectively.

(4) Radiative Attachment Coefficients

The coefficient of radiative attachment of electrons to atomic oxygen $\beta_r(O)$ has been found to a high order of precision by Branscomb and coworkers.[38] The principle of detailed balancing cannot be used in conjunction with O_2^- photodetachment cross sections to find the O_2^- electron radiative attachment coefficient $\beta_r(O_2)$ (except to find a lower limit); consequently, the latter has not yet been determined. Use of the principle of detailed balancing together with the O_2^- photodetachment cross sections[39] yields a lower limit of ~ 10^{-20} cm^3/sec. In order to have an effect comparable with that of $\beta_r(O)$ the coefficient $\beta_r(O_2)$ must be > 10^{-17} cm^3/sec. It is not at all apparent that the $\beta_r(O_2)$

could be three orders of magnitude larger than its computed lower limit. This point can only be settled by experiment, however. If radiative attachment to molecular oxygen is important above 85 km, this fact should be revealed by the presence of a term proportional to $\frac{n(O_2)}{n(O)}$ (assuming that associative detachment is the important nighttime detachment process at these altitudes) in the profile of λ. If this profile is determined with a sufficiently high order of accuracy (within $\sim$ 10 percent), the coefficient $\beta_r(O_2)$ can be evaluated by fitting equation (22) to the λ profile unless it is so small that it is completely negligible in comparison to $\beta_r(O)$.

(5) Photodetachment Reciprocal Mean Lifetime

The effective photodetachment reciprocal mean lifetime ρ in the D-region is unknown. Laboratory measurements of the photodetachment cross section[38] indicate a value for detachment of electrons from atomic oxygen of $\rho(O^-) = 1.5\ sec^{-1}$ and for detachment from molecular oxygen[39] of $\rho(O_2^-) = 0.4\ sec^{-1}$. The former value is probably of a fairly high order of accuracy, but the latter is open to serious question. This is due to the fact that the population of excited states of the O_2^- ion may have been different in the laboratory experiment than occurs in the ionosphere.* In addition to the uncertainty in $\rho(O_2^-)$ there is considerable doubt as to the contribution to the effective ρ made by detachment of electrons from O^-. This is determined by the rate constant for the charge exchange process

$$O_2^- + O \rightarrow O_2 + O^- \qquad (24)$$

Measurements of the negative ion-electron concentration ratio (λ) profile in the sunlit D-region offers a way out of this uncertainty.

---

*In their measurement of cross sections for photodetachment from O_2^-, Burch and coworkers[39] found an electron affinity for O_2 of $\sim$ 0.15 ev while in electron swarm experiments Phelps and Pack[40] found an affinity of $\sim$ 0.46 ev. The difference may well have been due to the fact that in the swarm experiments collisional de-excitation of the O_2^- occurred before detachment whereas in the photodetachment experiment it did not.

The ratio, λ, is given during the day by the equation

$$\lambda = \frac{\kappa[n(O_2)]^2}{\rho} \qquad (25)$$

for altitudes below 85 km. If profiles of λ and $n(O_2)$ are determined under any of the three conditions considered herein (PCA, SID, and quiet D-region) the value of ρ can in principle be determined. However, the relatively large values of the negative ion and electron concentrations present in the D-region during PCA's and SID's render these conditions more appropriate to the determination of ρ. If $n(O_2)$ can be determined to within 25 percent of its true value it may be possible to obtain the photodetachment reciprocal mean lifetime to within 50 percent.

If one measures the λ profile just before and just after sunrise or sunset during a PCA or auroral event one obtains a relation

$$\frac{\lambda^D}{\lambda^N} = \frac{\gamma_a n(O)}{\rho} \qquad (26)$$

where D and N refer to day and night, respectively. Under the reasonable assumption that γ_a and ρ do not vary appreciably with altitude one can thus use the ratio $\frac{\lambda^D}{\lambda^N}$ to extend to lower altitudes the atomic oxygen concentration measured above $\sim$ 85 km by airglow intensity observations.

There has been some speculation as to whether or not the photodetachment reciprocal lifetime ρ varies during the course of a solar flare.[41] If so, λ will vary during the course of the SID in accordance with the equation:

$$\frac{d\lambda}{dt} = -\frac{\kappa[n(O_2)]^2}{\rho^2}\frac{d\rho}{dt} \qquad (27)$$

An experiment capable of determining the negative ion and electron concentration profiles at three different times during the SID can in principle resolve this point. If λ varies sufficiently rapidly that its change in time is not masked by errors in determining $\frac{d\lambda}{dt}$, one can obtain the time dependence of ρ.

(6) Relationship of the Gross Relaxation Coefficients to Those for Individual Processes

With the exception of radiative attachment to molecular oxygen no geophysical experiment considered in this study can yield relaxation parameters associated with each molecular process; only the "average" associated with a particular type of process will result. The "average" coefficients are related to those associated with individual processes as follows

$$\bar{\alpha}_D = \frac{\sum_{j+} \alpha_D^{j+} N_j(+)}{\sum_{j+} N_j(+)} \tag{28a}$$

$$\bar{\alpha}_i = \frac{\sum_{+-jk} \alpha_i^{jk+-} N_j(+) N_k(-)}{\sum_{jk+-} N_j(+) N_k(-)} \tag{28b}$$

where the summations are over all species of negative ions, - , positive ions, +, and excited states j and k as indicated.

$$\bar{\gamma} = \frac{\gamma(O_2^-)N(O_2^-) + \gamma(O^-)N(O^-)}{N(O_2^-) + N(O^-)} \tag{28c}$$

$$\bar{\rho} = \frac{\rho(O_2^-)N(O_2^-) + \rho(O^-)N(O^-)}{N(O_2^-) + N(O^-)} \tag{28d}$$

b. Electron Collision Frequencies

(1) From Electron Temperatures

Numerous measurements of the momentum transfer cross section Q_d for slow electrons in molecular nitrogen and oxygen have been made in recent years. These are shown as functions of electron energy in Figures VI-9 and VI-10. At a given electron speed v the collision frequency, ν, is

$$\nu = n_k \, v \, Q_{dk} \tag{29}$$

where n_k is the concentration of neutral particles of type k. For low energy electrons Q_d has the form

$$Q_d = a_m v^m \tag{30}$$

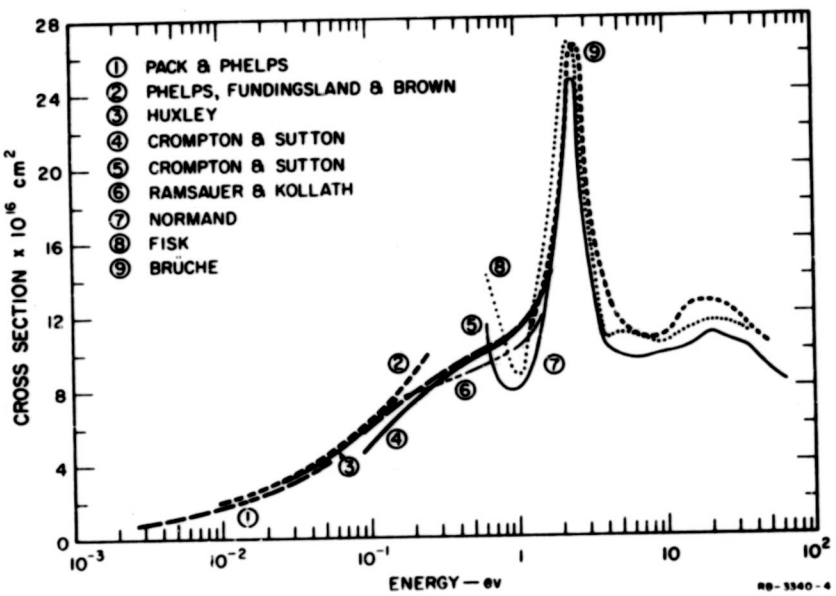
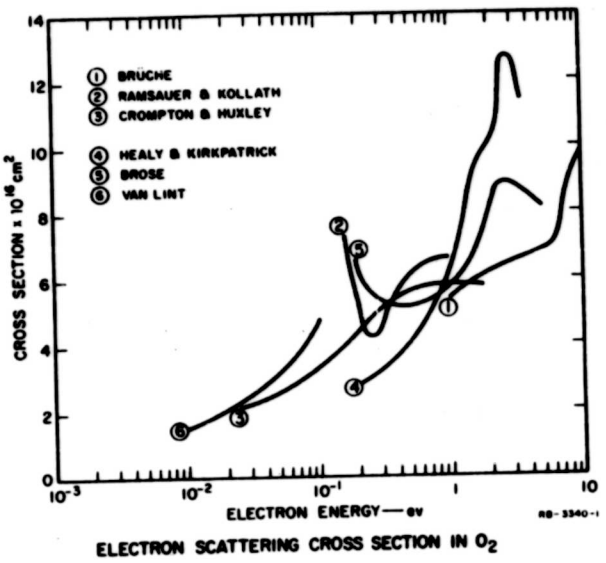


FIG. VI-9 TOTAL AND MOMENTUM TRANSFER CROSS SECTIONS FOR ELECTRONS (Q and Q_d, respectively) IN N_2 AS A FUNCTION OF ENERGY (1) Q_d FROM VELOCITY MEASUREMENTS,[42] (2) Q_d FROM MICROWAVE CONDUCTIVITY MEASUREMENTS,[43] (3) Q_d FROM DIFFUSION AND DRIFT VELOCITY MEASUREMENTS,[44] (4) MEAN Q_d DRUYVESTEYN DISTRIBUTION,[45] (5) Q_d OF COMPTON AND SUTTON, ASSUMING POWER LAW VELOCITY DEPENDENCE,[46] (6) Q_d ABSORPTION MEASUREMENT,[47] (7) Q_e ABSORPTION METHOD,[48] (8) Q ABSORPTION METHOD,[49] (9) ABSORPTION METHOD.[50]



ELECTRON SCATTERING CROSS SECTION IN O_2

FIG. VI-10 TOTAL AND MOMENTUM TRANSFER CROSS SECTIONS (Q and Q_d, respectively) FOR ELECTRONS IN O_2 AS A FUNCTION OF ENERGY. (1) Q ABSORPTION METHOD,[50] (2) Q ABSORPTION METHOD,[47] (3) Q_d FROM DIFFUSION AND DRIFT VELOCITY MEASUREMENTS,[51] ASSUMING POWER LAW VELOCITY DEPENDENCE,[46] (4) Q_d FROM DIFFUSION-DRIFT VELOCITY MEASUREMENTS,[52] (5) Q_d FROM DIFFUSION-DRIFT VELOCITY MEASUREMENTS,[53] DRUYVESTEYN DISTRIBUTION,[52] (6) Q_d FROM MICROWAVE MEASUREMENTS,[54] ANALYZED BY PHELPS.[55]

where m = 1 for molecular nitrogen and m ≈ 1 for molecular oxygen.[55] Hence in air

$$\nu = n_{air}\, a_{air}\, v^2 \tag{31}$$

If we neglect the effects produced by the presence of a magnetic field, the complex conductivity of a weakly ionized gas is related to the electron collision frequency $\nu(v)$ by the equation[56]

$$\sigma = -\frac{4\pi e^2}{3m} \int_0^\infty v^3 \, \frac{(\nu(v) - i\omega)}{\nu^2(v) + \omega^2} \, \frac{\partial f_0}{\partial v} \, dv \tag{32}$$

where e and m are the charge and mass, respectively, of the electron, ω is the frequency of an incident electromagnetic wave, and f_o is the electron velocity distribution function given by

$$f_o = A \exp \left[- \int_o^v \left[kT + \frac{3e^2E^2}{3m\, \xi(v)[\nu^2(v) + \omega^2]} \right]^{-1} mv\,dv \qquad (33)$$

In this equation k is Boltzmann's constant, E is the electric field amplitude of the incident electromagnetic field, T is the electron temperature (see Section VI B 3e), $\xi(v)$ is the fraction of excess electron energy lost by recoil in a collision with a gas molecule, and A is a normalizing function obtained from

$$N_e = 4\pi \int_o^\infty f_o\, v^2\, dv \qquad (34)$$

where N_e is the electron concentration. For weak fields and high frequencies equation (33) can be approximated by a maxwellian distribution. If there is a slight departure from equilibrium in the ionosphere during SID or PCA events, a small correction may have to be added to f_o. Methods for making this correction are given by Allis[57] and Delcroix.[58]

The D-region electron temperatures obtained by the rocket probes are substituted into the distribution function (33) and the conductivity is evaluated by use of equations (31) and (32). The absorption coefficient for electromagnetic waves in a weakly ionized medium is

$$k = \frac{2\pi}{c} \mathrm{Re}\ \sigma \qquad (35)$$

For the case $\omega >> \nu$, k in air is given by

$$k \approx \frac{5\ \omega_p^2\ \nu}{6c\ \omega^2} \qquad (36)$$

where ω_p is the plasma frequency. If $\omega \approx \nu$, the expression for k in air can not be put in an analytical form.[55]

(2) From HF Signal Absorption

For radio signal frequencies much larger than the electron collision frequency in air ($\omega \gg \nu$) one can use expression (36) to a fairly high order of accuracy in computing the absorption. In section VI B 3b we saw that under this condition the mean electron collision frequency in an altitude interval Δh was related to the differential absorption D in decibels, the mean square plasma frequency $\overline{\omega_p^2}$ and the two signal frequencies ω_1 and ω_2 by the equation

$$\bar{\nu} = 0.138 \frac{D}{\Delta h} \frac{c}{\overline{\omega_p^2}} \frac{\omega_1^2 \omega_2^2}{\omega_2^2 - \omega_1^2} \qquad (3)$$

An estimate of the differential absorptions involved can be obtained by using what are believed to be representative electron concentrations during SID's[59] and PCA events[60] and the electron collision frequencies of Phelps and Pack.[61] These are shown in Figure VI-11. Absorption coefficients computed with the aid of equation (36) and based on the data presented in Figure VI-11 are shown in Figure VI-12. In order to approach optimum conditions the signal frequency corresponding to the SID was chosen to be 10 mc; that corresponding to the PCA event was chosen to be 20 mc. The differential absorptions at various altitudes are shown in Table VI-6 for the case in which ω_2 is the fourth harmonic of ω_1 .

It is evident from Table VI-6 that if the differential absorption can be obtained to a precision of 0.05 db in an altitude interval of 4 km and the electron concentration to within 10 percent of its true value, the mean electron collision frequency in the interval can be measured to within ~ 15 percent. We are of course assuming ideal conditions here, i.e., that ω_1 is the optimum frequency for the electron concentration profile existing when the experiment is carried out. The actual uncertainty may be as large as ~ 50 percent.

This method may also be used during auroral events.

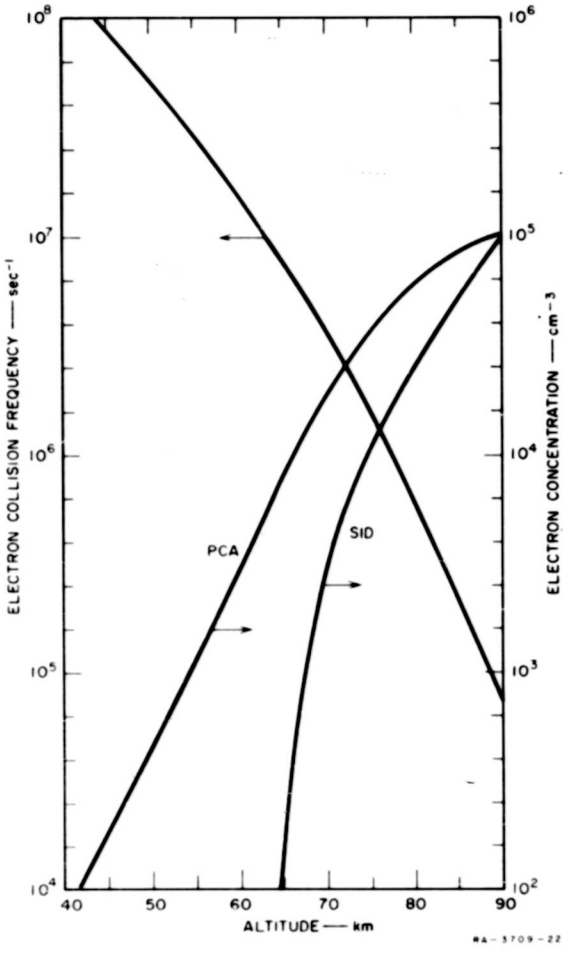


FIG. VI-11 TYPICAL ELECTRON CONCENTRATION PROFILES OCCURRING DURING SID'S,[59] AND PCA EVENTS,[60] AND ELECTRON COLLISION FREQUENCIES ACCORDING TO PHELPS AND PACK,[61]

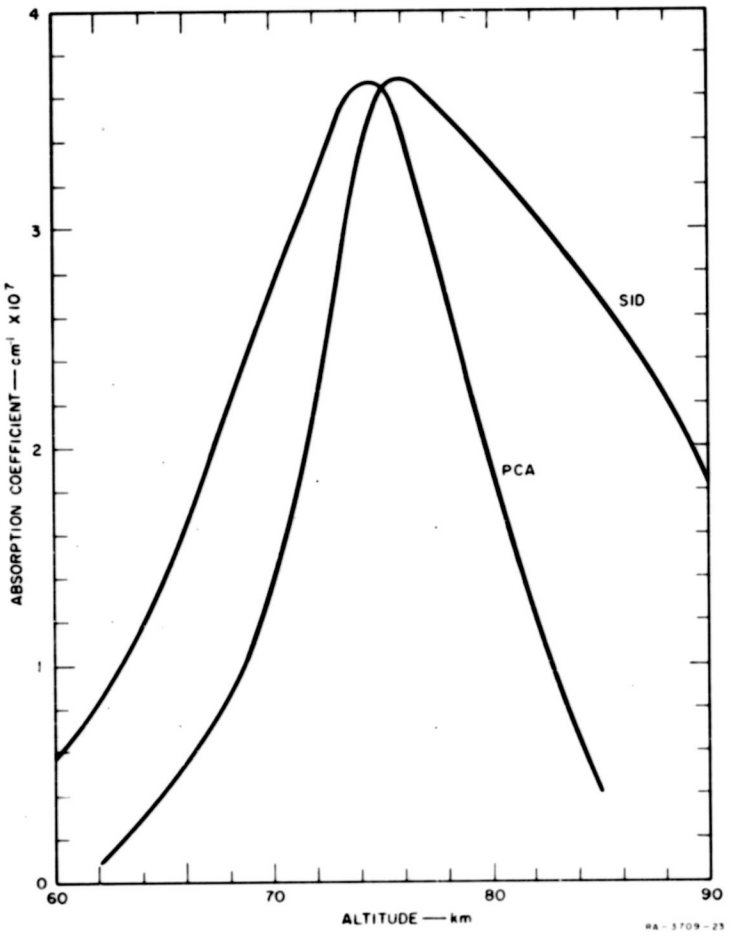


FIG. VI-12 HF ABSORPTION COEFFICIENTS BASED ON THE DATA PRESENTED IN FIGURE VI-11. THE SIGNAL FREQUENCIES ARE 10 mc (SID) AND 20 mc (PCA).

Table VI-6

DIFFERENTIAL ABSORPTION OF HF SIGNALS

Altitude (km)	Differential Absorption-db	
	SID; ω_1 = 10 mc, ω_2 = 40 mc	PCA; ω_1 = 20 mc; ω_2 = 80 mc
46	~ 0	0.28
50	~ 0	0.68
54	~ 0	1.25
58	~ 0	2.00
62	~ 0	2.96
66	0.10	4.14
70	0.43	5.40
74	1.25	6.63
78	2.54	7.65
82	3.70	8.35
86	4.68	8.70
90	5.33	--

9. Information Obtainable if Errors are Large or Part of the Equipment Malfunctions

It is conceivable, perhaps probable in some experiments, that a component intended for the measurement of one or more of the experimental parameters will malfunction or will provide data having large associated errors. Table VI-7 lists those derived parameters obtainable if some of the measurements are missing or have large associated errors.

C. Summary

The measurements that are considered to be pertinent and feasible and the relaxation parameters that can be determined from these measurements are summarized in Table VI-8. It is quite obvious that PCA events seem potentially to be the most rewarding. However, instrument development and cost per round are also expected to be much higher. Also the frequency of solar proton events can be expected to be low during the first part of the period of interest.

Table VI-7

INFORMATION OBTAINABLE IF ERRORS ARE LARGE OR PART OF THE EQUIPMENT MALFUNCTIONS

TYPE EVENT	INFORMATION OBTAINABLE IF MEASUREMENT OF													
	dN_e/dt		dN_i^-/dt		N_e		N_i^-		q		T_e		HF Absorp.	
	Fails	Has Large Error	Fails	Has Large Error	Fails	Has Large Error	Fails	Has Large Error	Fails	Has Large Error	Fails	Has Large Error	Fails	Has Large Error
SID	ρ (1)	ρ α_D, $d\rho/dt$ will have large assoc. error ν (1)	ρ α_D ν	ρ α_D $d\rho/dt$ will have large assoc. error	ν (2)	ν (2) α_D, ρ, $d\rho/dt$ will have large assoc. errors	ν α_D	ν α_D ρ, $d\rho/dt$ will have large assoc. errors	ν ρ $d\rho/dt$ (3)	ν ρ $d\rho/dt$ α_D may have large assoc. error (3)	ν (4) (5)	ν (4) (5)	ν (2) (6)	ν profile will have large assoc. error (2) (6)
PCA	--	--	--	--	ν (2)	ν (2) α_D, α_i, γ, ρ, $n(O)$ profile will have large assoc error	ν α_D	ν α_D α_i, γ, ρ, $n(O)$ profile will have large assoc. errors	ν γ ρ $n(O)$ profile	ν γ ρ $n(O)$ profile α_D and α_i will have large assoc errors	Same as above		Same as above	
Quiet D-Region	--	--	--	--	ν (2)	ν (2) α_D, ρ will have large assoc. errors	ν α_D	ν α_D ρ will have large assoc errors	ν ρ	ν ρ α_D will have large assoc. errors	Same as above		--	--

Table VI-7 *concluded*

TYPE EVENT	INFORMATION OBTAINABLE IF MEASUREMENT OF													
	dN_e/dt		dN_i^-/dt		N_e		N_i^-		q		T_e		HF Absorp.	
	Fails	Has Large Error	Fails	Has Large Error	Fails	Has Large Error	Fails	Has Large Error	Fails	Has Large Error	Fails	Has Large Error	Fails	Has Large Error
Auroral Brems-strahlung	γ, ρ All other parameters except $d\rho/dt$ if q is steady	γ, ρ Other parameters will have large assoc errors unless q is steady	ρ α_D γ ν	If it is measurable $d\rho/dt$ will have large assoc errors	No parameters	α_D, α_i, γ, ρ will have large assoc errors	ν α_D	ν α_D ρ, γ will have large assoc errors	ν γ ρ	ν γ ρ α_D, α_i will have large assoc errors	--	--	(6)	(6)

Notes: (1) If this occurs because only one or two rockets of the series of three provide adequate measurements of N_e, dN_e/dt may still be obtained (with somewhat reduced precision) from riometer measurements of reduction in cosmic noise intensity.

(2) The electron collision frequency may be obtained from electron temperature measurements.

(3) If satellite operations indicate that in the particular flare the X-ray intensity decreases sufficiently rapidly after its maximum, α_D may still be obtained with reasonably good precision from dN_e/dt and N_e data corresponding to the last probe of the series.

(4) The electron collision frequency may be obtained from HF absorption and N_e measurements.

(5) All other measurable parameters except the variation of α_D with temperature can be obtained.

(6) All other measurable parameters can be obtained.

SYMBOLS USED

α_D - dissociative recombination coefficient

α_i - ion-ion recombination coefficient

ρ - photodetachment rate

γ - collisional-type detachment coefficient

ν - electron collision frequency

N_e - electron concentration

N_i^- - negative ion concentration

q - electron production rate

T_e - electron temperature

Table VI-8

SUMMARY OF DATA THAT CAN BE DERIVED FROM GEOPHYSICAL EXPERIMENTS

PARAMETER	PCA	SID	QUIET D-REGION	AURORAL BREMSSTRAHLUNG
Effective dissociative recombination coefficient $\bar{\alpha}_D$	During steady portion. The uncertainty in α_D is approximately the same as that in the measurement	During decay phase. Uncertainty is largely dependent upon errors in measurements of q and dN_e/dt	Dominant + ion may be different than occurs during disturbance	If columns of free electrons and ions are sufficiently steady or smoothly varying in time
Effective ion-ion recombination coefficient $\bar{\alpha}_i$	During steady portion. Uses measurements of q, N_e, and λ made before and after sunrise or sunset	Doubtful	No	As in PCA if columns of ionization are steady
Effective nighttime detachment coefficients $\bar{\gamma}_c$, $\bar{\gamma}_a$	By determining dependences of λ upon $n(O_2)$ and $n(O)$ at night	No	No	As in PCA if columns of ionization are steady
Coefficient of radiative attachment to O_2 $\beta_r(O_2)$	By determining if there is a term in eqn for λ proportional to $n(O_2)/n(O)$ at high altitudes ($\geq$ 90 km) at night	No	No	Doubtful
Effective photodetachment mean reciprocal lifetime $\bar{\rho}$	By determining λ profiles during daylight	Same	Same	Doubtful
Time variation of $\bar{\rho}$	Possibly during decay phase of a "spike"	By measuring time rate of change of λ during decay-phase	No	Doubtful
Extension of atomic concentration $n(O)$ to lower altitudes	By measuring λ profiles just before and just after sunrise or sunset and "normalizing" on the basis of airglow determinations above 90 km	No	No	Doubtful
Electron collision frequencies				
(a) Temp measurement	Yes	Yes	Yes	Yes
(b) HF absorption measurement	Yes	Yes	Yes	Yes

Opportunities for quiescent D-region experiments will, of course, be almost unlimited and the cost of instrumentation can be much lower than for proton events. However, the amount of information obtainable may be quite low. The full potential of quiescent D-region experiments cannot be evaluated at this time, although there are definite indications that there is considerable value in such experiments.

Auroral bremsstrahlung events may also provide more frequent opportunities for research during the early part of the 1963-67 period. As the summary table (Table VI-8) shows, these experiments have considerable promise. Again, however, exploratory measurements are required to provide sufficient information for good experimental design.

Experiments during SID's would be the most economical in that instrument development costs and cost per probe fired should be the lowest of the group of experiments considered. Unfortunately, the amount of information obtainable is low and the flare frequency required for a reasonable program is not expected to be encountered until late in the 1963-67 period.

In the dicussion of the earlier portions of this section on specific experiments, it was apparent that a range of instrumentation exists for each kind of experiment. The necessary measurements conceivably can be made with a minimum number of instruments if sufficient exploratory experiments and instrument development is included in the research program. The necessity for duplicate measurements, large dynamic range, and a large number of spectral bands, lies in the fact that the present state of knowledge of these events is low and that instruments for these applications are not well developed. Table VI-9 summarizes the instrumentation required for both "minimum" and "optimum" experiments. "Minimum" experiments implies that either low probability of success is acceptable or that sufficient research and instrument development has been completed to insure a higher probability of success. "Optimum" experiments implies the necessity for conducting the geophysical experiments as soon as practicable, and thus providing a minimum of exploration and instrument development.

Table VI-9

SUMMARY OF INSTRUMENTATION REQUIREMENTS

EVENT	PCA		SID		AURORAL BREMSSTRAHLUNG		QUIESCENT CONDITIONS	
Instrumentation	Minimum Experiment	Optimum Experiment	Minimum Experiment	Optimum Experiment	Minimum Experiment	Optimum Experiment	Minimum Experiment	Optimum Experiment
Proton dE/dx chamber	X	X						
Proton spectrometer		X						
Electron dE/dx chamber						X		
Three wide-band K-edge X-ray detectors			X				X	
Several narrow-band K-edge X-ray detectors				X		X		X
X-ray scintillation spectrometer				X	X	X		
L α ion chamber								X
Langmuir probe	X	X	X	X	X	X	X	X
Impedance probe	X	X	X	X	X	X	X	X
Ion trap		X		X		X		X
HF absorption		X		X		X		X
Density		X		X		X		X
NO concentration								X
Radar tracking	X	X	X	X	X	X	X	X
Riometer		X		X		X		X
Flare patrol		X	X	X			X	X
Visual auroral observation		X			X	X		
Balloon observation	X	X		X	X	X		
Satellite observation*		X		X		X		X

*Desirable, but not necessary.

REFERENCES

1. Chubb, T. A., H. Friedman, R. W. Kreplin, W. A. Nichols, A. E. Urzicker, and M. J. Votaw, Solar Radiation Satellite, IGY Bulletin No. 42, Trans. Amer. Geophys. Union 41, No. 4 (December 1960)

2. Kreplin, R. W., U. S. Naval Research Laboratory, Private communication.

3. McIlwain, C. W., State University of Iowa, Private communication.

4. Meyerott, R. E., Lockheed Missiles and Space Division, Private communication.

5. Anderson, K. A., University of California, Private communication.

6. Davis, L. R. and C. E. Fichtel, et al., International conference on cosmic rays and the earth storm, Proceedings of the Kyoto Conference Sept. 4-15, 1961. To be published.

7. Wegner, H. E., dE/dx and E Semiconductor Detector Systems for 25 Mev He^3 and Alpha Particles, IRE Trans. Nuc. Sci. NS-8, 103-111 (1961)

8. Fichtel, C. E. and D. E. Guss, Heavy Nuclei in Solar Cosmic Rays. Proc. of Kyoto Conference. To be published.

9. Davis, L. R., O. E. Berg, and L. H. Merideth, Direct Measurements of Particle Fluxes in and Near Auroras in Space Research, H. Kallman-Bijl. Ed., North-Holland (Amsterdam, 1960)

10. Weir, R. A., Private communication.

11. Seddon, J. C., A. D. Pickar, and J. E. Jackson, Continuous Electron Density Measurements up to 200 Km, J. Geophys. Res. 59, 4 (1954)

12. Jackson, J. E., Upper Atmosphere Research Report No. XXIX, NRL report 4960, Naval Research Laboratory, Washington, D.C. (1957)

13. Kane, J. A., Reevaluation of Ionospheric Electron Densities and Collision Frequencies Derived from Rocket Measurements of Refractive Index and Attenuation, NASA Technical Note D-503, National Aeronautics and Space Administration, Washington, D.C. (1960)

14. Mechtly, E. A., et al., Instrumentation for Rocket Measurements of Electron Density in the Ionosphere, Scientific Report No. 127, Pennsylvania State University, Ionosphere Research Laboratory, University Park, Penn. (1960)

15. Haycock, O. C., Experimental Plan and Instrumentation for the Determination of the Electron Density in the Ionosphere, Scientific Report No. 1, University of Utah, Upper Air Research Laboratories (1957)

16. Pfister, W. and J. C. Ulwick, The Analysis of Rocket Experiments in Terms of Electron Density Distributions, J. Geophys. Res. 63, 2 (1958)

17. Rothman, R. and T. Morita, Transmission Through an Ionized Medium in the Presence of a Strong Magnetic Field, Tech. Report 74, SRI Proj. 2494, Contract AF 19(604)-3458, Stanford Research Institute, Menlo Park, California (1961)

18. Nisbet, J. S. Electron Densities in the Upper Ionosphere from Rocket Measurements, Scientific Report No. 126, Pennsylvania State University, Ionosphere Research Laboratory, University Park, Penn. (1959)

19. Prenatt, R. E., Faraday Rotation Measurements at Fort Churchill, J. Geophys. Res. 64, 9 (1959)

20. Haycock, O. C., Measuring Antenna Impedance in the Ionosphere, Electronics January 13, 1961

21. Bourdeau, R. E., et al., The Ionosphere Direct Measurements Satellite Instrumentation (Explorer VIII), Presented at National IAS-ARS meeting, Los Angeles, California, June (1961)

22. Jackson, J. E. and J. A. Kane, Performance of an RF Impedance Probe in the Ionosphere, J. Geophys. Res. 65, 2209 (1960)

23. Severin, J. A. and C. M. Crain, A Capacitance-Controlled Oscillator for the Measurement of the Dielectric Constant of Atmospheric Air, Report No. 5-29, Contract AF 33(616)-5024, Electrical Engineering Research Laboratory, The University of Texas, Austin, Texas (1957)

24. Bourdeau, R. E., E. C. Whipple, Jr., and J. F. Clark, Analytic and Experimental Electrical Conductivity between the Stratosphere and the Ionosphere, J. Geophys. Res. 64, 1363 (1959)

25. Hok, D. and W. G. Dow, in Rocket Exploration of the Upper Atmosphere, Edited by Boyd and Seaton, Pergamon Press Ltd., London (1954)

26. Carignan, G. R. and L. H. Brace, The Dumbell Electrostatic Ionosphere Probe: Engineering Aspects, Scientific Report JS-2, University of Michigan, Space Physics Laboratory, Ann Arbor, Mich. (1961)

27. Bourdeau, R. E., et al., Ionospheric Measurements Using Environmental Sampling Techniques, NASA Technical Note D-491, National Aeronautics and Space Administration, Washington, D.C. (1960)

28. Ichimiya, T., et al., Measurement of Positive-Ion Density in the Ionosphere by Sounding Rocket, Nature 190, 156 (1961)

29. Spencer, N. W., Bi-polar Probe Instrumentation No. 1, Scientific Report FS-1, University of Michigan Research Institute, Ann Arbor, Mich. (1958)

30. Takayama, K., H. Ikegami and S. Miyazaki, Plasma Resonance in a Radio Frequency Probe, Phys. Rev. Lett. 5, 238 (1960)

31. Krassovsky, V. I., Exploration of the Upper Atmosphere with the Help of the Third Soviet Sputnik, Proc. I.R.E., 47, 289 (1959)

32. Weir, R. A. Doctoral Thesis, University of California, to be published.

33. Brown, R. R. and R. A. Weir, Ionospheric Effects of Solar Protons. Arkiv för Geofysik 3, 523 (1961)

34. Kasner, W. H., W. A. Rogers, and M. A. Biondi, Electron-Ion Recombination Coefficients in Nitrogen and Oxygen, Phys. Rev. Lett. 7, 321 (1961)

35. Whitten, R. C. and I. G. Poppoff, Associative Detachment in the D-region, J. Geophys. Res. (to appear in March 1962)

36. Chanin, L. M., A. V. Phelps, and M. A. Biondi, Measurement of the Attachment of Slow Electrons in Oxygen, Phys. Rev. Lett. 2, 344 (1959)

37. Young, R. A. (Private communication)

38. Branscomb, L. M., D. S. Burch, S. J. Smith and S. Geltman, Photodetachment Cross Section and the Electron Affinity of Atomic Oxygen, Phys. Rev. 111, 504 (1958)

39. Burch, D. S., S. J. Smith, and L. M. Branscomb, Photodetachment of O_2^-, Phys. Rev. 112, 171 (1958)

40. Phelps, A. V. and J. L. Pack, Collisional Detachment in Molecular Oxygen, Phys. Rev. Lett. 6, 111 (1961)

41. Mitra, A. P. (Private communication)

42. Pack, J. L. and A. V. Phelps, Drift Velocities of Slow Electrons in Helium, Neon, Argon, Hydrogen and Nitrogen, Phys. Rev. 121, 798 (1961)

43. Phelps, A. V., O. T. Fundingsland, and S. C. Brown, Microwave Determination of the Probability of Collision of Slow Electrons in Gases, Phys. Rev. 84, 559 (1951)

44. Huxley, L. G. H., A Discussion of the Motion in Nitrogen of Free Electrons with Small Energies with Reference to the Ionosphere, J. Atmos. Terr. Phys. 16, 46 (1959)

45. Crompton, R. W. and D. I. Sutton, Experimental Investigation of the Diffusion of Slow Electrons in Nitrogen and Hydrogen, Proc. Roy. Soc. A215, 467 (1952)

46. Shkarofsky, I. P., M. P. Bachynski, and T. W. Johnston, Collision Frequency Associated with High Temperature Air and Scattering Cross Sections of the Constituents, Report No. 7-801.5: December 1959, RCA Victor Co., Ltd., Montreal, Canada.

47. Ramsauer, C. and R. Kollath, Über den Wirkungsquerschnitt der Nichtedelgasmoleküle gegenüber Electronen unterhalb 1 Volt, Ann. d. Phys. 3.4., 91 (1930)

48. Normand, C., The Absorption Coefficient for Slow Electrons in Gases, Phys. Rev. 35, 1217 (1930)

49. Fisk, J. B., On the Cross Sections of Cl_2 and N_2 for Slow Electrons, Phys. Rev. 51, 25 (1937)

50. Brüche, E., Über den Querschnitt von Wasserstoff--und Stickstoff--molekülen gegenüber langsamen Electronen, Ann. d. Phys. 82, 912 (1927)

51. Crompton, R. W. and L. G. H. Huxley (private communication)

52. Healey, R. H. and C. B. Kirkpatrick, from R. H. Healey and J. W. Reed, The Behavior of Slow Electrons in Gases, Amalgamated, Sydney (1941)

53. Brose, H. L., The Motions of Electrons in Oxygen, Phil. Mag. 50, 536 (1925)

54. Van Lint, V. A. Recombination and Attachment in Ionized Gases, Report No. TR 59-43 (August 31, 1959), General Atomic Division of General Dynamics Corporation, San Diego, Calif.

55. Phelps, A. V., Propagation Constants for Electromagnetic Waves in Weakly Ionized, Dry Air, J. Appl. Phys. 31, 1723 (1960)

56. Molmud, P., Langevin Equation and the AC Conductivity of Non-Maxvellian Plasmas, Phys. Rev. 114, 29 (1959)

57. Allis, W. P., Motions of Ions and Electrons, Handbuch der Physik, Vol. 21, Springer-Verlag (1956)

58. Delcroix, J. L., Introduction to the Theory of Ionized Gases, Interscience (New York, 1960)

59. Whitten, R. C. and I. G. Poppoff, A Model of Solar-Flare-Induced Ionization in the D-region, J. Geophys. Res. 66, 2279 (1961)

60. Bailey, D. K., Abnormal Ionization in the Lower Ionosphere Associated with Cosmic-Ray Flux Enhancements, Proc. IRE 47, 255 (1959)

61. Phelps, A. V. and J. L. Pack, Electron Collision Frequencies in Nitrogen and in the Lower Ionosphere, Phys. Rev. Lett. 3, 340 (1959)

DASA REQUIRED MINIMUM DISTRIBUTION LIST

GENERAL IONIZATION PANEL PUBLICATIONS

(15 January 1962)

(one copy each addressee)

AIR FORCE ACTIVITIES

HQ USAF (AFCIN) Washington 25, DC
HQ USAF (AFRDC) Washington 25, DC
HQ USAF (AFORQ) Washington 25, DC
HQ USAF (AFDAP) Washington 25, DC
HQ USAF (AFTAC) Washington 25, DC
AFSWC, Kirtland AFB New Mexico
ATTN: SWRPA
ATTN: SWRPL
ATTN: CO Naval Air Special Weapons Facility Kirtland AFB New Mexico
ATTN: SWOI
ATTN: SWRPR
ATTN: SWRPS
ATTN: SWRP
ATTN: SWRPT
ATTN: SWRPI
ATTN: SWRJ
AFOSR(SREC) ATTN: Technical Information and Intelligence Division
Washington 25, DC
ARL (RRLO) ATTN: Mr. Cody Wright-Patterson AFB Ohio
ATIC (AFCIN 4F2A) ATTN: Major Pearce Wright-Patterson AFB Ohio
HQ USAF (AFRDR/NU) ATTN: Major E. Lowry, Washington 25, DC
OAR (RRN) Bldg T-D ATTN: Major Munyon, Washington 25, DC
ASD ATTN: WWAD, Tech Library, Wright-Patterson AFB Ohio
SSD AF Unit Post Office, Los Angeles 45, California, ATTN: Tech Library
6555 Test Wg (Dev) ATTN: DWZS, LtCol J. G. Henry Patrick AFB Florida
AFMDC (MDGRT) Holloman AFB New Mexico
IT Wright-Patterson AFB Ohio
AFMTC (MTASI) Patrick AFB Florida
AEDC (AEOI) Arnold AFS Tennessee
APGC (PGTRI) Eglin AFB Florida
RADC ATTN: ACOIL-2 Documents Library, Griffiss AFB New York
BSD AF Unit Post Office, Los Angeles 45, California, ATTN: Tech Library
ESD L G Hanscom Field Bedford Mass
AFSC (RDR-2) Andrews AFB, ATTN: Capt Bay Berrier, Washington 25, DC
AFSC, Andrews AFB ATTN: SCR, DCS/R&E, Washington 25, DC

AFCRL L C Hanscom Field Bedford Mass
ATTN: CRT
ATTN: CRTPM
ATTN: CRZI
ATTN: CRZC
ATTN: CRZA
ATTN: CRZK

ARMY ACTIVITIES

Commanding Officer, White Sands Missile Range, White Sands Missile Range, New Mexico, ATTN: Tech Library
Chief of Ordnance, Department of the Army, Washington 25, DC
Chief Signal Officer, Department of the Army, ATTN: Sig R&D, Washington 25, DC
Army Signal Agency, ATTN: Mr. W. Webb, White Sands Missile Range, New Mexico
Commanding Officer, U.S. Army Signal Research and Development Laboratory, Ft Monmouth, New Jersey, ATTN: Dr. W. McAfee
Director, U.S. Army Ordnance, Ballistic Research Laboratories ATTN: Mr. E. Baicy, Aberdeen Proving Grounds, Maryland
Chief of Research and Development, Department of the Army ATTN: LtCol Roger Conarty, Washington 25, DC
Commanding Officer, Army Research Office, Box CM, Duke Station ATTN: Dr. Robert Mace, Durham, North Carolina
Chief, Army Ballistic Missile Agency, ATTN: Tech Library, Redstone Arsenal, Alabama
Director, Office of Special Weapons Developments, U.S. Continental Army Command, Fort Bliss, Texas
Director, Evan Signal Laboratory, Belmar, New Jersey, ATTN: Weapons Effects Section
ARGMA, Huntsville, Alabama, ATTN: Tech Library
Commanding Officer, Army Research Office, Box CM, Duke Station, Durham, North Carolina, ATTN: Dr. H. Robe
Director, U.S. Army Ordnance, Ballistic Research Laboratories, Aberdeen Proving Grounds, Maryland, ATTN: Mr. Warren Berning
Commanding Officer, U.S. Army Signal Research and Development Laboratory Ft Monmouth, New Jersey, ATTN: Tech Library
Director, U.S. Army Ordnance, Ballistic Research Laboratories ATTN: Dr. F. Kaufman, Aberdeen Proving Grounds, Maryland
Director, U.S. Army Ordnance, Ballistic Research Laboratories ATTN: Library, Aberdeen Proving Grounds, Maryland
Commanding Officer, Diamond Ordnance Fuze Laboratories, Connecticut Avenue and Van Ness Street, N.W. ATTN: Tech Ref Branch, Washington 25, DC
Chief of Research and Development, Department of the Army, Washington 25, DC

NAVY ACTIVITIES

Chief of Naval Research, Navy Department, ATTN: Mr. James Winchester, Washington 25, DC

Commander, Naval Missile Center, Point Mugu, California, ATTN: Code 212.11
Director, U.S. Naval Research Laboratory, ATTN: Dr. P. Mange and Dr. Philip Shapiro, Washington 25, DC
Chief of Naval Operations, Navy Department, ATTN: CDR W. Eaton, OP-75, Washington 25, DC
Director, U.S. Naval Research Laboratory, ATTN: Tech Library, Washington 25, DC
Chief of Naval Research, Navy Department, ATTN: Dr. F. Byrne, Washington 25, DC

OTHER DOD ACTIVITIES

Director, Advanced Research Projects Agency, Washington 25, DC
Director, Advanced Research Projects Agency, ATTN: LtCol Roy Weidler, Washington 25, DC
Director, Weapons Systems Evaluation Group, Washington 25, DC
HQ DASA, ATTN: Document Library Branch (5 Copies), Washington 25, DC
HQ DASA, Radiation Division, ATTN: Major B. McCormac; Major J. E. Mock, Washington 25, DC

AEC ACTIVITIES

Director, Argonne National Laboratory, P.O. Box 299, Lemont, Illinois, ATTN: Tech Library
Director, Oak Ridge National Laboratory, P.O. Box "P", Oak Ridge, Tennessee, ATTN: Tech Library
Brookhaven National Laboratory, Technical Information Division, Document Group, New York, ATTN: Classified Document Section
Director, Los Alamos Scientific Laboratory, P.O. Box 1663, Los Alamos, New Mexico, ATTN: Report Librarian; Dr. Herman Hoerlin
Director, University of California, Lawrence Radiation Laboratory, P.O. Box 808, Livermore, California, ATTN: Technical Information Division
Chief, Technical Information Service Extension, U.S. Atomic Energy Commission, P.O. Box 62, Oak Ridge, Tennessee
President, Sandia Corporation, Sandia Base, Albuquerque, New Mexico, ATTN: Classified Document Division
U.S. Atomic Energy Commission, ATTN: Technical Reports Library, Washington 25, DC

OTHER

Director, Armour Research Foundation, 10 West 35th Street, Chicago, Illinoia, ATTN: Document Library
Aeronutronic, Division of the Ford Motor Company, Ford Road, Newport Beach, California
University of California, Lawrence Radiation Laboratory, Berkeley 4, California, ATTN: Dr. Ken Watson
Space Technology Laboratories, Inc., 5730 Arbor Vitae Street, Los Angeles 45, California
Stanford University, Stanford, California, ATTN: Security Officer

Boeing Aerospace Division, Seattle, Washington, ATTN: Dr. E. L. Chupp
G. C. Dewey Company, 202 E. 44th Street, New York, New York
Kaman Aircraft Corporation, Nuclear Division, Garden of the Gods Road, Colorado Springs, Colorado, ATTN: Dr. Frank Shelton
Director, Stanford Research Institute, Menlo Park, California, ATTN: Document Custodian for Dr. Charles Cook; I. G. Poppoff
University of Washington, Applied Physics Laboratory, 1013 E. 40th Street, Seattle 5, Washington, ATTN: Dr. R. R. Geballe
General Dynamics CONVAIR, 3165 Pacific Highway, San Diego, California
General Atomic, A Division of General Dynamics Corporation, P.O. Box "S", Old San Diego Station, San Diego, California, ATTN: Dr. Victor Van Lint
General Electric Company, Technical Military Planning Operation, 735 State Street, Santa Barbara, California, ATTN: Mr. Walter Hausz; Dr. Walter Dudziak
Electro-Optical Systems, Inc., 125 N. Vinedo Avenue, Pasadena, California, ATTN: Dr. Henry Richter
Director, Stanford Research Institute, Menlo Park, California, ATTN: Document Custodian for Dr. Allen Peterson
Geophysics Corporation of America, Burlington Road, Bedford, Massachusetts
Lockheed Missiles and Space Division, Technical Information Center, 3251 Hanover Street, Palo Alto, California, ATTN: Dr. Roland Meyerott
Cornell Aeronautical Laboratory, Inc., Box 235, Buffalo 21, New York
E. H. Plesset Associates, Inc., 1281 Westwood Boulevard, Los Angeles 24, California
Director, Research Analysis Corporation, 6935 Arlington Road, Bethesda 14, Maryland, ATTN: Library
The RAND Corporation, 1700 Main Street, Santa Monica, California, ATTN: Tech Library
General Electric Company, Technical Military Planning Operation, 735 State Street, Santa Barbara, California, ATTN: Dr. Roy Hendrick
Edgerton, Germeshausen & Grier, Inc., 160 Brookline Avenue, Boston 15, Massachusetts, ATTN: Dr. M. Shuler
Director, Lincoln Laboratory, P.O. Box 73, Lexington 73, Massachusetts, ATTN: Mr. James Pannell
Director, Armour Research Foundation, 10 West 35th Street, Chicago 16, Illinois, ATTN: Document Library for Mr. C. Haaland
The RAND Corporation, 1700 Main Street, Santa Monica, California ATTN: Dr. Robert Lelevier
National Aeronautics and Space Administration, ATTN: Dr. R. Bourdeau, Washington 25, DC
Technical Operations, Inc., South Avenue, Burlington, Massachusetts, ATTN: Paul Richards, Dr. I. L. Kofsky
Republic Aviation Corporation, 223 Jericho Turnpike, Mineola, New York
Republic Aviation Corporation, Executive Offices, Main Plant, Farmingdale, Long Island, New York
Radio Corporation of America, David Sarnoff Research Center, 201 Washington Road, W. Windsor Township, Princeton, New Jersey
Allied Research Associates, Inc., 43 Leon Street, Boston 15, Massachusetts, ATTN: Security Office
Scientific Instrumentation, Office of Lunar and Planetory Programs, National Aeronautics and Space Administration, 1520 H Street, N.W., ATTN: Dr. Martin Swetnick, Washington 25, DC

Goddard Space Flight Center, National Aeronautics and Space Administration,
Greenbelt, Maryland, ATTN: Mr. John Naugle
Pennsylvania State University, University Park, Pennsylvania
ATTN: Professor A. H. Waynick
State University of Iowa, Physics Department, Iowa City, Iowa,
ATTN: Document Control Station for Dr. J. A. Van Allen
General Electric MSVD, 3198 Chestnut Street, Philadelphia, Pennsylvania,
ATTN: Dr. M. H. Bortner
Director, National Bureau of Standards, Central Radio Propagation
Laboratory, Boulder, Colorado, ATTN: Alan Shapley; T. E. Van Zandt
General Electric Company, Technical Military Planning Operation,
735 State Street, Santa Barbara, California, ATTN: DASA Data Center
Westinghouse Electric Corporation, Research Laboratories, Beulah Road
(Churchill Boro), Pittsburgh 35, Pennsylvania, ATTN: Dr. M. Biondi
Director, National Bureau of Standards, ATTN: Dr. L. M. Branscomb,
Washington 25, DC
New York University, College of Engineering, University Heights,
New York 53, New York, ATTN: Dr. Sidney Borowitz
Mitre Corporation, Middlesex Turnpike, Bedford, Massachusetts,
Thru: AFCRL. CCRA-7-15-E, L G Hanscom Field, Bedford, Massachusetts
Institute for Defense Analyses, 1710 H Street, N.W., Washington 25, DC

STANFORD
RESEARCH
INSTITUTE

MENLO PARK
CALIFORNIA

Regional Offices and Laboratories

Southern California Laboratories
820 Mission Street
South Pasadena, California

Washington Office
808 17th Street, N.W.
Washington 5, D.C.

New York Office
270 Park Avenue, Room 1770
New York 17, New York

Detroit Office
The Stevens Building
1025 East Maple Road
Birmingham, Michigan

European Office
Pelikanstrasse 37
Zurich 1, Switzerland

Representatives

Honolulu, Hawaii
Finance Factors Building
195 South King Street
Honolulu, Hawaii

London, Ontario, Canada
85 Wychwood Park
London 14, Ontario, Canada

London, England
15 Abbotsbury Close
London W. 14, England

Milan, Italy
Via Macedonio Melloni 40
Milano, Italy

Tokyo, Japan
911 Iino Building
22, 2-chome, Uchisaiwai-cho, Chiyoda-ku
Tokyo, Japan

UNCLASSIFIED

UNCLASSIFIED